University of Sussex

The electroweak phase transition in two-Higgs-doublet models and implications for LHC searches

Gláuber Carvalho Dorsch

Submitted for the degree of Doctor of Philosophy

University of Sussex

August 2015

Declaration

The following publications have resulted from the work I have done during my PhD studies at Sussex:

[1] G. C. Dorsch, S. J. Huber and J. M. No, *"A strong electroweak phase transition in the 2HDM after LHC8,"* JHEP **1310** (2013) 029 [arXiv:1305.6610 [hep-ph]].

[2] G. C. Dorsch, S. J. Huber and J. M. No, *"Cosmological Signatures of a UV-Conformal Standard Model,"* Phys. Rev. Lett. **113** (2014) 121801 [arXiv:1403.5583 [hep-ph]].

[3] G. C. Dorsch, S. J. Huber, K. Mimasu and J. M. No, *"Echoes of the Electroweak Phase Transition: Discovering a second Higgs doublet through $A_0 \to ZH_0$,"* Phys. Rev. Lett. **113** (2014) 21, 211802 [arXiv:1405.5537 [hep-ph]].

This thesis is based on references [1] and [3] above.

I hereby declare that this thesis has not been and will not be submitted in whole or in part to another University for the award of any other degree.

Signature:

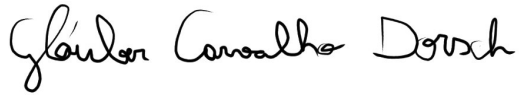

Gláuber Carvalho Dorsch

"The Divine Being is nothing other than the Human being, or rather, the being of man abstracted from the limits of the individual (i.e. the real, corporeal man) and objectified, contemplated and worshiped as another being, as a being distinguished from his own. All attributes of the Divine Being are, therefore, attributes of humankind."

Ludwig Feuerbach, *The Essence of Christianity*

University of Sussex

Gláuber Carvalho Dorsch

Submitted for the degree of Doctor of Philosophy in Physics

The electroweak phase transition in two-Higgs-doublet models and implications for LHC searches

The nature of the electroweak phase transition in two-Higgs-doublet models is revisited in light of the recent LHC results. A scan over an extensive region of their parameter space is performed, showing that a strongly first-order phase transition is favoured by a Standard Model-like light neutral scalar, together with a moderately heavy pseudo-scalar, $m_{A^0} \gtrsim 300$ GeV, and a large mass splitting $m_{A^0} - m_{H^0} \gtrsim m_Z$ between the latter and the heavier CP-even particle. Altogether, these results point to the observation of the decay $A^0 \to H^0 Z$ as a "smoking gun" signature of these scenarios. We analyze the LHC search prospects for this decay in the $\ell\ell b\bar{b}$ and $\ell\ell W^+W^-$ final states, arguing that current data may be sensitive to this signature in the former channel, and with great potential for a discovery in both channels in the 13 TeV run.

Acknowledgements

The present work would not have been conceivable without the collaboration and support from many people to whom I am greatly indebted.

First and foremost, I would like to sincerely thank my advisor, Stephan Huber, not only for the vote of confidence when conceding me the opportunity of being part of this group, but also for his constantly friendly, efficient and objective supervision, which was undoubtedly the main cause for the flourishing of this work.

My appreciation is extended to Jose Miguel No and Ken Mimasu, from whom I also learned enormously, and without whose collaboration this work would have been only a shade of what it curently is.

I am also grateful to Mikko Laine and Veronica Sanz, for useful discussions which largely enriched this thesis, and also for accepting to referee it.

Furthermore, I wholeheartedly thank the whole TPP group at Sussex, for maintaining an amicable atmosphere of intense mutual collaboration, leading to a pleasant and fruitful working environment for scientific enquiry.

To the education bestowed upon me by my parents I owe the scientific curiosity which has led me to pursue a career as a researcher, and I am forever indebted to them for their unconditional support and innumerous sacrifices which enabled me to reach the point of realizing the present work.

Last but not least, I would like to thank the love of my life, Thaisa C. da C. Guio, for the constant companionship, the recomforting friendship, and for providing me every single day with a good reason to smile and to carry on in spite of all hardships.

This work was financed by CAPES (Brazil) via the Science Without Borders program.

Contents

List of Tables

List of Figures

Chapter 1

Introduction

1.1 The problem of baryogenesis

Although the existence of antimatter has been known since Dirac's prediction of the positron in 1928 — later confirmed by Anderson's measurements in 1933 [1] —, it was not until the later development of a coherent framework of relativistic quantum field theories that the importance of these unusual particles came to be fully contemplated. For it can be shown that a Lorentz invariant quantum theory is *causal* if, and only if, every particle has a "mirror" partner with its same mass and spin but opposite charges. Thus, rather than being mere accidents or artifacts of Dirac's exotic equation, antiparticles must be present in every self-consistent theory, and are therefore just as fundamental as the particles themselves. In fact, each particle-antiparticle pair is *a priori* completely symmetrical, being excitations of one and the same quantum field, and as long as interactions do not take place, the choice of what is to be called matter or antimatter is nothing but a mere convention.

The picture might change when interactions are taken into account, since they could favour the creation of a charge of a particular sign over its counterpart. And although the electromagnetic and strong forces do not behave in such way, weak interactions *do* distinguish particles from antiparticles (see section 1.2). However, all experimental tests also suggest that both baryon and lepton numbers are separately conserved in weak decays — at least in those occurring at our high-energy machines —, leading to a certain scepticism as to whether a baryonic excess could be generated this way. Still, a trivial question begs to differ: why is a symmetry between matter and antimatter not observed in our everyday life? Why is the world around us constituted almost exclusively of matter particles?

One *a priori* possible way to avoid the problem is to hypothesize that the predominance

of matter over antimatter is only a local feature of our region of the Universe, which could be compensated by an excess of antimatter elsewhere. But then the question that naturally follows is: how close to us can the nearest antimatter-dominated region be? Or, put another way, how big is this matter-dominated region we happen to live in? We can safely state that it must be at least as big as the Solar System, for if there were a significant amount of antimatter so close to the Sun, its annihilation with solar wind particles would be the dominant source of γ-ray bursts in the sky [2]. Secondly, despite numerous attempts, not a single antihelium nucleus has ever been found in direct cosmic rays detection [3, 4], and the current accuracy of the measurements leads to an upper limit of 10^{-7} for the fraction of antimatter over matter in the galaxy[1]. This negative result in the search for heavy antinuclei cannot be underestimated: if *a single* anticarbon were found in cosmic rays, this would be a confirmation that there is an anti-star fusing antihydrogen and antihelium [2]. Finally, it has been shown that if the Universe were indeed a patchwork of matter- and antimatter-dominated regions, they would inevitably overlap some time between the recombination and structure formation epochs, and the resulting annihilations would yield a cosmic diffuse gamma-ray spectrum incompatible with the observations [5]. The conclusion is that this spectrum can only be as we observe if the matter-dominated region is at least of the size of the whole visible Universe.

In fact, current measurements of the fraction of baryonic matter in the Universe [6, 7] lead to a ratio of the net number of baryons per number of photons

$$\frac{n_B}{n_\gamma} \simeq 6.75 \times 10^{-10}. \tag{1.1}$$

This means that, on average, there was an excess of one baryon for every one billion matter-antimatter annihilation events taking place in the early Universe.

Another attempt to avoid further theoretical difficulties would be to assume the asymmetry to have always existed, taking a baryonic excess as an initial condition of our Universe. However, apart from being theoretically unpleasing and unappealing to suppose an asymmetrical initial state with no better reason than an *ad hoc* argument, such initial asymmetry would be "diluted away" if we accept that the Universe underwent a period of exponential inflation, resulting in a symmetric Universe soon after the rapid expansion [8].

A more appealing alternative is to assume that the Universe was initially symmetric, and that the asymmetry was generated dynamically at some later stage of its history.

[1]The antiparticles found up to date in cosmic ray searches are positrons and antiprotons, which can be explained as being secondary products in reactions occuring as the cosmic rays travel from their source to the detector on the Earth.

This is called *baryogenesis*, and it can only occur if the three Sakharov conditions are satisfied [9], namely there must be (i) baryon number non-conservation; (ii) C and CP violation; (iii) departure from thermodynamical equilibrium. The reason for the first requirement is obvious. The second condition is needed if the interactions are to distinguish between matter and antimatter. More specifically, if charge symmetry is conserved then every process generating an excess of baryons would proceed with the same rate as the charge-conjugate process generating an excess of anti-baryons. Similarly, if CP is an exact symmetry of the model, the width of a process generating an excess of left-handed baryons would equal that of the CP conjugate process generating an excess of right-handed anti-baryons, and the net baryonic number (adding up the excess of left- and right-handed baryons) would still vanish. Finally, the third condition is required because, by definition, a state of thermodynamical equilibrium is such that the rate of any process equals that of its reverse, in which case no net baryon asymmetry could be generated. Alternatively, it could be noted that in thermodynamical equilibrium the number density of baryons and anti-baryons is given by the Fermi-Dirac distribution $(e^{-E^2/T^2}+1)^{-1}$, and the CPT theorem ensures that particles and anti-particles have the same mass, implying the same number density.

1.2 Baryogenesis in the SM

It is quite astonishing that the Standard Model of Particle Physics (SM) in principle contains all these necessary ingredients to explain the cosmological problem of the baryon asymmetry of the Universe. And, of course, all of them involve the weak interaction.

Starting with the requirement of violation of C-symmetry, note that all weakly-interacting neutrinos are left-handed (and anti-neutrinos are always right-handed). Now, C conjugation takes a neutrino to an anti-neutrino (and vice-versa) without changing handedness, so that the charge-conjugate of an existing operator involving a left-handed neutrino would contain couplings to left-handed *anti*-neutrinos, and is therefore forbidden. For instance, the charge-conjugate of the decay

$$\pi^+ \to \mu^+ + \nu_\mu,$$

in which the emitted neutrino is always left-handed, is never observed, and muonic decays of π^- are always associated with emission of a right-handed anti-neutrino.

This observation has initially led to the speculation that maybe weak interactions do not preserve charge and parity (C and P) separately, but only their product, CP. However,

this turns out not to be the case either, as CP is also violated in the SM due to the existence of three fermionic generations. Indeed, let V_L^u and V_L^d be the 3×3 unitary matrices that rotate up- and down-type left-handed quarks from the flavour to their mass eigenstates. After this basis change the charged weak interactions between quarks are governed by the term

$$\mathcal{L} \supset -\frac{g}{\sqrt{2}}\,\overline{u_L}\,\gamma^\mu W_\mu^+ (V_L^u\, V_L^{d\,\dagger})\, d_L + \text{H.c.}, \tag{1.2}$$

where g is the $SU(2)_L$ coupling constant, u_L and d_L are fermionic triplets (accounting for the three generations of up- and down-type quarks, respectively) and $V_L^u\, V_L^{d\,\dagger} \equiv V_{\text{CKM}}$ is the so-called CKM matrix describing the mixing between different quark flavours [10, 11]. Being a 3×3 unitary matrix, V_{CKM} contains one complex phase which cannot be rotated away by field redefinitions [12], and which has the physical significance of inducing CP violating effects, as experimentally confirmed by measurements of kaon and B-meson properties [13] (for a review see ref. [14]).

As for the requirement of displacement from thermodynamical equilibrium, there are *a priori* two potential sources for it in the SM, namely the expansion of the Universe, which proceeds with a rate given by the Hubble parameter H, and the *electroweak phase transition* (EWPT), the process through which the Higgs field acquires its vacuum expectation value (VEV) and breaks the electroweak symmetry, giving mass to gauge bosons and fermions and leaving a remnant electromagnetic symmetry unbroken.

To better understand this latter process first note that, since the Universe is expanding, in earlier stages of its history all its content must have been enclosed in a much smaller volume, resulting in a larger energy density and larger temperature (see ref. [15] for a pedagogic review of the Hot Big Bang cosmology). At about 10^{-10} s after the Big Bang the average temperature of the Universe was $\mathcal{O}(100$ GeV), too hot even for quarks and gluons to hadronize (which takes place at energies below $\Lambda_{\text{QCD}} \simeq 250$ MeV [16]), and the Universe was then pervaded by a plasma of SM particles. Under these conditions, part of the energy released by the Higgs field as it gets a VEV must be spent in generating the masses of these plasma constituents [17], and the larger the density of particles in the plasma is, the smaller the VEV must be[2] in order to minimize the system's free-energy after symmetry breaking. But beyond a certain critical temperature T_c the plasma is so thick that more energy would be required to generate its mass than can be gained by shifting the Higgs VEV, and electroweak symmetry breaking cannot occur spontaneously. Thus electroweak symmetry is restored at high temperatures [18, 19].

[2]Recall that particle masses are proportional to the Higgs VEV.

The Universe then starts from a stage in which the electroweak symmetry is preserved, and, as it expands and its temperature drops below a certain T_c, a transition from the *symmetric* to the *broken* phase can take place. The dynamics of this phase transition will depend crucially on the details of the underlying model, especially on the particle content and their interactions with the Higgs field. If the Higgs VEV varies discontinually in this process, the phase transition is said to be of *first order* and it proceeds via nucleation of bubbles of the broken phase in a "sea" of symmetry-preserving vacuum, much like boiling water. This introduces a second time-scale of displacement from equilibrium, namely the duration of the phase transition, i.e. the time it takes for the bubbles of broken phase to fill the entire Universe.

Let us turn now to the requirement of baryon number violation. Although in the SM both baryon and lepton number are accidental symmetries of the Lagrangian, and the difference $B-L$ is an exact symmetry of the theory, the sum $B+L$ has an anomaly [20, 21] leading to[3]

$$\partial_\mu J^\mu_B = \frac{3}{64\pi^2}\epsilon^{\mu\nu\rho\sigma}\left(g^2 F^a_{\mu\nu}F^a_{\rho\sigma} - g'^2 B_{\mu\nu}B_{\rho\sigma}\right), \tag{1.3}$$

which relates baryon number to the instantaneous configuration of the gauge fields. Now these gauge fields have infinitely many different vacuum states, all related among themselves by gauge transformations and thus having the same energy. But for $SU(2)$ not all of them are physically equivalent, since in this case gauge transformations may belong to different homotopy classes, so that some pairs of gauge related states are not *continuously* obtainable one from the other by means of gauge transformations. A transition between these states would then involve an energy cost and would have physical consequences [22, 23].

Indeed, it is possible to rewrite the r.h.s. of eq. (1.3) as a total divergence $\partial_\mu K^\mu$ [24], with

$$K^\mu = \frac{3}{32\pi^2}\epsilon^{\mu\nu\rho\sigma}\left[g^2\left(W^a_\nu F^a_{\rho\sigma} - \frac{g}{3}\epsilon^{abc}W^a_\nu W^b_\rho W^c_\sigma\right) - g'^2 A_\nu B_{\rho\sigma}\right], \tag{1.4}$$

where W_μ, A_μ are respectively the $SU(2)_L$ and $U(1)_Y$ potentials. To each gauge configuration one can then associate a so-called Chern-Simons number,

$$\begin{aligned} N_{\rm CS}[W] &\equiv \frac{g^2}{32\pi^2}\int d^3x\,\epsilon^{ijk}\left(W^a_i F^a_{jk} - \frac{g}{3}\epsilon^{abc}W^a_i W^b_j W^c_k\right), \\ n_{\rm CS}[A] &\equiv \frac{g'^2}{32\pi^2}\int d^3x\,\epsilon^{ijk}A_i B_{jk}, \end{aligned} \tag{1.5}$$

[3] Here, the overall factor of 3 is the number of fermionic families, g and g' are respectively the $SU(2)_L$ and $U(1)_Y$ gauge couplings, while $F_{\mu\nu} \equiv \partial_\mu W_\nu - \partial_\nu W_\mu - g\,[W_\mu, W_\nu]$ and $B_{\mu\nu} \equiv \partial_\mu A_\nu - \partial_\nu A_\mu$ are the field strength tensors for these two gauge groups.

which are integer-valued at vacuum configurations — in fact $n_{\rm CS}[A_{\rm vac}] = 0$ since it is proportional to the field strength itself —, and which characterize the homotopy class to which this vacuum belongs. A transition from one vacuum to another with different such integer then induces, through the anomaly, a corresponding change in the net baryon number,

$$\Delta B = \left[\int d^3x\, J^0_B\right]_{t=-\infty}^{t=+\infty} = \int d^4x\, \partial_\mu J^\mu_B = \left[\int d^3x\, K^0\right]_{t=-\infty}^{t=+\infty} = 3\,\Delta N_{\rm CS}. \qquad (1.6)$$

The probability for this to occur via tunneling at zero-temperature can be computed from a semi-classical approximation [25] and is found to be $O(e^{-16\pi^2/g^2}) \sim 10^{-162}$ [26]. This prohibitively small number is the reason why B violation is never observed today. However, at high temperatures the system may use the energy available in the surrounding plasma to jump over the barrier instead of having to tunnel through it, and the process is then much less suppressed, with a rate per unit volume in the broken phase given by [27, 28]

$$\Gamma^{\rm broken}_{\rm sph} \sim T^4 \exp\left(-\frac{4\pi}{g}\frac{v(T)}{T}B(T)\right), \qquad (1.7)$$

where $v(T) = 2m_W(T)/g$ is the Higgs VEV at temperature T and $B(T) \sim \mathcal{O}(1)$ is obtained by computing the energy of the classical field configuration sitting on top of the energy barrier separating the two vacua [29] (i.e. a saddle-point solution of the energy functional), so-called a *sphaleron*[4] [30]. In the unbroken phase the analysis is more complicated, as there is no sphaleron solution around which to perform a semi-classical expansion, but a statistical approach (confirmed by lattice simulations) leads to an unsuppressed rate $\Gamma^{\rm unbroken}_{\rm sph} \approx \alpha_W^5 T^4$ [31, 32, 33].

The efficiency of these processes is measured by comparing their rate to the Hubble expansion parameter H, which for a radiation-dominated Universe reads

$$H^2 = \frac{\pi^2 g_* T^4}{90 M^2_{\rm Planck}}, \qquad (1.8)$$

with $g_* \approx 106.75$ the number of effective degrees of freedom in the plasma. If the total rate $\Gamma/T^3 \ll H$, the sphaleron process is effectively turned off, while $\Gamma/T^3 \gg H$ implies that the process is extremely efficient and proceeds in thermal equilibrium. This is clearly the case in the unbroken phase for $T \lesssim 10^{12}$ GeV, so that any asymmetry generated by $B-L$ conserving processes at an earlier epoch would be washed out afterwards [27]. Similarly,

[4] From ancient greek $\sigma\phi\alpha\lambda\epsilon\rho\acute{o}\nu$, "likely to make one stumble, trip or fall". Its Chern-Simons number equals $\frac{1}{2}$, as expected from its being a configuration lying in-between vacua with $\Delta N_{\rm CS} = 1$. Through the anomaly one can also say it has $\frac{3}{2}$ for baryon and lepton number, in the sense that the variation in these quantum numbers in a transition from one vacuum to the *sphaleron* configuration is half the total variation in a transition between two neighbouring vacua.

no baryon asymmetry could result from the EWPT if the sphalerons are still efficient after the transition takes place. Thus a *necessary* condition for successful electroweak baryogenesis is that supercooling takes place, causing the sphalerons to be switched off in the broken phase[5], $\Gamma_{\rm sph}^{\rm broken}/T^3 \ll H$, which then yields [34, 35]

$$\frac{v_c}{T_c} \gtrsim 1.0 \tag{1.9}$$

with $v_c \equiv v(T_c)$. Clearly the Higgs VEV must vary discontinuously, and from the fact that there is a lower bound on this discontinuity one says that eq. (1.9) corresponds to a requirement of a *strongly first order electroweak phase transition*.

We are now in a position to understand why the Standard Model actually can *not* properly account for the baryon asymmetry of the Universe.

The first reason for this failure is that, in the SM, the electroweak phase transition would be first order only for Higgs masses $m_h \lesssim m_W$ [36, 37, 38, 39], well below the observed value $m_h \approx 125$ GeV measured by ATLAS [40] and CMS [41] in July 2012. In fact, for this value of the Higgs mass the would-be "electroweak phase transition" is actually a cross-over, i.e. a perfectly continuous process, and therefore does not introduce any new source of displacement from thermal equilibrium apart from the Universe's expansion. Thus, whenever the B violating sphalerons are active, they are in thermal equilibrium, and the net generated asymmetry is close to zero.

The other problem is the insufficient amount of CP violation provided by the CKM matrix alone [42], due not only to the smallness of the Jarlskog invariant $J \approx 3.06 \times 10^{-5}$ [43, 44], but also aggravated by the huge suppression from the tiny Yukawa couplings. Indeed, the amount of CP violation in the SM can be quantified by [45]

$$d_{\rm CP} = J\,(m_t^2 - m_c^2)(m_t^2 - m_u^2)(m_c^2 - m_u^2)(m_b^2 - m_s^2)(m_b^2 - m_d^2)(m_s^2 - m_d^2), \tag{1.10}$$

where the factors of quark mass differences appear because, if any two quarks of same charge were degenerate, the CKM matrix could be made real by a suitable field redefinition and no CP violation would take place. This dimensionful quantity should be compared to the relevant energy scale of the problem, which for electroweak baryogenesis is the temperature of the phase transition $T \sim \mathcal{O}(100$ GeV). The net baryon asymmetry can then be roughly estimated as

$$\frac{n_B}{s} \sim \frac{d_{\rm CP}}{g_* T^{12}} \sim 10^{-21} \tag{1.11}$$

[5]It follows, in particular, that the expansion of the Universe cannot be the sole source of displacement from equilibrium.

where s is the entropy density in the Universe. That this is off the observed value by more than 10 orders of magnitude is a strong indicative that CP violation in the SM is too small for baryogenesis.

The above argument relies on the assumption that the plasma temperature is the only relevant energy scale of the problem, so its conclusion could be circumvented by elaborating a more intricate mechanism in which lower scales would also be relevant. This was attempted in ref. [46], where coherent scattering of low-momentum ($p \ll T$) quarks against the bubble wall was considered as the main source of the baryonic asymmetry. But this mechanism was ultimately dismissed, because damping in the plasma causes low energy quarks to actually decohere, making it impossible for an inherently quantum effect such as CP violation to manifest itself [42, 47]. The conclusion is that electroweak baryogenesis requires additional sources of CP violation apart from the complex phase in the CKM matrix [48][6].

1.3 Beyond the Standard Model

Together with the absence of a reasonable dark matter candidate — a stable, neutral particle whose production and decay rates during the thermal evolution of the Universe lead to the correct particle abundance as required by cosmological observations [51] — and the fact that in the SM neutrinos are massless — in contradiction with measurements of neutrino mixing —, the origin of the matter-antimatter asymmetry of the Universe is therefore amongst the few experimentally-based motivations to look for physics beyond the SM (BSM) below the Planck scale[7].

A currently promising scenario for baryogenesis, which is also related to the solution of the problem of neutrino masses, is via *leptogenesis* [54, 55]. Although massive neutrinos could easily be accomodated in the SM via the introduction of right-handed Dirac neutrinos with tiny Yukawa couplings, this simplistic solution is usually frowned upon for aggravating the naturalness problem in the flavour sector [56, 57]. A more plausible alternative is that neutrinos be Majorana fermions, leading to a natural explanation for the small masses due to the see-saw mechanism [58, 59], which could be tested in searches

[6] Other mechanisms to obtain the baryon asymmetry with just SM CP violation have also been proposed, such as the so-called Cold Electroweak Baryogenesis, but a thorough investigation of their viability is still an open issue [49, 50].

[7] At $M_{\text{Planck}} \sim 10^{19}$ GeV gravitational effects become relevant, which are not included in the SM since it is still not known how to fit them in the framework of a quantum field theory (if this is at all possible). But because M_{Planck} is many orders of magnitude above the TeV scale, this fundamental incompleteness of the SM is hardly a concern for the study of the TeV scale phenomena accessible at modern colliders (except in models with extra spatial dimensions, where the fundamental scale of gravity can be much lower [52, 53]).

for lepton number violating effects such as neutrinoless double-β decays [60]. In fact, lepton number violation is typically required in mechanisms for neutrino mass generation, even in effective approaches via higher-dimensional operators in the Lagrangian. Now, at temperatures below the mass of the right-handed Majorana neutrino, these lepton number violating decays will be unidirectional — therefore out of equilibrium —, and due to CP-violation in the leptonic mixing matrix a net lepton number excess is generated, which is then converted to a baryon excess via sphalerons (recall that $B-L$ is an exact symmetry). This is the core of the leptogenesis mechanism [61].

Another very attractive scenario is *electroweak baryogenesis*. In this case displacement from thermodynamical equilibrium is provided by the electroweak phase transition, which must be strongly of first order as discussed in the previous section. As the bubbles of true vacuum expand in the symmetric background, particles in the plasma scatter off the bubble wall and, due to CP violation, a chiral excess is generated which is converted in a baryonic excess via sphaleron processes [46, 62, 63, 64, 65, 66, 67]. In order to enhance the SM prediction of the phase transition strength, as well as the amount of effective CP violation, the BSM sector must couple rather strongly to the SM particles, in particular to the electroweak symmetry breaking sector. Furthermore, its characteristic energy scale must not be much larger than the electroweak scale in order for the new particles to be abundant in the plasma during the phase transition. It follows that not only the new physics introduced, but the whole mechanism of electroweak baryogenesis should be testable at current and near-future collider experiments, which is what makes this proposal especially attractive [68].

The nature of the electroweak phase transition, and the ensuing baryon asymmetry, has been extensively studied in many BSM scenarios such as supersymmetric theories [69, 70, 71, 72, 73, 74, 75, 76] as well as in simpler extensions such as the SM with an extra scalar singlet [77, 78, 79] and in two-Higgs-doublet models (2HDMs). In the latter it is found that the correct value for the baryon asymmetry can be predicted in some simplified cases [80, 81], for specific regions of its parameter space [63, 82, 83] and in a general CP-violating scenario [84]. However, a general study of the dependence of the electroweak phase transition with the various parameters of a 2HDM is challenging, due to the high dimensionality of the parameter space — 14 free parameters in the most general case, reduced to 10 when a softly broken $\mathbb{Z}_2$ symmetry is imposed, as discussed below.

The *purpose of this work* is precisely to shed some light on this still largely unexplored issue. We perform a random scan over an extensive region of the 2HDM parameter space,

looking for points with a strong first order electroweak phase transition in order to establish the extent to which 2HDMs are viable candidates for baryogenesis, and which regions of the parameter space are preferred for this purpose [85]. With this knowledge at hand, we proceed to analyse what such a cosmological bound can teach us about the phenomenology of the model, especially whether it could be used to indicate favourable search strategies for testing these scenarios at collider experiments [86].

Granted, the simple addition of a second doublet to the scalar sector does not solve many of the problems affecting the SM, such as the lack of gauge unification, the hierarchy problem, the strong CP problem [87] or the flavour puzzle [88]. But the converse is often true: scalar sectors with two Higgs doublets are well motivated, emerging naturally in many SM extensions such as in supersymmetric [89, 90] and Composite Higgs scenarios [91, 92], in many axionic solutions to the strong CP problem [93], GUT theories, etc. Under an exact $\mathbb{Z}_2$ symmetry[8] it could also provide a dark matter candidate [94, 95] and allow for radiative generation of neutrino masses [96]. Finally, although it is one of the simplest extensions of the SM, the 2HDM contains all the necessary ingredients required for baryogenesis: (i) it modifies the scalar sector, introducing new bosons coupling to the driver of the electroweak phase transition and thus likely enhancing its strength; (ii) it can accomodate additional sources of CP violation, either explicit or spontaneous. For all these reasons, 2HDMs are quite popular as an effective low energy scalar sector, and their phenomenology have been extensively studied in the literature [97, 98, 99, 100, 101, 102, 103, 104, 105, 106, 107, 108, 109]. The current work differs from these in the cosmological motivation behind the benchmarks here analysed.

The general features of the model are introduced in chapter 2. Let us emphasize from the outset that, because CP violation is *not* essential for the study of the electroweak phase transition — which is the focus of the current work —, we will *disregard* this effect for simplicity. This not only reduces the number of free parameters by one, but also simplifies many analytic expressions, allowing us to explain our results in an easier and more transparent way. Of course, for the actual computation of the generated baryon asymmetry some CP violation has to be reintroduced. However, constraints from electron and neutron EDMs will generally enforce any CP violating phase to be quite small, namely $\mathcal{O}(10^{-2})$ [110, 111, 112], in which case their impact on the phase transition strength is mild [113] and the results presented here are still valid[9].

[8] In this case the model is also called Inert Doublet Model.

[9] Whether the required smallness of the CP violating phase still allows for the generation of the observed baryon asymmetry is an issue worth of further investigation, but it lies outside the scope of this work.

The most general Yukawa Lagrangian is presented in section 2.1, where it is shown that the existence of two scalar doublets coupling to fermions leads to dangerous tree-level flavour changing neutral currents (FCNC). We discuss how the harmful terms are forbidden by imposing a $\mathbb{Z}_2$ symmetry which naturally enforces each fermion type to couple to one doublet only. There are four possible combinations, and the model is categorized accordingly as 2HDM Type I, II, X (also called Lepton Specific) and Y (Flipped). The top quark has by far the largest coupling to the scalar sector, and so is chosen to always couple to the same doublet in all four types just listed. We note in passing that the scalar sector of the Minimal Supersymmetric Standard Model (MSSM) is a Type II 2HDM, this being the reason why most works on 2HDMs have focused of this model type. Here we will also look in detail into Type I, as this model type is much less constrained than the other three.

Theoretical and experimental constraints on the model parameters are discussed in section 2.4. Stability of the electroweak vacuum is required up to a cutoff $\Lambda \simeq 10$ TeV, and tree-level unitarity is imposed on $2 \to 2$ scattering amplitudes, thus setting an upper bound on the quartic couplings. From the experimental side, we ensure that the new scalars' contribution to loop-induced quantities such as electroweak precision observables, FCNC processes (specifically $\overline{B} \to X_s\gamma$) and B meson mixing do not drastically alter the SM predictions, which are in good agreement with the precision measurements. Finally, we discuss the constraints imposed by direct searches for new scalars at collider experiments, including the measured properties of the 125 GeV resonance recently observed.

For the evaluation of the phase transition strength the relevant mathematical tool is the effective potential, which we compute perturbatively to 1-loop order in sections 2.3 and 3.1 (at zero and finite temperature, respectively). We will see that the contribution from light particles, such as down-type quarks and leptons, is negligible due to their small couplings to the scalar sector. This means that the phase transition strength is insensitive to the specific structure of the Yukawa sector, being the same for all four types mentioned above. In fact the model type will only have an impact on the constraints coming from $\mathrm{BR}(\overline{B} \to X_s\gamma)$ and collider searches.

The details of our scan and our method for evaluating the phase transition strength are presented in section 3.2, with results and analysis given in section 3.3. Our findings point to a favoured region of the parameter space with a rather exotic phenomenology, where the pseudoscalar decays largely into a Z boson and a heavy non-SM-like scalar.

These scenarios have been little explored in collider searches so far, as they are largely

non-existent in supersymmetric extensions. A detailed analysis of the discovery prospects for this decay channel is performed in chapter 4 for two benchmark points, where we find that a 5σ discovery can be reached at 13 TeV with a luminosity $\mathcal{L} \sim 20 - 200$ fb^{-1}, within reach of the next LHC run.

Chapter 5 is reserved for our conclusions.

Chapter 2

Two-Higgs-doublet models

Two-Higgs-doublet models (2HDMs) figure among the most minimalistic extensions of the Standard Model, differing from it only by the addition of an extra scalar $SU(2)_L$ doublet to its field content (hence the name of the model). The scalar sector of the theory is then composed of

$$\Phi_1 = \begin{pmatrix} \varphi_1^+ \\ \varphi_1^0 \end{pmatrix} = \frac{1}{\sqrt{2}} \begin{pmatrix} \sqrt{2}\,\varphi_1^+ \\ h_1 + i\,\eta_1 \end{pmatrix}, \qquad \Phi_2 = \begin{pmatrix} \varphi_2^+ \\ \varphi_2^0 \end{pmatrix} = \frac{1}{\sqrt{2}} \begin{pmatrix} \sqrt{2}\,\varphi_2^+ \\ h_2 + i\,\eta_2 \end{pmatrix}, \tag{2.1}$$

where the upper components of the doublets are charged under $U(1)_{\text{em}}$, while the bottom ones are neutral.

The most general renormalizable potential for two doublets Φ_1 and Φ_2 that is invariant under $SU(2)_L \times U(1)_Y$ can be written as[1]

$$\begin{aligned} V_{\text{tree}}(\Phi_1, \Phi_2) = &- \mu_1^2 \Phi_1^\dagger \Phi_1 - \mu_2^2 \Phi_2^\dagger \Phi_2 - \frac{1}{2}\left(\mu^2 \Phi_1^\dagger \Phi_2 + \text{H.c.}\right) + \\ &+ \frac{\lambda_1}{2}\left(\Phi_1^\dagger \Phi_1\right)^2 + \frac{\lambda_2}{2}\left(\Phi_2^\dagger \Phi_2\right)^2 + \lambda_3 \left(\Phi_1^\dagger \Phi_1\right)\left(\Phi_2^\dagger \Phi_2\right) + \\ &+ \lambda_4 \left(\Phi_1^\dagger \Phi_2\right)\left(\Phi_2^\dagger \Phi_1\right) + \frac{1}{2}\left[\lambda_5 \left(\Phi_1^\dagger \Phi_2\right)^2 + \text{H.c.}\right] + \\ &+ \Big\{ \left(\Phi_1^\dagger \Phi_2\right)\left[\lambda_6 \left(\Phi_1^\dagger \Phi_1\right) + \lambda_7 \left(\Phi_2^\dagger \Phi_2\right)\right] + \text{H.c.} \Big\}, \end{aligned} \tag{2.2}$$

where μ^2, λ_5, λ_6 and λ_7 can be complex, opening the possibility of having additional sources of CP violation coming from the scalar sector. Note, however, that complex phases in the parameters in the potential are not sufficient to guarantee CP violation. First, because at least one complex phase can be absorbed by a field redefinition which cannot alter the physics. Moreover, since the two doublets have the same quantum numbers, it

[1] The condition of invariance under the gauge group requires that the terms of the potential always appear in products of the form $\Phi^\dagger\Phi$. Moreover, since we want the potential to be renormalizable, it can only have up to quartic interactions, that is, terms of the form $\left(\Phi^\dagger\Phi\right)\left(\Phi^\dagger\Phi\right)$. The most general potential is obtained when we consider all possible combinations of Φ_1 and Φ_2 for these quadratic and quartic terms.

is a matter of choice whether we describe the system in terms of Φ_1 and Φ_2 or of linear combinations thereof, and after such *basis transformation* the potential would still look like eq. (2.2), albeit with different values for the parameters [114, 115, 116]. The sufficient and necessary condition for the 2HDM potential to be *explicitly* CP conserving is that a basis choice exists in which all parameters are real [117, 118].

Due to the gauge symmetries, a general minimum of this potential can always be written as

$$\langle\Phi_1\rangle = \frac{1}{\sqrt{2}}\begin{pmatrix} 0 \\ v\cos\beta \end{pmatrix}, \quad \langle\Phi_2\rangle = \frac{1}{\sqrt{2}}\begin{pmatrix} u \\ v\sin\beta\, e^{i\xi} \end{pmatrix}, \tag{2.3}$$

with $u \in \mathbb{C}$. The case $u \neq 0$, when the charged component acquires a VEV, implies in breaking of $U(1)_{\text{em}}$ and a consequent non-vanishing mass for the photon. This is of course not realized in our Universe, so we will henceforth focus on $u = 0$ only. On the other hand, the phase ξ can be shifted from the VEV to the parameters in the potential via a redefinition $\Phi_2 \to e^{-i\xi}\Phi_2$.

In this case one can define the fields rotated to the so-called Higgs basis as

$$\left.\begin{aligned} \Phi_1' &= \cos\beta\,\Phi_1 + \sin\beta\,\Phi_2 \\ \Phi_2' &= -\sin\beta\,\Phi_1 + \cos\beta\,\Phi_1 \end{aligned}\right\} \implies \langle\Phi_1'\rangle = \frac{1}{\sqrt{2}}\begin{pmatrix} 0 \\ v \end{pmatrix}, \qquad \langle\Phi_2'\rangle = 0, \tag{2.4}$$

so that Φ_1' behaves like the SM scalar doublet. This then means that

$$G^+ = \cos\beta\;\varphi_1^+ + \sin\beta\;\varphi_2^+ \qquad \text{(charged Goldstone)}, \tag{2.5}$$

$$H^+ = -\sin\beta\;\varphi_1^+ + \cos\beta\;\varphi_2^+ \qquad \text{(charged Higgs)}, \tag{2.6}$$

$$G^0 = \cos\beta\;\eta_1 + \sin\beta\;\eta_2 \qquad \text{(neutral Goldstone)}, \tag{2.7}$$

$$h_{\text{SM}} = \cos\beta\;h_1 + \sin\beta\;h_2 \qquad \text{(SM Higgs)}, \tag{2.8}$$

so that β plays the role of a *mixing angle* between the charged mass eigenstates (G^+, H^+).

Likewise, we can rotate the neutral flavour eigenstates to mass eigenstates H_i with a rotation matrix R such that

$$\begin{aligned} \begin{pmatrix} H_1 \\ H_2 \\ H_3 \end{pmatrix} &= \begin{pmatrix} 1 & 0 & 0 \\ 0 & c_3 & s_3 \\ 0 & -s_3 & c_3 \end{pmatrix}\begin{pmatrix} c_2 & 0 & -s_2 \\ 0 & 1 & 0 \\ s_2 & 0 & c_2 \end{pmatrix}\begin{pmatrix} c_1 & s_1 & 0 \\ -s_1 & c_1 & 0 \\ 0 & 0 & 1 \end{pmatrix}\begin{pmatrix} h_1 \\ h_2 \\ -s_\beta\,\eta_1 + c_\beta\,\eta_2 \end{pmatrix} = \\ &= \underbrace{\begin{pmatrix} c_1c_2 & s_1c_2 & -s_2 \\ c_1s_2s_3 - s_1c_3 & s_1s_2s_3 + c_1c_3 & c_2s_3 \\ c_1s_2c_3 + s_1s_3 & s_1s_2c_3 - c_1s_3 & c_2c_3 \end{pmatrix}}_{R}\begin{pmatrix} h_1 \\ h_2 \\ -s_\beta\,\eta_1 + c_\beta\,\eta_2 \end{pmatrix}, \end{aligned} \tag{2.9}$$

where $c_i \equiv \cos(\alpha_i)$ and $s_i \equiv \sin(\alpha_i)$.

In the particular case of CP conservation the real components of the scalar fields cannot mix with the complex ones, so $\alpha_2 = \alpha_3 = 0$. The neutral physical states then read

$$\begin{aligned} A^0 &= -\sin\beta\ \eta_1 + \cos\beta\ \eta_2 && \text{(CP-odd Higgs)}, \\ h^0 &= \cos\alpha\ h_1 + \sin\alpha\ h_2 && \text{(lightest CP-even Higgs)}, \\ H^0 &= -\sin\alpha\ h_1 + \cos\alpha\ h_2 && \text{(heaviest CP-even Higgs)}, \end{aligned}$$

with $\alpha \equiv \alpha_1$ the mixing angle between the two CP-even scalars. Note that our definition of α differs from the general 2HDM literature by an additive factor of $\pi/2$. We find our choice more convenient, since the case when $h^0 = h_{\rm SM}$ corresponds here to $\alpha = \beta$. In general, however, the SM-like Higgs is an admixture of h^0 and H^0,

$$h_{\rm SM} = \cos(\beta-\alpha)\, h^0 + \sin(\beta-\alpha)\, H^0. \tag{2.10}$$

In principle $\beta - \alpha \in [0, 2\pi)$, but it is easy to see that a shift $\beta - \alpha \to \beta - \alpha + \pi$ is equivalent to a field redefinition $(h^0, H^0) \to -(h^0, H^0)$ in the CP-even sector and has no physical consequence. Therefore we can restrict the range of this angle to the physically relevant interval $\beta - \alpha \in \left[-\frac{\pi}{2}, \frac{\pi}{2}\right)$.

2.1 Yukawa sector

Turning now to the Yukawa interactions of fermions with the two doublets, let U and D be fermion triplets, corresponding to the three families of up and down type quarks in their flavour eigenstates, respectively (i.e., of positively and negatively charged quarks under $U(1)_{\rm em}$)[2]. Likewise, let E and N be the triplets corresponding to the three families of leptons and neutrinos. From the properties of the electroweak interaction we know that the left-handed components of these spinors must form doublets under $SU(2)_L$, which we write as $Q_L = (U_L \quad D_L)^T$ and $L_L = (N_L \quad E_L)^T$, whereas the right-handed components U_R, D_R and E_R are singlets[3]. The most general Yukawa interactions of fermions with the two scalar doublets can then be written as

$$\begin{aligned} \mathcal{L}_{\rm Yukawa} = &- \overline{Q_L}\left(Y_1^D \Phi_1 + Y_2^D \Phi_2\right) D_R - \overline{Q_L}\left(Y_1^U \widetilde{\Phi}_1 + Y_2^U \widetilde{\Phi}_2\right) U_R + \text{H.c.} \\ &- \overline{L_L}\left(Y_1^E \Phi_1 + Y_2^E \Phi_2\right) E_R + \text{H.c.}, \end{aligned} \tag{2.11}$$

where $Y_i^{D,U,E}$ are 3×3 Yukawa coupling matrices (acting on the flavour indices of the spinors) and $\widetilde{\Phi}_{1,2} \equiv\ i\sigma_2 \Phi_{1,2}^*$.

---

[2] A suitable rotation in flavour space takes $D \to (d \quad s \quad b)$ and $U \to (u \quad c \quad t)$.

[3] We do not consider right-handed neutrinos.

These Yukawa terms will give mass to the fermions when the neutral components of the scalar doublets acquire VEVs, yielding

$$\mathcal{L}_{\text{Yukawa}}^{\text{mass}} = -\overline{U_L}\left(Y_1^U\langle\varphi_1^0\rangle + Y_2^U\langle\varphi_2^0\rangle\right)U_R + \text{H.c.} + (U \to D, E). \tag{2.12}$$

Clearly the diagonalization of the fermion mass matrix $M_F = Y_1^F\langle\varphi_1^0\rangle + Y_2^F\langle\varphi_2^0\rangle$ does not imply diagonalization of the 3×3 Yukawa coupling matrices Y_1^F and Y_2^F separately. This means that, after rotating the quarks to their mass eigenbasis, there appear interaction terms of the form

$$\mathcal{L}_{\text{FCNC}} = -\overline{d_L}\, y_1^d\, \varphi_1^0\, d_R - \overline{u_L}\, y_1^u \left(\varphi_1^0\right)^* u_R + 1 \to 2 + \text{H.c.} \tag{2.13}$$

with non-diagonal $y_i^{d,u}$, which describes interactions whereby the flavour of the quarks is changed via an exchange of a neutral boson. As these *flavour changing neutral currents* (FCNC) are highly suppressed in nature, the fact that such effect is present at tree-level in our model is a rather undesirable feature of which we need to get rid somehow.

A particularly simple and convenient way to deal with this problem[4], which is also most widely adopted in the literature, is to consider that each type of fermion couples to one doublet only [126]. This can be achieved by imposing a $\mathbb{Z}_2$ symmetry on the Lagrangian, under which the fields transform as $\Phi_1 \to -\Phi_1$, $d_R \to \pm d_R$ and $\ell_R \to \pm\ell_R$, the others remaining invariant. The top quark has by far the dominant coupling to the scalar sector, and we can then use it as a reference to distinguish the two doublets. Put another way, we can *define* Φ_2 to be the doublet coupling to up-type quarks (so u_R is even under $\mathbb{Z}_2$ by construction). There are then four possibilities to couple down-type quarks and leptons either to the same doublet that couples to the top or to the other one, and 2HDMs are often categorized according to this choice as shown in Table 2.1[5].

For consistency, the scalar potential must also be symmetric under these transformations (otherwise the undesirable terms will reappear in the Lagrangian as renormalization counter-terms), so we must have $\mu = \lambda_6 = \lambda_7 = 0$. But in this case there can be no CP violation in the scalar sector, neither explicit (since only λ_5 would possibly have a complex phase which could then be reabsorbed by field redefinitions) nor spontaneous [127]. Thus

[4]Other ways include Minimal Flavour Violation [119, 120, 121, 122], general Yukawa alignment [123] and the so-called Yukawa texture *Ansatz* of $Y_{ij} \sim \sqrt{2m_i m_j}/v$ [124], to name a few. It is worth mentioning that the Yukawa alignment hypothesis is not stable under radiative corrections [125], except in special cases as the one we consider here, where the Yukawa *Ansatz* is imposed via — and therefore is protected by — a discrete symmetry.

[5]In the 2HDM literature Type X is sometimes denoted *Lepton Specific* whereas Type Y is called *Flipped*. It is also worth mentioning that the scalar sector of the Minimal Supersymmetric Standard Model (MSSM) is a Type II 2HDM.

	Φ_1	Φ_2	u_R	d_R	ℓ_R
Type I	$-$	$+$	$+$	$+$	$+$
Type II	$-$	$+$	$+$	$-$	$-$
Type X	$-$	$+$	$+$	$+$	$-$
Type Y	$-$	$+$	$+$	$-$	$+$

Table 2.1: $\mathbb{Z}_2$ charge of scalar doublets and fermions in the different 2HDM Types.

an exact discrete symmetry is not really interesting for baryogenesis. A way out of this is to allow for an explicit soft breaking of the $\mathbb{Z}_2$ symmetry with $\mu \neq 0$ [128]. Because the symmetry is thus broken only softly, there are still no significant FCNCs generated thereby. And because the discrete symmetry is broken explicitly, there are no domain wall problems when both doublets acquire a VEV [129, 130]. This is the case we will consider from now on, so the tree-level potential has the form in eq. (2.2) with

$$\lambda_6 = \lambda_7 = 0. \tag{2.14}$$

The full Yukawa Lagrangian can then be written as

$$\begin{aligned}\mathcal{L}_{\text{Yukawa}} = &- \frac{m_f}{v} H_i \left(y_{f,i} \overline{f} f + \widetilde{y}_{f,i} \overline{f}\, i\,\gamma_5\, f\right) \\ &- H^+ \overline{u} \frac{V_{\text{CKM}}}{\sqrt{2}v} \left[\left(m_d\, y_{d,H^+} - m_u\, y_{u,H^+}\right) + \gamma_5 \left(m_d\, y_{d,H^+} + m_u\, y_{u,H^+}\right)\right] d + \text{H.c.} \\ &- H^+ \frac{m_e}{\sqrt{2}v} \overline{\nu}\; y_{e,H^+} \left(1+\gamma_5\right) e + \text{H.c.}\end{aligned} \tag{2.15}$$

with the scalar-fermion couplings for Types I, II, X and Y summarized in the following tables. Notice from Table 2.1 that Types I and X (resp. Types II and Y) are equivalent as long as only quarks are taken into account, whereas for a purely leptonic case the equivalence pairing is Type I $\sim$ Type Y and Type II $\sim$ Type X.

	$y_{u,i}$	$y_{d,i}$	$\widetilde{y}_{u,i}$	$\widetilde{y}_{d,i}$	y_{u,H^+}	y_{d,H^+}
Type I/X	$R_{i2}/\sin\beta$	$R_{i2}/\sin\beta$	$-R_{i3}/\tan\beta$	$R_{i3}/\tan\beta$	$1/\tan\beta$	$1/\tan\beta$
Type II/Y	$R_{i2}/\sin\beta$	$R_{i1}/\cos\beta$	$-R_{i3}/\tan\beta$	$-R_{i3}\tan\beta$	$1/\tan\beta$	$-\tan\beta$

Table 2.2: Couplings of scalars to quarks.

	$y_{e,i}$	$\widetilde{y}_{e,i}$	y_{e,H^+}
Type I/Y	$R_{i2}/\sin\beta$	$R_{i3}/\tan\beta$	$1/\tan\beta$
Type II/X	$R_{i1}/\cos\beta$	$-R_{i3}\tan\beta$	$-\tan\beta$

Table 2.3: Couplings of scalars to leptons.

2.2 Physical parameters

We have argued above that a physically plausible 2HDM potential must have a minimum of the form

$$\langle\Phi_1\rangle_{\text{EW min}} = \frac{1}{\sqrt{2}}\begin{pmatrix} 0 \\ v\cos\beta \end{pmatrix}, \qquad \langle\Phi_2\rangle_{\text{EW min}} = \frac{1}{\sqrt{2}}\begin{pmatrix} 0 \\ v\sin\beta \end{pmatrix}, \tag{2.16}$$

in order to preserve $U(1)_{\text{em}}$. At such minimum the gauge bosons have masses

$$m_W^2 = \frac{g^2v^2}{4} \qquad \text{and} \qquad m_Z^2 = \frac{m_W^2}{\cos^2\theta_W} \tag{2.17}$$

(with $\cos\theta_W \approx 0.8819$ the cosine of the Weinberg angle), implying that at least one such vacuum state must have $v \approx 246$ GeV, which we shall henceforth call the *electroweak minimum*.

The condition that this be indeed an extremum of V_{tree} allows us to write, for the CP conserving and softly broken $\mathbb{Z}_2$-symmetric case,

$$\begin{aligned} 2\mu_1^2 &= v^2\left(\lambda_1\cos^2\beta + \lambda_{345}\sin^2\beta\right) - 2M^2\sin^2\beta, \\ 2\mu_2^2 &= v^2\left(\lambda_2\sin^2\beta + \lambda_{345}\cos^2\beta\right) - 2M^2\cos^2\beta, \end{aligned} \tag{2.18}$$

where $M^2 \equiv \mu^2/\sin(2\beta)$ and $\lambda_{345} \equiv \lambda_3+\lambda_4+\lambda_5$. We then exchange two bare mass parameters in V_{tree} by the parameter M, which sets the overall scale for the masses of the additional scalars, and the electroweak scale v, which is the natural scale for h_{SM} as usual.

From the diagonalization of the mass matrix (see Appendix A) with the rotation R defined in eq. (2.9) we also see that the quartic couplings can be written as

$$\begin{aligned} \lambda_1 &= \frac{1}{v^2\cos^2\beta}\left(m_{h^0}^2\cos^2\alpha + m_{H^0}^2\sin^2\alpha - M^2\sin^2\beta\right), \\ \lambda_2 &= \frac{1}{v^2\sin^2\beta}\left(m_{h^0}^2\sin^2\alpha + m_{H^0}^2\cos^2\alpha - M^2\cos^2\beta\right), \\ \lambda_3 &= \frac{1}{v^2\sin(2\beta)}\Big[\left(2m_{H^\pm}^2 - M^2\right)\sin(2\beta) - \left(m_{H^0}^2 - m_{h^0}^2\right)\sin(2\alpha)\Big], \\ \lambda_4 &= \frac{1}{v^2}\left(M^2 + m_{A^0}^2 - 2\,m_{H^\pm}^2\right), \\ \lambda_5 &= \frac{1}{v^2}\left(M^2 - m_{A^0}^2\right), \end{aligned} \tag{2.19}$$

so that λ_{1-5} regulate the mutual splittings among the scalar masses, as well as how they deviate from their base values v and M.

These relations allow us to use, as the defining physical parameters of the model, the masses of the scalars (m_{h^0}, m_{H^0}, m_{A^0}, $m_{H^\pm}$) and their mixing angles (β, α), together with the overall scale of new physics M.

2.3 Zero temperature 1-loop effective potential

So far we have been dealing with the *classical* theory of two-Higgs-doublet models, having obtained the properties of the scalar fields — the physical states, their masses and VEVs — by inspection of the tree-level potential V_{tree}.

However, quantum mechanical fluctuations will cause these properties to deviate from the expressions derived above, and must then be taken into account by computing the contribution from all (1PI) loop diagrams to the relevant n-point correlation function. Still it would be convenient if these computations could be summarized in an *effective potential*, from which one could get the properties of the full quantum system by inspection, in analogy to what we have previously done for the classical case. We will now show that this can indeed be done [131, 132].

We start by recalling Dirac's insight that the quantum mechanical amplitude for a certain process is related to the classical action functional via $Z \sim e^{iS}$ [133, 134]. The relationship is not an equality because e^{iS} is the amplitude for the process along a certain definite "path" only, and the superposition principle tells us that the full quantum amplitude is the sum over all possible such contributions. More rigorously, the vacuum-to-vacuum transition amplitude in the presence of an external current J reads

$$Z[J] \equiv e^{iW[J]} \equiv \langle 0^+|0^-\rangle_J = \int \mathcal{D}\phi\, e^{i(S[\phi]+J\cdot\phi)}, \tag{2.20}$$

where for the moment we will use the simplified notation

$$J \cdot \phi \equiv \int d^4x\, J(x)\phi(x). \tag{2.21}$$

Note that W is a functional of J, not of the field configurations (which have been integrated over). In particular,

$$\frac{\delta W}{\delta J(x)} = \langle 0^+|\phi(x)|0^-\rangle_J \equiv \phi_{\text{cl}}(x), \tag{2.22}$$

and $\phi_{\text{cl}}(x)$ can be interpreted as a classical field configuration in the presence of the current J, since all quantum fluctuations have been averaged over[6]. But we can now perform a

[6]The terminology here, albeit adequate, can be misleading. ϕ_{cl} is "classical" in the sense that quantum

Legendre transform to define a functional

$$\Gamma[\phi_{\rm cl}] \equiv W[J] - J \cdot \phi_{\rm cl} \tag{2.23}$$

depending only on the classical field configurations and such that $Z[J] = e^{i(\Gamma[\phi_{\rm cl}]+J\cdot\phi_{\rm cl})}$. Comparing to Dirac's initial insight[7], we see that $\Gamma[\phi_{\rm cl}]$ plays the role of an *effective quantum action*, an action functional that encapsulates the sum over all possible quantum fluctuations.

We can now expand Γ in powers of momentum and, in analogy to the classical case, call the *effective potential* $V_{\rm eff}$ the negative of all momentum independent terms in the expansion, i.e.

$$\Gamma[\phi_{\rm cl}] = \int d^4x \left(-V_{\rm eff}(\phi_{\rm cl}) + \mathcal{O}(\partial_\mu \phi_{\rm cl})\right). \tag{2.24}$$

On the other hand, it can be shown that the n-th derivative of Γ w.r.t. $\phi_{\rm cl}$ are the 1PI Green's functions (including all loop diagrams) [135]. We therefore achieve our aim of recovering the quantum properties of the system by taking derivatives of $V_{\rm eff}$ in analogy to the procedure we followed in the classical field theory.

Having laid down the general formalism, we now turn to the explicit computation of the effective potential in the 2HDM. As usual this can be done only perturbatively, and here we will focus only on the first quantum corrections (i.e. we compute the effective action to next-to-leading order). One way of doing this is by directly calculating and summing the contribution from all possible 1-loop diagrams with arbitrarily many external legs [132]. We will take an alternative, but obviously equivalent route, and start from the full path integral in eq. (2.20) [136]. In the spirit of variational calculus, we parametrize the quantum fluctuations around the tree-level path as

$$\phi(x) = \phi_{\rm tree}(x) + \eta(x). \tag{2.25}$$

By definition $\phi_{\rm tree}$ satisfies the classical equations of motion

$$\left.\frac{\delta S}{\delta \phi}\right|_{\phi_{\rm tree}} + J = 0, \tag{2.26}$$

and this defines an implicit functional relationship between $\phi_{\rm tree}$ and J. Being just a shift by a constant (in field space), the Jacobian of the transformation in eq. (2.25) is trivial and, after expanding $S[\phi_{\rm tree}+\eta]$ in powers of η, the path integral reads

$$e^{iW[J]} = e^{i(S[\phi_{\rm tree}]+J\cdot\phi_{\rm tree})} \int \mathcal{D}\eta \, \exp\left[\frac{i}{2}\,\eta\,\left.\frac{\delta^2 S}{\delta\eta\,\delta\eta}\right|_{\phi_{\rm tree}}\eta + \ldots\right], \tag{2.27}$$

---

effects *have already been* taken into account and averaged over — this is in fact how classicality emerges out of a fundamentally quantum world. This is not to be confused with the configuration that extremizes the classical action S, which provides only the leading order contribution to $\phi_{\rm cl}$.

[7] Note that, in the presence of an external current J, the classical action is shifted as $S[\phi] \to S[\phi] + J\cdot\phi$.

with the term linear in η vanishing by virtue of eq. (2.26), and the ellipsis representing terms coming from higher order diagrams in perturbation theory. The remaining path integral has a Gaussian form and can therefore be analytically solved, yielding

$$W[J] = S[\phi_{\text{tree}}] + J \cdot \phi_{\text{tree}} - i \log \left[\det \left(i\mathcal{D}^{-1}(\phi_{\text{tree}}) \right)^{-1/2} \right] + \mathcal{O}(\text{2-loop}), \tag{2.28}$$

where we have defined the inverse propagator

$$i\mathcal{D}^{-1}(\phi_{\text{tree}}) \equiv - \left. \frac{\delta^2 S[\phi]}{\delta\phi\, \delta\phi} \right|_{\phi_{\text{tree}}} = \partial_\mu \partial^\mu + m^2(\phi_{\text{tree}}). \tag{2.29}$$

To get the effective action we now need to do a Legendre transform. From eq. (2.22),

$$\phi_{\text{cl}} = \frac{\delta W}{\delta J} = \left(\frac{\delta S}{\delta \phi_{\text{tree}}} + J \right) \frac{\delta \phi_{\text{tree}}}{\delta J} + \phi_{\text{tree}} + \mathcal{O}(\text{1-loop}), \tag{2.30}$$

which implies $\phi_{\text{tree}} = \phi_{\text{cl}} + \mathcal{O}(\text{1-loop})$, the first term vanishing due to eq. (2.26). Plugging this back into eq. (2.28) and again using eq. (2.26) finally yields

$$\Gamma[\phi_{\text{cl}}] = S[\phi_{\text{cl}}] + \frac{i}{2} \text{Tr} \left[\log \left(i\mathcal{D}^{-1}(\phi_{\text{cl}}) \right) \right] + \mathcal{O}(\text{2-loop}). \tag{2.31}$$

Note that, at tree-level, the effective action coincides with the classical action, thus further justifying the nomenclature. To compute the first quantum correction we will consider the case

$$\phi_{\text{cl}}(x) = \phi_{\text{cl}} \ \equiv \ \text{constant}, \tag{2.32}$$

i.e. we will take the vacuum to be translation invariant. This is most of the time a realistic assumption, and we will comment later on its implications and possible relaxation (see section 3.1.2). The constancy of ϕ_{cl} makes the propagator invariant under translations, which means that $i\mathcal{D}^{-1}(\phi_{\text{cl}}; k)$ is diagonal in momentum space. We can then write

$$\begin{aligned} \Gamma[\phi_{\text{cl}}] &= S[\phi_{\text{cl}}] + \frac{i}{2} \text{Tr} \left[\mathbb{I} \log \left(-k^2 + m^2(\phi_{\text{cl}}) \right) \right] + \dots \\ &= - \int d^4x\, V_{\text{tree}}(\phi_{\text{cl}}) + \int d^4x \sum_i \frac{i}{2} \int \frac{d^4k}{(2\pi)^4} \log \left(-k^2 + m_i^2(\phi_{\text{cl}}) \right) + \dots \\ &= - \left[V_{\text{tree}}(\phi_{\text{cl}}) + \sum_i \frac{1}{2} \int \frac{d^4k_E}{(2\pi)^4} \log \left(k_E^2 + m_i^2(\phi_{\text{cl}}) \right) + \dots \right] \int d^4x \end{aligned} \tag{2.33}$$

after a Wick rotation $k^0 \to ik^0$. The sum is over all scalars in the theory. The spacetime volume $\int d^4x$ is a consequence of the translation invariance of the propagator (or, equivalently, of the constancy of ϕ_{cl}). On the other hand, recalling the expansion in eq. (2.24) of the effective action in powers of momenta, and that all terms $\mathcal{O}(\partial_\mu \phi_{\text{cl}})$ vanish, we see that the coefficient in brackets is nothing but $V_{\text{eff}}(\phi_{\text{cl}})$, the effective potential we have been looking for.

The integral in the first quantum correction to the effective potential (henceforth called $V_1(\phi_{\rm cl})$) can be analytically solved. The 4-dimensional volume element in spherical coordinates is $d^4k_E = |k_E|^3 d|k_E| d\Omega_3$, and integration over the 3-dimensional solid angle returns a factor of $2\pi^2$, so

$$V_1(\phi_{\rm cl}) = \sum_i \frac{1}{16\pi^2} \int_0^\Lambda dk_E k_E^3 \log\left(k_E^2 + m_i^2(\phi_{\rm cl})\right), \tag{2.34}$$

where Λ is the cut-off scale beyond which the theory ceases to be a good effective description of Nature, and at which some new physics described in terms of other degrees of freedom kicks in. After integrating by parts and neglecting field-independent terms as well as subdominant $\mathcal{O}(m^2/\Lambda^2)$ (since $\Lambda \gg m_i \ \forall\ i$) we arrive at

$$V_1 = \sum_i \frac{1}{64\pi^2} \left[m_i^4 \left(\log \frac{m_i^2}{\Lambda^2} - \frac{1}{2} \right) + 2\Lambda^2 m_i^2 \right]. \tag{2.35}$$

The last step in the calculation consists in getting rid of the cut-off dependence by absorbing them into the (unobservable) bare parameters of the tree-level potential via a renormalization procedure. Put another way, we can say that the parameters appearing in $V_{\rm tree}$ also depend on Λ in such a way that, in the full effective potential $V_{\rm eff} = V_{\rm tree} + V_1 + \ldots$, all cut-off dependence cancels out [137]. The key point behind this procedure is that the outcome of a measurement can only give information about the parameters of the full quantum theory, and nothing can be known about their individual contributions from each order in the perturbative expansion[8].

That the mentioned cancellations can indeed take place follows from the fact that $\Lambda^2 \sum_i m_i^2$ merely shifts the value of the bare mass parameters and therefore does not introduce any new field dependence in the effective potential. Likewise, we can split

$$m_i^4 \log \frac{m_i^2}{\Lambda^2} = m_i^4 \log \frac{m_i^2}{Q^2} + m_i^4 \log \frac{Q^2}{\Lambda^2} \tag{2.36}$$

and the latter term simply shifts the values of the bare quartic couplings[9]. The scale Q is introduced here on dimensional grounds to make the argument of the logarithms dimensionless.

All in all, the bottom line is that the only genuinely new field dependence introduced

[8] A theory is said to be *renormalizable* when all cut-off dependence can be eliminated by fixing the value of finitely many physical parameters — or, in other words, when only finitely many counter-terms are needed to get rid of the cut-off dependence. Thus renormalizability is a fundamental requirement for the theory to be predictive.

[9] Alternatively, note that $\sum_i m_i^2 = \mathrm{Tr}(M)$ and $\sum_i m_i^4 = \mathrm{Tr}(MM)$, where M is the squared mass matrix. From the fact that these are gauge-invariant quantities involving only up to quartic powers of the fields, it follows that they must have the general form of eq. (2.2).

by the 1-loop diagrams come from the first term in eq. (2.36), so we can finally write

$$V_1 = \sum_i \frac{1}{64\pi^2} m_i^4 \left(\log \frac{m_i^2}{Q^2} - \frac{1}{2} \right) + V_{\rm CT}. \tag{2.37}$$

The factor of 1/2 is kept in by convention, whereas $V_{\rm CT}$ has the same form as the tree-level potential and accounts for possible cut-off independent terms which remain after the cancellations just mentioned take place.

The calculation we have shown here gives only the contribution to the scalar fields' effective potential coming from fluctuations of the scalar fields themselves, i.e. from diagrams with scalars running in the loops (since only the scalar fluctuations have been integrated over). To get the full result, eq. (2.27) should be integrated also over all fermions and vector fields. It turns out that each degree of freedom of these fields gives a contribution of the same form of eq. (2.37), the contribution from fermions carrying also a negative sign due to the fermionic loop [138]. Therefore the final result reads

$$V_{\rm eff} = V_{\rm tree} + \sum_i \frac{n_i}{64\pi^2} m_i^4 \left(\log \frac{m_i^2}{Q^2} - \frac{1}{2} \right) + V_{\rm CT}. \tag{2.38}$$

The dominant contributions to the quantum correction are from the heavy particles in the model, namely the gauge bosons ($V = Z$, W^+ and W^-, each with $n_V = 3$ polarization d.o.f), the top quark ($n_t = -1 \times 2 \times 2 \times 3$ for chirality, spin and colour d.o.f), and the scalars themselves ($n_\phi = 1$). The masses entering eq. (2.38) are the particle masses at an arbitrary point in field space, which read

$$m_{W,Z}^2(\phi_i) = m_{W,Z}^2 \frac{\left(\Phi_1^\dagger \Phi_1 + \Phi_2^\dagger \Phi_2 \right)}{v^2}, \qquad m_t^2(\phi_i) = m_t^2 \frac{\Phi_2^\dagger \Phi_2}{v^2 \sin^2 \beta}, \tag{2.39}$$

and the scalar masses are obtained by diagonalizing the mass matrix (see Appendix A). Note that the Goldstone bosons' masses vanish *only* at the minimum of the potential, but not in general. Since we are working in Landau gauge, their contribution as loop mediators must also be included in eq. (2.38), and is typically non-negligible.

Finally, the counter-terms in $V_{\rm CT}$ are fixed by setting the physical parameters whose experimental values will be used in defining the theory, as well as the energy scale Q at which the experiments were carried out. This *renormalization scale* Q must be of the order of the masses of the particles contributing to the 1-loop potential in eq. (2.38), to ensure the smallness of the logarithmic terms so that the 1-loop quantum correction remains subdominant with respect to the tree-level contribution — otherwise the validity of the perturbative expansion at 1-loop order breaks down. Once these are fixed, the counter-terms can be computed by e.g. requiring the tree-level value of the defining physical

quantities to match the experimental value and demanding that the 1-loop contribution does not modify them.

Here we will choose the masses of the SM particles as well as the physical parameters described in section 2.2 (namely the scalar masses and their mixing angles) as the physical observables defining the theory, and will take $Q \equiv v/\sqrt{2} \approx m_t$. Following the prescription just described, this means that the position of the electroweak minimum and the scalar mass matrix at tree and 1-loop level are the same, i.e.

$$\frac{\partial V_{\rm CT}}{\partial h_i} + \sum_k \frac{n_k}{32\pi^2} m_k^2 \log\left(\frac{m_k^2}{Q^2}\right) \frac{\partial m_k^2}{\partial h_i} = 0 \tag{2.40}$$

and

$$\frac{\partial^2 V_{\rm CT}}{\partial\phi_i \partial\phi_j} + \sum_k \frac{n_k}{32\pi^2} \left[\frac{\partial m_k^2}{\partial\phi_i}\frac{\partial m_k^2}{\partial\phi_j}\left(\log\frac{m_k^2}{Q^2} + 1\right) + m_k^2 \log\left(\frac{m_k^2}{Q^2}\right)\frac{\partial^2 m_k^2}{\partial\phi_i\partial\phi_j}\right] = 0, \tag{2.41}$$

where ϕ_i stands for the fields in the doublets.

But there is a caveat in carrying out the condition in eq. (2.41). For the Goldstone bosons, the first term in eq. (2.41) is infrared divergent, so that trying to define the physical mass by taking derivatives of $V_{\rm eff}$ actually yields unphysical results[10]. This happens because, by definition, the effective potential takes into account only diagrams with vanishing external momenta, whereas the physical mass must be evaluated on-shell, with $p^2 = m^2$. A rigorous solution to the problem has been developed in ref. [82]. Here we choose to adopt the more straightforward approach of replacing the vanishing Goldstone masses in the logarithmic divergent term by an IR cutoff at $m^2_{\rm IR} = m^2_{h^0}$, which gives a good approximation to the exact procedure of on-shell renormalization, as argued in ref. [84].

2.4 Constraints

We now turn to the constraints that the model has to satisfy both for theoretical consistency as well as for agreement with experimental data.

2.4.1 Stability of electroweak vacuum

In order for the predicted values of the gauge bosons' masses to agree with the experimental data, it is necessary not only that the scalar potential have an electroweak minimum as in eq. (2.16) with $v \approx 246$ GeV, but also that this be the actually realized vacuum state

[10] At 2-loop order these IR divergences appear already in the first derivative of $V_{\rm eff}$, so that even the minimization procedure of the potential is ill-defined. A rigorous way to handle these divergences is to resum the problematic diagrams involving Goldstone bosons. However, the numerical impact of these resummations in the final shape of the potential is very small [139, 140].

of the scalar fields. This will not necessarily be the case if the electroweak vacuum is not the global minimum of the potential, in which case the system has a finite probability of tunnelling out of it. This is the well-known issue of *stability of the electroweak vacuum*.

Already in the SM this is a potential problem [141, 142, 143]. For even though at tree-level the electroweak vacuum is guaranteed to be unique and thus *stable*, the negative and non-negligible quantum corrections from the top quark will pull the effective potential down towards negative values and may generate a potentially dangerous second minimum at some large scale $\Lambda \gg v$. The electroweak vacuum is then said to be *unstable* if its lifetime is shorter than the age of the Universe, in which case this Λ is interpreted as the cutoff beyond which the SM is no longer a good effective theory. Else, it is said to be *metastable*.

A naïve first approach to this problem is to check for these secondary minima by "brute force" evaluation of the effective potential. However, this may require excursions into the region of very large field values, $\phi \approx \Lambda \gg v$, for which the logarithms in eq. (2.38) will be large and induce a breaking of the perturbative expansion, even if the couplings are small. A proper way to deal with this problem is to resum these logarithms by computing the running of the couplings and considering the RG improved potential [143, 144, 145]. Again, the top quark will yield a negative contribution to the β-function of the Higgs quartic coupling λ and, depending on its magnitude, may cause this λ to become negative at some scale. If this scale is above M_{Planck} then no problem arises, since the SM is not expected to work in this regime. Otherwise, it is necessary to compute the lifetime of this vacuum to ensure its metastability [146].

The results to a 2-loop approximation are depicted in fig. 2.1, which has been taken from ref. [147]. On the left, the running Higgs quartic coupling λ is shown as a function of the RGE scale for values of the top mass, the QCD coupling constant and the Higgs mass varying by $\pm 3\sigma$ around their central values. As discussed above, the larger the top Yukawa coupling is, the sooner the quartic coupling becomes negative. But in any case instability sets in only at scales $\Lambda \gtrsim 10^{10}$ GeV$\gg v$, thus justifying the need to resum the logarithms, as stated above. To the right is a phase diagram indicating that, with the currently known values of the SM parameters, the electroweak vacuum is in a rather fine-tuned region of metastability.

Let us now turn to the 2HDM case. Recall that, if the electroweak vacuum *is* the global minimum of the potential, then it is said to be *stable*. In a tree-level analysis, this is the case only if the potential is bounded from below, i.e. if $V_{\text{tree}} > 0$ whenever the fields

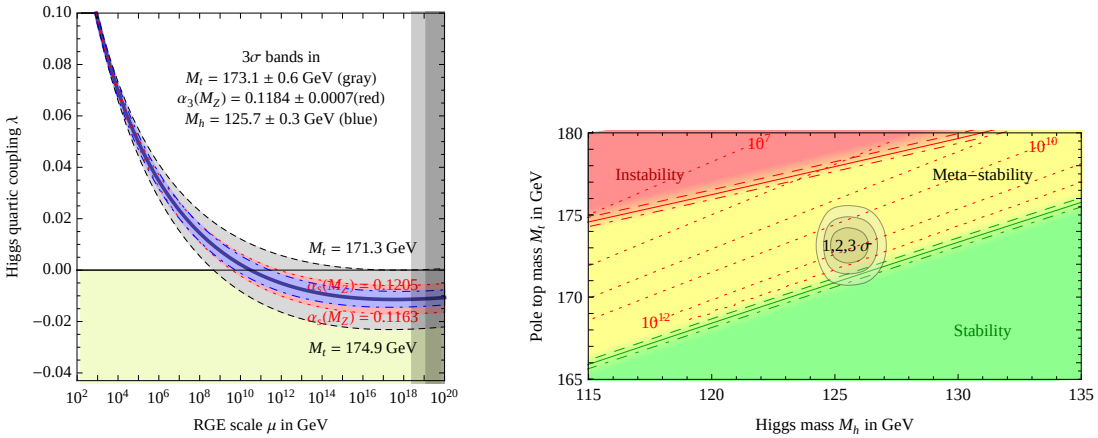

Figure 2.1: (Left) Running Higgs quartic coupling λ with the RGE scale. Results are shown for various values of the top mass, the strong coupling and the Higgs mass, all varying by $\pm 3\sigma$. (Right) Phase diagram showing the nature of the electroweak vacuum as a function of the top and Higgs mass. The red dotted lines indicate the scale at which the the quartic coupling becomes negative. For the current values of the SM parameters to within a 3σ precision, the electroweak vacuum is metastable. Figures taken from ref. [147].

approach infinity in any direction. In this limit it suffices to analyse the quartic terms in the potential, so the requirement of a bounded potential imposes bounds on the quartic couplings λ_{1-5}[11]. Indeed, with a judicious choice of directions one can show that

$$\begin{gathered} \lambda_1 > 0, \quad \lambda_2 > 0, \quad \lambda_3 > -\sqrt{\lambda_1 \lambda_2}, \\ \lambda_3 + \lambda_4 - |\lambda_5| > -\sqrt{\lambda_1 \lambda_2} \end{gathered} \tag{2.42}$$

are necessary conditions to guarantee boundedness from below, and for the $\mathbb{Z}_2$ symmetric case it can be shown that they are also sufficient [148, 149].

Boundedness from below is itself necessary, but not sufficient, to guarantee stability of the electroweak minimum. This is because, contrary to the SM case, in general the 2HDM scalar potential has a rich vacuum structure already at tree-level, with multiple inequivalent stationary points, and it is then necessary to ensure that the electroweak minimum will be the deepest among them.

This vacuum structure of the tree-level 2HDM potential has been extensively studied in the literature [150, 151, 152], culminating in a fundamental theorem stating that, in the most general 2HDM, V_{tree} can have *at most* two minima of any kind [153]. Two corollaries follow from this.

[11] The condition that the quartic terms of the potential be positive definite at large field values in all directions in field space, $V_4 > 0$, is called a *strong stability requirement*, and is actually not satisfied by some interesting models like the MSSM [97]. In these cases a milder requirement would be to demand $V_4 \geq 0$, and that the quadratic terms in the potential be positive-definite in the directions where $V_4 \to 0$.

First, if the potential has a minimum preserving $U(1)_{\rm em}$, as in the cases considered in our study, then no other minima exist that break this symmetry [154, 155]. This is because charge-breaking vacua always come in conjugated pairs[12], so their coexistence with an electroweak minimum would imply in $V_{\rm tree}$ having more than two extrema, in contradiction with the theorem just mentioned. The models here considered are therefore safe against spontaneous breaking of $U(1)_{\rm em}$ at tree-level.

For the very same reason, a minimum that spontaneously breaks a discrete symmetry (e.g. CP) cannot coexist with minima that preserve it.

But there is still the possibility that the potential has two charge- and CP-conserving minima, the deepest one having norm $\langle \Phi_1^\dagger \Phi_1 + \Phi_2^\dagger \Phi_2 \rangle \neq v^2$ and thus yielding different masses for the gauge bosons than those we observe. In a general $\mathbb{Z}_2$ symmetric (possibly CP violating) 2HDM, a necessary and sufficient condition for this *not* to be the case, and for the electroweak minimum to be the global minimum of $V_{\rm tree}$, is that [156, 157]

$$\left[\left(\frac{m_{H^\pm}^2}{v^2} + \frac{\lambda_4}{2}\right)^2 - \frac{|\lambda_5|^2}{4}\right]\left[\frac{m_{H^\pm}^2}{v^2} + \frac{\sqrt{\lambda_1\lambda_2} - \lambda_3}{2}\right] > 0. \tag{2.43}$$

Two notes are in order at this point. First, as already stated above, it is not strictly necessary that the electroweak minimum be the global minimum of the potential, as long as its lifetime is larger than the age of the Universe. However, computing this tunneling effect in a multi-dimensional field space is a complicated task [156] which is beyond the scope of this work, so that this possibility will *not* be considered.

Second, these conditions are the requirements for *tree-level* stability only, and it is necessary to verify that they are not spoiled by loop corrections. Since the effective potential does not have a simple polynomial shape, no theorems similar to the ones presented above have been proven at loop-level yet.

As in the above discussion on the SM case, one possible approach here is to work with the RG improved potential, imposing that the running couplings satisfy eq. (2.42) all the way up to a cut-off Λ beyond which we do *not* expect the 2HDM to be a good effective theory, so that some additional UV physics may be needed to complete it. We choose here $\Lambda = 10$ TeV. The fact that this is relatively close to the electroweak scale[13] allows us to use the simpler approach of demanding the effective potential to be positive definite for field values up to $\phi_i \approx \Lambda$. Indeed, we have checked explicitly that both methods are essentially equivalent.

[12]The value of the potential at a minimum of the form shown in eq. (2.3) remains the same under a transformation $u \to -u$.

[13]Compare it to the stability cut-off in the SM, $\Lambda \gtrsim 10^{10}$ GeV.

We also rule out the existence of a deeper minimum in the vicinity (within a radius of 1 TeV) of the electroweak vacuum by scanning for other minima of the effective potential in this region and requiring them to lie above the electroweak one.

2.4.2 Unitarity

Another important constraint comes from the requirement that the S-matrix remain unitary up to high energies, at least up to the scale $\Lambda \gg v$ beyond which the model breaks down or enters a strongly coupled regime [158]. This requirement is equivalent to the so-called *optical theorem*, which relates the total cross section of a two-particle collision to the imaginary part of the $2 \to 2$ forward scattering matrix element [135],

$$2\sqrt{s}\,|\vec{\mathbf{p}}| \sum_n \sigma_{2\to n} = \mathrm{Im}\mathcal{M}(s, \theta = 0), \tag{2.44}$$

with $\sqrt{s}$ the centre-of-mass energy, $\vec{\mathbf{p}}$ the momentum of one of the incoming particles and θ the angle between the incoming and outcoming beams[14], all measured in the centre-of-mass frame. In the case of high energy collisions that we consider here, $|\vec{\mathbf{p}}| \approx \sqrt{s}/2$. Thus the unitarity constraint effectively sets an upper bound on the $2 \to 2$ cross-section and, consequently, on the associated coupling constants.

Indeed, the matrix element of a $2 \to 2$ scattering process can be decomposed in partial wave components as

$$\mathcal{M}(s, \theta) = \sum_l (2l + 1) P_l(\cos\theta)\, a_l(s) \tag{2.45}$$

so that the $2 \to 2$ cross section in the high energy limit reads

$$\sigma = \int d\Omega\, \frac{|\mathcal{M}|^2}{64\pi^2 s} = \frac{1}{16\pi\, s} \sum_l (2l + 1)|a_l(s)|^2, \tag{2.46}$$

where we have used the orthogonality of the Legendre Polynomials,

$$\int_0^\pi \sin\theta\, P_l(\cos\theta)\, P_n(\cos\theta) d\theta = \frac{2}{2l + 1}\delta_{ln}. \tag{2.47}$$

From eq. (2.44) together with $\sigma \leq \sum_n \sigma_{2\to n}$ (the total cross section is greater than or at least equal to the $2 \to 2$ cross section) one then obtains [158, 159]

$$\begin{aligned} 16\pi\, \mathrm{Im}(a_l) \geq |a_l|^2 = \mathrm{Re}(a_l)^2 + \mathrm{Im}(a_l)^2 \Rightarrow \\ \mathrm{Re}(a_l)^2 + [\mathrm{Im}(a_l) - 8\pi]^2 = (8\pi)^2 \Rightarrow \\ |\mathrm{Re}(a_l)| < 8\pi \;\forall\; l \in \mathbb{N}. \end{aligned} \tag{2.48}$$

[14] Note that there is no dependence on the azimuthal angle ϕ in a $2 \to 2$ scattering.

Unitarity of the model is then ensured by computing the matrix elements of all possible $2 \to 2$ scattering processes and imposing that its largest eigenvalue be smaller than the bound in eq. (2.48). The fact that unitarity can be a problem only in high energetic scatterings allows us to concentrate on this case only, simplifying the analysis considerably. Indeed, this assumption has already been used in writing $|\vec{\mathbf{p}}| \approx \sqrt{s}/2$ in eq. (2.44) as well as in writing the differential cross section in the simple form of eq. (2.46). Furthermore, in this limit:

- the s-wave amplitudes dominate the scattering process, so we only need to evaluate the bound on a_0;
- quartic interactions (with couplings Q_{ijkl}) dominate over trilinears, so $|a_0| = |Q_{ijkl}|$;
- the bounds coming from scattering of transverse modes of gauge bosons are well below those from their longitudinal components, so we can focus on the latter only [160];
- the equivalence theorem [160, 161, 162] states that the vectorial longitudinal components scatter as the Goldstone bosons from which they originally sprang.

In summary, the unitarity analysis can be done by focusing solely on the scalar sector and results in bounds on the quartic couplings of the scalar potential.

Unitarity constraints in 2HDMs have been worked out in refs. [159, 163, 164]. Since for the unitarity analysis only the eigenvalues of the S-matrix are relevant, and since these are unmodified by a change of basis, it does not matter whether we compute the matrix elements using the flavour or the physical eigenstates. We choose the former for simplicity, as in this case they will be very simple combinations of the λ_{1-5}. Note, furthermore, that for high-energetic scatterings the hypercharge Y and weak isospin σ are conserved, which, together with the $\mathbb{Z}_2$ symmetry, simplifies the S-matrix to a block diagonal form, each block no larger than a 2×2 matrix. The eigenvalues of the scalar-scalar scattering matrices can then be written in a closed analytic form as

$$
\begin{aligned}
& & \Lambda^{\text{odd}}_{20} &= \lambda_3 - \lambda_4, \\
\Lambda^{\text{even}}_{21\pm} &= \frac{1}{2}\left(\lambda_1 + \lambda_2 \pm \sqrt{(\lambda_1 - \lambda_2)^2 + 4|\lambda_5|^2}\right), & \Lambda^{\text{odd}}_{21} &= \lambda_3 + \lambda_4, \\
\Lambda^{\text{even}}_{01\pm} &= \frac{1}{2}\left(\lambda_1 + \lambda_2 \pm \sqrt{(\lambda_1 - \lambda_2)^2 + 4\lambda_4^2}\right), & \Lambda^{\text{odd}}_{01\pm} &= \lambda_3 \pm |\lambda_5|, \\
\Lambda^{\text{even}}_{00\pm} &= \frac{1}{2}\left[3(\lambda_1 + \lambda_2) \pm \sqrt{9(\lambda_1 - \lambda_2)^2 + 4(2\lambda_3 + \lambda_4)^2}\right], & \Lambda^{\text{odd}}_{00\pm} &= \lambda_3 + 2\lambda_4 \pm 3|\lambda_5|,
\end{aligned}
$$

and the constraints then read

$$
\max\left(|\Lambda^{\mathbb{Z}_2}_{Y\sigma\pm}|\right) < 8\pi. \tag{2.49}
$$

2.4.3 Electroweak precision observables

The existence of additional scalar particles running in the loops causes the gauge bosons' two-point functions to receive corrections relative to their SM values, so-called "oblique" corrections. As a consequence, some combinations of gauge boson masses and their couplings, whose experimental values are known to agree with the SM prediction to great accuracy, get extra contributions from the new physics introduced. It then becomes a challenge for the model to predict a deviation that remains within the precision of the experimental measurement. The best example is provided by the ρ parameter,

$$\rho = \frac{m_W^2}{m_Z^2 \cos^2\theta_W},$$

which is intimately related to the electroweak symmetry breaking sector of the theory, and whose value is known to agree with the SM prediction to better than 0.4% at 2σ [165]. Because they contain only scalar *doublets*, 2HDMs predict $\rho = 1$ at tree-level (as in the SM). At loop level, however, there are extra contributions with respect to the SM ones[15] [166, 167], and one has

$$\begin{aligned}\Delta\rho^{\text{2HDM}} = \frac{1}{32\pi^2 v^2}\Big[&F_{H^\pm,A^0} + \sin^2(\beta-\alpha)(F_{H^\pm,h^0} - F_{A^0,h^0}) \\ &+ \cos^2(\beta-\alpha)\left(F_{H^\pm,H^0} - F_{A^0,H^0}\right) \\ &+ 3\sin^2(\beta-\alpha)\left(F_{Z,H^0} - F_{Z,h^0} - F_{W,H^0} + F_{W,h^0}\right)\Big],\end{aligned} \tag{2.50}$$

with

$$F_{x,y} = \frac{m_x^2 + m_y^2}{2} - \frac{m_x^2\, m_y^2}{m_x^2 - m_y^2}\ln\left(\frac{m_x^2}{m_y^2}\right). \tag{2.51}$$

The condition that $\rho \sim \rho_{SM} \approx 1$ is satisfied only if there is an approximate mass degeneracy between the charged and one of the neutral scalars, which is related to the limit in which custodial symmetry is recovered [168]. Indeed, it is easy to see, for instance, that $m_{A^0} = m_{H^\pm}$ satisfies the constraint trivially when $m_Z = m_W$.

The ρ parameter is only an instance of observables that receive oblique corrections in 2HDMs. For a general extension of the SM preserving the $SU(2)_L \times U(1)_Y$ gauge structure, these corrections can be parametrized by the Peskin-Takeuchi parameters S, T and U [169] and some higher-order extensions of them [170, 171]. Nevertheless it turns out that for 2HDMs only $\Delta\rho \equiv \rho - 1 \equiv \alpha_{EM} T$ is relevant, since the experimental bounds on the remaining parameters are hardly violated [168, 172].

[15] In the SM, custodial symmetry is violated by $U(1)_Y$ interactions and Yukawa couplings, but is preserved by the scalar potential.

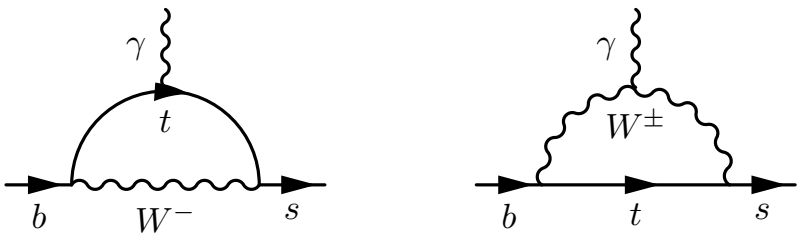

Figure 2.2: Typical diagrams contributing to $b \to s\gamma$ in the SM due to $W^\pm$ boson exchange.

Another important electroweak precision constraint, unrelated to the oblique parameters above, comes from $Z \to b\bar{b}$ decays [173, 101]. We checked explicitly that this constraint is milder than the one coming from $B^0 - \overline{B^0}$ mixing, which we will take into account next.

2.4.4 Flavour constraints

The impact of flavour constraints on 2HDMs has been extensively studied in ref. [174]. For models with a $\mathbb{Z}_2$ symmetry and with $\tan\beta \lesssim 10$, the only relevant bounds come from $B^0 - \overline{B^0}$ mixing and $b \to s\gamma$ decays. Since these observables do not involve leptons in any manner, they are equivalent in Types I and X (resp. Types II and Y).

The $b \to s\gamma$ decay is an FCNC process which, because of the $\mathbb{Z}_2$ symmetry, gets its leading order contribution only at loop level. This is also what happens in the SM, with the W boson mediating the b to s transition, as shown in fig. 2.2. In this case it can be shown that, to NNLO order, the predicted branching ratio agrees well with the experimental measurement (within theoretical and experimental uncertainties) [175]. In 2HDM there are additional diagrams obtained by replacing the $W^\pm$ by a $H^\pm$ in fig. 2.2 (with vertices $b \to tH^\pm$ and $tH^\pm \to s$), and we must then ensure that the full radiative contributions are still within the precision of the experiments.

The only 2HDM parameters involved in this decay process are $m_{H^\pm}$ and $\tan\beta$ (from the couplings of $H^\pm$ to fermions). The constraints are of course milder for increasing $m_{H^\pm}$. As for the dependence on $\tan\beta$, for Types I/X both vertices above mentioned enter with a factor $1/\tan\beta$, so the 2HDM contribution to the amplitude scales with $(\tan\beta)^{-2}$ and the constraint is milder as $\tan\beta$ grows. In Types II/Y, where one vertex contributes with $\tan\beta$ and the other with $1/\tan\beta$, the end result is essentially $\tan\beta$-independent.

A proper calculation and numerical implementation of the relevant observable, $\mathrm{BR}(\overline{B} \to X_s\gamma)$, is quite involved and time consuming [176, 177, 178, 179]. Since the resulting exclusion lines have already been computed by other studies, we borrow their results directly [174, 179]. Note that for Types II/Y a recent study to NNLO constrains [179]

$$m_{H^+} \gtrsim 380 \text{ GeV} \qquad \text{at } 95\% \text{ C.L.} \tag{2.52}$$

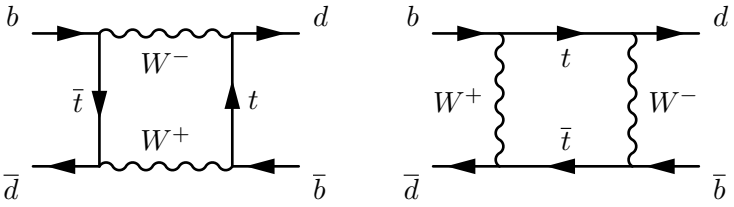

Figure 2.3: Diagrams of dominant contributions to $B^0 - \overline{B^0}$ mixing in the SM. Additional contributions from the 2HDM are obtained by exchanging one or both W's by a charged scalar $H^\pm$.

The dominant SM contributions to $B^0 - \overline{B^0}$ mixing are shown in fig. 2.3. Additional contributions from 2HDMs come from exchange of charged scalars $H^\pm$ in place of one or both W's in the diagrams shown. This constraint is type-independent, since only the top Yukawa coupling enters the computation. The result can be found in refs. [180, 174].

The exclusion regions from these flavour constraints in Types I/X and Types II/Y are shown in fig. 2.4.

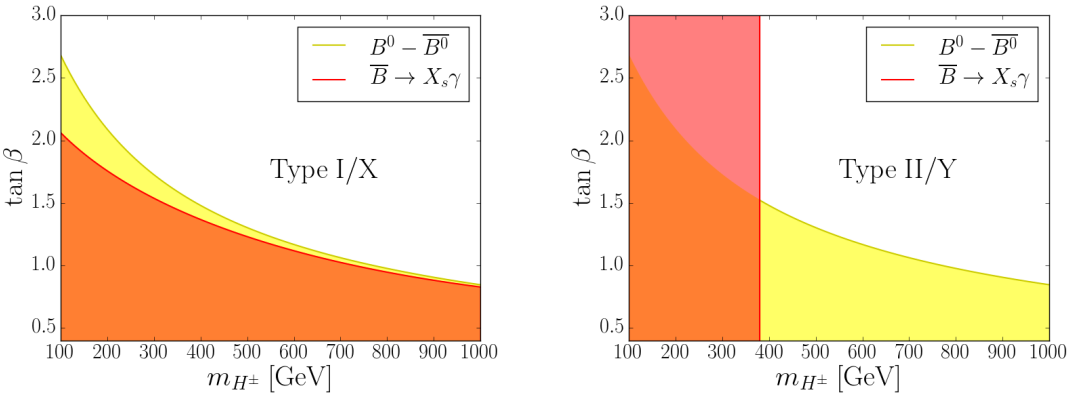

Figure 2.4: Exclusion regions from $\overline{B} \to X_s\gamma$ (red) and $B^0 - \overline{B^0}$ mixing (yellow) in Types I/X (left) and Types II/Y (right).

2.4.5 Collider constraints

Direct searches

Direct searches for scalar resonances at LEP, Tevatron and LHC also impose important bounds on the model parameters. Whenever a search finds no resonances, the data can be used to set 95% C.L. upper bounds on the cross section of the designated search channel, and the model is then excluded (to this confidence level) if its prediction lies above this experimental limit,

$$R_\sigma \equiv \frac{\sigma_{95\%\text{ C.L.}}}{\sigma_{\text{model}}} < 1. \tag{2.53}$$

Due to the relatively low energy reach at LEP, searches for neutral scalars in these

experiments have focused mainly on $H_i \to q\bar{q}$ and $H_i \to \tau\tau$ [181], which are the dominant decay modes for $m_{H_i} \lesssim 2m_W$. In hadron colliders, on the other hand, the cleanest channels are diboson (WW, ZZ) and diphoton decays [182, 183, 184, 185, 186, 187, 188], followed by $Z\gamma$ [189, 190] and, to a lesser extent, $\tau\tau$ [191, 192, 193, 194, 195]. Indeed, it is interesting to note that the branching ratio of scalars into two photons is typically small, $\mathcal{O}(10^{-3})$, due to its being a loop induced effect, but a $\gamma\gamma$ signal is so clear at the LHC that this has actually been one of the main channels leading to the Higgs boson observation in 2012 and to accurate measurements of its properties [196, 197, 198]. The very opposite occurs with the $b\bar{b}$ final state: despite this being the dominant decay in the SM for $m_h \lesssim 2m_W$ and also in the 2HDM quite generally, a search in this channel at a hadron collider is extremely disfavoured due to the overwhelming QCD background. The only possibility of seeing this decay mode in such machines is to focus on associated production of the Higgs with other particles (e.g. Higgs-strahlung) [199, 200, 201], whose tagging can be used to distinguish the signal from the background. Recently, a search has also been performed in the vector boson fusion (VBF) channel, with the two outgoing quarks tagged for the mentioned differentiation, and the results show agreement with the SM prediction [202].

Other channels which are absent in the SM have also been scrutinized, mainly motivated by supersymmetric scenarios, e.g. $H_i \to$ invisibles [203, 204, 205, 206], $H^0 \to h^0 h^0$ and $A^0 \to Zh^0$ (with h^0 behaving as the SM Higgs) [207, 208, 209].

It is also worth mentioning that direct searches for a charged Higgs boson at LEP have placed a 95% C.L. model-independent bound

$$m_{H^\pm} > 79.3 \text{ GeV},$$

assuming only that $H^\pm$ decays exclusively into $c\bar{s}$ and $\tau^+\nu_\tau$, which is realistic in the 2HDM for this mass range [210, 211, 212, 213]. Additional searches have been performed at Tevatron and LHC via $t \to H^+ b$ [214, 215, 216, 217] and $H^+ \to t\bar{b}$ [218, 219], resulting in $\tan\beta$-dependent bounds.

Computing the model predictions

In order to apply these constraints to the 2HDM parameters we need to compute the predicted cross section for the various searched events mediated by a scalar S, $\sigma_{i\to S\to f}$. For this purpose we restrict ourselves to the vastly simplifying *narrow width approximation*, valid when the total decay rate of S is small compared to its mass, $\Gamma_S \ll m_S$. In this case interference effects can be neglected and we can write $\sigma_{i\to S\to f} = \sigma_S \times \text{BR}(S \to f)$, with

σ_S the scalar's production cross section and $\mathrm{BR}(S \to f)$ its branching ratio into the final products of that specific event. In our case, narrow width will mean $\Gamma_S \lesssim 0.2\, m_S$.

At an e^+e^- collider such as LEP the main production processes of neutral scalars are Higgs-strahlung, VBF and pair production, shown in fig. 2.5. Note that production in pairs is the only way of obtaining a charged Higgs at LEP (with $V = W^\pm$ in the diagram) and also a pseudoscalar (in association with a CP-even scalar), since A^0 does not couple to gauge bosons in a CP-conserving scenario. The relevant couplings in this case (normalized to a reference value $g/2\cos\theta_W$) are

$$g_{hAZ} = \sin(\beta - \alpha), \qquad g_{HAZ} = \cos(\beta - \alpha). \tag{2.54}$$

But since LEP had a maximum energy reach of $\sqrt{s} = 209$ GeV, pair production would only be possible if the scalars were moderately light, $m_S \lesssim 100$ GeV, a situation not contemplated in the present work.

On the other hand the coupling of the CP-even states to gauge bosons (normalized to the SM values) are

$$g_{hVV} = \cos(\beta - \alpha), \qquad g_{HVV} = \sin(\beta - \alpha), \tag{2.55}$$

so LEP constraints on H^0 are mild for $\alpha \approx \beta$.

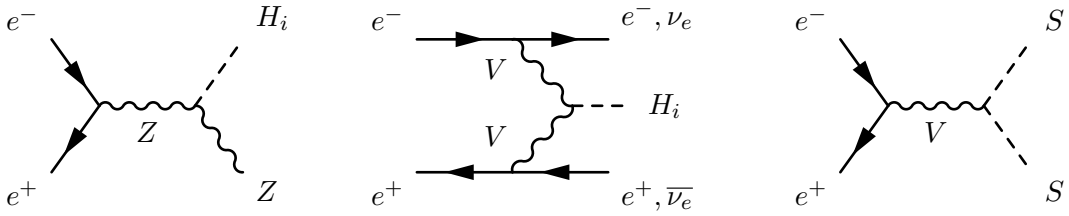

Figure 2.5: Neutral scalar production processes at LEP. (Left) Higgs-strahlung. (Centre) Vector Boson Fusion. (Right) Pair production.

At a hadron collider, such as Tevatron and LHC, there are two other important production processes, namely gluon-gluon fusion and top fusion, whose diagrams are shown in fig 2.6 (left and right, respectively). Higgs-strahlung, VBF and pair production are also possible, with diagrams analogous to the ones shown in fig. 2.5, but with quarks instead of leptons in the external legs, and with W's also mediating associated production. Note that, in a hadron collider, even in the alignment limit all neutral scalars are produced via gluon-gluon and top fusion.

Whenever the process has an analog in the SM, we compute its cross section by simply rescaling the SM values with the appropriate effective coupling (see ref. [220] for a review

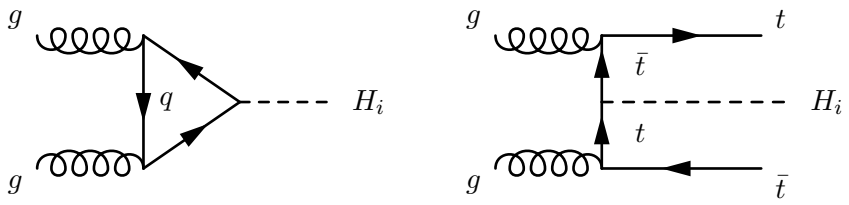

Figure 2.6: Additional production processes of neutral scalars at hadron colliders such as Tevatron and LHC. (Left) Gluon fusion. (Right) Top fusion.

on the state-of-the-art computation of SM cross sections). Thus, for Higgs-strahlung, VBF and top fusion we have

$$\sigma(H_i V) \equiv g^2_{H_i VV}\, \sigma_{\rm SM}(hV), \tag{2.56}$$

$$\sigma(\text{VBF}) \equiv g^2_{H_i VV}\, \sigma_{\rm SM}(\text{VBF}), \tag{2.57}$$

$$\sigma(t\bar{t}H_i) \equiv (y^2_{u,i} + \widetilde{y}^2_{u,i})\, \sigma_{\rm SM}(t\bar{t}h), \tag{2.58}$$

with g_{H_iVV} given in eq. (2.55), and the top couplings $y_{u,i}$ and $\widetilde{y}_{u,i}$ shown in Table 2.2.

For pair production, which is not present in the SM, the reference cross section is the SM value for Higgs-strahlung off a vector boson, multiplied by an appropriate phase space factor to account for the two spin zero particles in the final state [221].

The gluon-gluon fusion channel is more involved due to its being a loop process already at leading order. Our approach in this case is to compute the effective ggH_i vertex by solving the quark loop and obtaining the corresponding form factor [221, 222]. This means that the loop is effectively "shrunk" to a point and the same rescaling argument is applicable.

Because $m_t \gg m_b$, the top loop is typically the dominant contribution to this process. The only possible exception occurs in Types II/Y, where the top Yukawa coupling is suppressed by a factor of $\tan\beta$ whereas the bottom one is enhanced by the same factor. This means that, if $\tan\beta \gg 1$, the large bottom Yukawa can compensate for the small bottom mass (which leads to a suppression in the loop form factor), and the bottom loop may become important. However, since we will concentrate on $\tan\beta \lesssim 10$, only the top loop will be considered in what follows.

For the CP-even states the form factor is the same as in the SM and all diagrams scale with the top coupling in the same way (including those of higher order corrections), so that the cross section in this case is

$$\sigma(ggH_i) \equiv y^2_{u,i}\, \sigma_{\rm SM}(ggh), \qquad H_i = h^0, H^0. \tag{2.59}$$

For the pseudoscalar we use the fact that the form factors also enter in the $H_i \to gg$ decay width to define

$$\sigma(ggA^0) \equiv \frac{\Gamma(A^0 \to gg)}{\Gamma_{\rm SM}(h \to gg)}\, \sigma_{\rm SM}(ggh). \tag{2.60}$$

A caveat in this definition is that, although accurate at leading order, at NLO QCD some diagrams are different for the decay and the production processes, most notably those involving emission of additional soft gluons in the final state [221]. However, using the public code SusHi 1.5.0 [223] we checked that our definitions for the gluon-gluon fusion cross section deviate by no more than 8% from the full NNLO QCD + NLO EW computation.

We turn now to the decay widths, which are calculated as following (see Appendix B):

- for decays into fermions, $H_i \to f\bar{f}$ and $H^\pm \to f\bar{f}'$, we include up to $\mathcal{O}(\alpha_s^2)$ QCD corrections [220, 221] as well as the off-shell decay $H^+ \to t^*\bar{b} \to W^+ b\bar{b}$ [224]. Most QCD corrections are taken into account if we use the running quark mass $m_q(m_{H_i})$ in the computation of the width, rather than the pole or the $\overline{\rm MS}$ mass $m_q(m_q)$. We therefore compute the running of α_s [225] and of quark masses [225, 226] (including matching conditions) to NNNLO[16];

- decays into two off-shell massive gauge bosons, $H_i \to W^*W^*$ and $H_i \to Z^*Z^*$, are calculated following ref. [227];

- $H_i \to \gamma\gamma$ [228] and $H_i \to Z\gamma$ [221, 229] are computed at leading order (i.e. at 1-loop);

- for a CP-even decaying into two gluons, we simply rescale the tabulated SM width [230] by the top coupling, $y_{u,i}^2$. On the other hand $A^0 \to gg$ is computed including NLO QCD corrections for the simplest case of heavy top, $m_{A^0} \ll 2m_t$ [231, 232];

- finally, decays into other scalars via $H_i \to H_j V^*$, $H^+ \to H_j W^{+*}$ and $H_i \to H_j H_k$ are included as in refs. [227, 233].

We cross-checked our computations with the codes HDECAY 6.20 [234] and 2HDMC 1.6.4 [235], finding excellent agreement. Even in the potentially worrisome case of $A^0 \to gg$ for heavy pseudoscalars, where our assumption of heavy top breaks down, our result deviates less than 6% from the full computation performed in HDECAY. While it is true that this channel is not particularly important for experimental searches — since the two gluons in the final state cannot be disentangled from the huge QCD background produced in hadron

[16] That is, we consider the 4-loop RGE and 3-loop matching conditions.

colliders, and because its impact in the total width (and therefore in the branching ratios) is negligible —, it is nevertheless important that we have this degree of accuracy in the computation of its width, as it enters in our definition of the pseudoscalar's production cross-section in eq. (2.60).

Finally, if $m_{H^\pm} < m_t$ the charged scalar can be produced via top decay $t \to H^+ b$, whose width we compute to leading order following refs. [221, 236].

With these theoretical predictions we can compute the ratio R_σ in eq. (2.53) for the various searches performed at LEP, Tevatron and LHC. For this we use the code HiggsBounds 4.2.0 [237, 238], which contains tabulated values of $\sigma_{95\%\text{ C.L.}}$ for a long list of searches, so that it takes the model's predictions for production cross sections and branching ratios as inputs, and returns the minimal R_σ as well as the most sensitive channel. The model is excluded if $\min\{R_\sigma\} < 1$.

The measured properties of the observed 125 GeV scalar resonance

Further constraints are imposed on the model by the observation of a neutral scalar resonance at LHC with mass $m_h \approx 125$ GeV [40, 41, 239, 240, 241], as it forces one of the H_i to have properties matching those of the observed particle. Important among these are the so-called signal strength modifiers for the various search channels, defined simply as

$$\mu_f \equiv \frac{\sigma(pp \to H_i \to f)}{\sigma_{\text{SM}}(pp \to h \to f)}. \tag{2.61}$$

So far the measurements agree with the expected from a SM Higgs boson, which means that $\mu_f \approx 1$ within experimental errors for most channels [242, 243, 244].

In this work we will assume that the discovered resonance is the lightest among the two CP-even states in the 2HDM, thus setting $m_{h^0} = 125$ GeV. The SM-like behaviour of the observed state will then impose rather stringent limits on $\beta - \alpha$ depending also on the other parameters of the model, particularly on $\tan\beta$. This is because the coupling of h^0 to fermions can be written as

$$y_{u,h^0} = \frac{\sin\alpha}{\sin\beta} = \cos(\beta-\alpha) - \frac{\sin(\beta-\alpha)}{\tan\beta}, \tag{2.62}$$

$$y_{e,h^0} = \begin{cases} y_{u,h^0}, & \text{Type I/Y} \\ \cos(\beta-\alpha) + \tan\beta\,\sin(\beta-\alpha), & \text{Type II/X} \end{cases} \tag{2.63}$$

with the couplings to down-type quarks pairing with either of the above according to Table 2.1. For small values of $\tan\beta$ even a slight deviation from alignment will induce a large deviation in the top coupling from its SM value, with a consequent enhancement/suppression in the gluon-gluon and top fusion production cross section, thus affect-

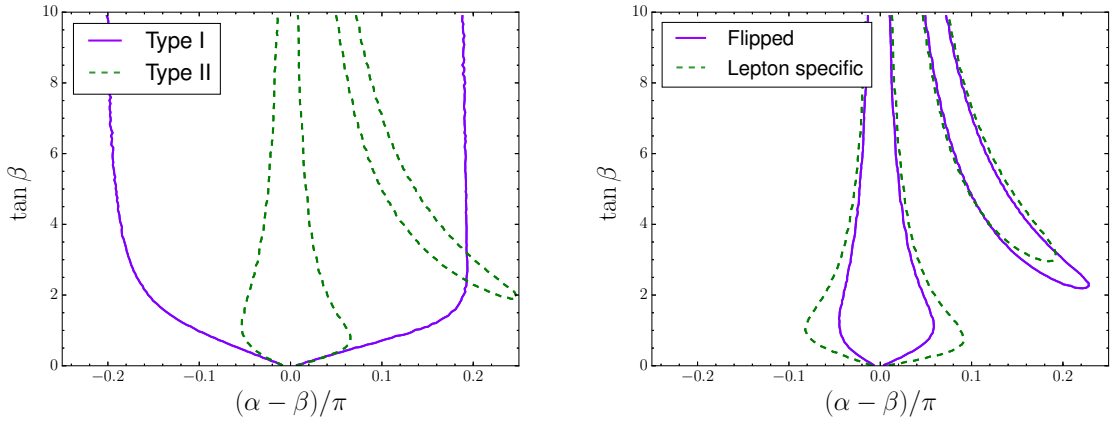

Figure 2.7: Allowed regions for $\alpha - \beta$ and $\tan\beta$ taking into account the properties of the discovered 125 GeV Higgs.

ing the signal strength modifiers in all channels which have not been tagged for VBF or Higgs-strahlung production. All models are therefore tightly constrained in the region of very low $\tan\beta$. Conversely, for $\tan\beta \gg 1$, Type I tends to be less constrained (and the constraint becomes increasingly less $\tan\beta$-dependent), whereas Types II, X (Lepton Specific) and Y (Flipped) are strongly disfavoured away from alignment due to large deviations in the couplings to $\tau\tau$ and $b\bar{b}$ final states. The contours delimiting the allowed regions are shown in fig. 2.7, which is in good agreement with the findings of refs. [103, 245]. The narrow disconnected allowed regions present in Types II, X and Y correspond to $\alpha \approx \beta - \pi$, where the fermionic couplings have SM-like absolute values but carry a flipped sign (see refs. [246, 247] for a phenomenological study of these scenarios).

Beyond the intricate dependence of the constrained regions with the model parameters, a quite general result enforced by the SM-likeness of the 125 GeV Higgs is that

$$|\beta - \alpha| \lesssim \frac{\pi}{4}. \tag{2.64}$$

This is because outside this domain the most SM-like scalar in the model is H^0, for which $m_{H^0} > m_{h^0} = 125$ GeV. An exception would be the case close to degeneracy, $m_{H^0} \approx m_{h^0}$, which we do not consider here.

We use HiggsSignals 1.3.2 [248] to test the compatibility of the model with the signal strength measurements. The input of the program are the same as for HiggsBounds, from which it performs a χ^2 analysis comparing the model's predictions for the mass and the signal strengths to the experimental data, returning the likelihood that one of the scalars H_i in the model will generate the local peak observed at $m_h \approx 125$ GeV. We consider the model to be excluded if the returned p-value is smaller than 5%.

Chapter 3

The phase transition

In a cold, nearly empty Universe, spontaneous symmetry breaking takes places because the energy of the Higgs self-interactions is minimized as the Higgs fields acquire non-vanishing VEVs. But in the early Universe, when the scalar fields are surrounded by a plasma of particles, the net free-energy of the entire system has contributions not only due to Higgs' self-interactions but also due to interactions with this thermal bath. That is to say, the effective potential becomes

$$V_{\text{eff}}^{T} = V_{\text{tree}} + V_1 + V_T \equiv V_0 + V_T, \tag{3.1}$$

with the zero-temperature part V_0 given in eq. (2.38) and a thermal contribution V_T to be computed in section 3.1 below.

The net free-energy density of the scalar fields and the plasma at a given temperature T in the broken phase is then

$$\begin{aligned} \mathcal{F}_T &\equiv V_{\text{eff}}^{T}(\text{broken}) - V_{\text{eff}}^{T}(\text{sym}) \\ &= \mathcal{F}_0 + V_T(\text{broken}) - V_T(\text{sym}) \\ &\equiv \Delta u - T\Delta s, \end{aligned} \tag{3.2}$$

where we have used the known thermodynamical definition of free-energy density in terms of energy density u and entropy density s. The first contribution, $\Delta u \equiv \mathcal{F}_0 < 0$, is the fixed amount of energy density released by the scalar fields by breaking the symmetry. The latter part, on the other hand, is always positive and monotonically increasing with temperature, associated to the entropy change in the system as particles in the plasma acquire their masses. As these particles grow more numerous, eventually a critical temperature T_c is reached above which the maximum amount of energy available to be exchanged with the system's environment and thereby increase its entropy, given by $\mathcal{F}_0$, is not enough to compensate for the entropy decrease in the system itself. The thermal part of the effective

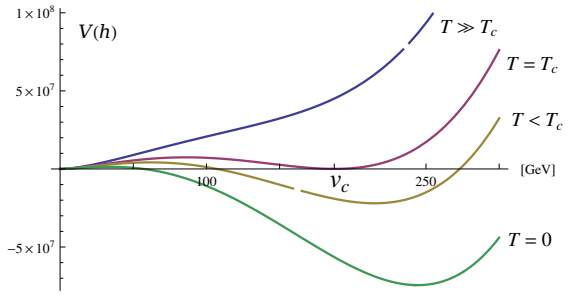

Figure 3.1: Thermal effective potential for various temperatures illustrating a strong first order phase transition.

potential then dominates, $\mathcal{F}_T > 0$, and electroweak symmetry breaking cannot proceed spontaneously.

This is illustrated in fig. 3.1, where the effective potential is shown for various temperatures in a fixed direction in field space. The symmetric phase is chosen as the reference point, so $V_{\text{eff}}^T(0) = 0$. In the next section we will discuss how the presence of a barrier between the symmetric and the broken phase, as shown in the figure, is indicative of a first order phase transition. Intuitively, this is because the barrier requires symmetry breaking to proceed via tunneling, with a certain tunneling probability per unit volume [25, 29, 249]. The electroweak symmetry may then be broken in some regions of space while being preserved in others, resulting in a highly inhomogeneous space filled with bubbles of different vacuum states.

3.1 Finite temperature 1-loop effective potential

In section 2.3 we have computed the 1-loop effective scalar potential at zero temperature, when the system propagates in a vacuum with no particles. This choice was implicitly made in eq. (2.33), where boundary conditions were imposed to calculate the Fourier expansion of the inverse propagator — namely, all the boundaries were implicitly set at infinity when all momentum components were taken to vary continuously. In particular we assumed that there is an infinite time interval separating the "incoming"/unevolved vacuum state $|0^-\rangle$ in eq. (2.20) from the "outgoing" one[1], $|0^+\rangle$, and that the dynamics is accurately described by the action S during all this period.

But when the system is surrounded by a thermal bath of particles these assumptions become rather unrealistic, since the propagation of the scalars is now affected by collisions

[1]The terminology of "ingoing" and "outgoing" states is not fully appropriate here, since we are not dealing with a scattering process.

with the plasma. In this case the appropriate starting point is the thermal partition function,

$$Z[J] \equiv \mathrm{Tr}(e^{-\beta H}) = \int \mathcal{D}\phi \, \exp\left(- \int_0^\beta d\tau \int d^3x \left[\mathcal{L}_E + J(x)\phi(x) \right] \right), \tag{3.3}$$

with $\beta^{-1} \equiv T$ the temperature of the system. Note that this can be obtained from the zero-temperature case in eq. (2.20) by performing the usual Wick rotation $t \to i\tau$ and limiting the "time" interval to $\tau \in [0, \beta)$. Furthermore, because the partition function is the trace of the thermal evolution operator $e^{-\beta H}$, the initial and final state of the system ought to be the same, which amounts to imposing periodic boundary conditions,

$$\phi(\tau, \boldsymbol{x}) = \phi(\tau + \beta, \boldsymbol{x}). \tag{3.4}$$

Thus there is an effective "compactification of time τ" in this interval $[0, \beta)$.

Consequently, the time-component of the 4-momentum is quantized as $k^0 = \omega_{n,\mathrm{bos}} \equiv 2\pi n/\beta$ for $n \in \mathbb{Z}$, which are called Matsubara modes, and

$$\int \frac{d^4k}{(2\pi)^4} \to \sum_{n=-\infty}^{\infty} \frac{1}{\beta} \int \frac{d^3k}{(2\pi)^3}. \tag{3.5}$$

As in the zero-temperature case, each gauge boson degree of freedom yields the same contribution as the scalars [138, 250]. For fermions, on the other hand, the boundary conditions analogous to eq. (3.4) are *anti*-periodic as usual, so the Matsubara modes are $\omega_{n,\mathrm{fer}} \equiv (2n+1)\pi/\beta$, $n \in \mathbb{Z}$.

From eqs. (2.33) and (3.5) the 1-loop contribution to the effective potential then becomes

$$V_1^T(\phi_{\mathrm{cl}}) = \sum_i n_i \sum_{n=-\infty}^{\infty} \frac{1}{2\beta} \int \frac{d^3k_E}{(2\pi)^3} \log\left(\omega_{n,i}^2 + k_E^2 + m_i^2(\phi_{\mathrm{cl}}) \right). \tag{3.6}$$

The sum over the Matsubara modes can actually be performed analytically [138, 250], yielding

$$V_1^T = \sum_i n_i \left[\int \frac{d^3k}{(2\pi)^3} \frac{E_i}{2} + \frac{T^4}{2\pi^2} \int_0^\infty x^2 \ln\left(1 \mp e^{-\sqrt{x^2 + m_i^2/T^2}} \right) dx \right] \equiv V_1 + V_T, \tag{3.7}$$

where $E_i^2 = \vec{k}^{\,2} + m_i^2$ and the sign inside the logarithm is $-$ for bosons and $+$ for fermions.

The first term is to be compared with the zero-temperature result obtained previously in eq. (2.35)[2]. The purely thermal part of the 1-loop contribution, V_T, has a low temperature expansion

$$V_T^{\mathrm{low}\ T} = - \sum_{i=B,F} |n_i| \, T^4 \left(\frac{m_i}{2\pi T} \right)^{3/2} e^{-\frac{m_i}{T}} \left(1 + \frac{15}{8} \frac{T}{m_i} \right), \tag{3.10}$$

[2]Indeed, we can rewrite the 1-loop zero-temperature contribution to the effective potential from

so that heavy particles are Boltzmann suppressed, as expected. On the other hand, at high-temperatures [138]

$$\begin{aligned} V_T^{\text{high } T} \approx \sum_B n_B \left(-\frac{\pi^2}{90} T^4 + \frac{1}{24} T^2 m_B^2 - \frac{1}{12\pi} T m_B^3 - \frac{m_B^4}{64\pi^2} \log \frac{m_B^2}{c_B T^2} \right) \\ + \sum_F |n_F| \left(-\frac{7\pi^2}{720} T^4 + \frac{1}{48} T^2 m_F^2 + \frac{m_F^4}{64\pi^2} \log \frac{m_F^2}{c_F T^2} \right), \end{aligned} \tag{3.11}$$

with $c_F = \pi^2 \exp\left(\frac{3}{2} - 2\gamma\right)$ ($\gamma \approx 0.577216$ is the Euler-Mascheroni constant) and $c_B = 16 c_F$. Note that the logarithmic terms partly cancel the ones from the zero-temperature effective potential in eq (2.38). As we have already argued in the discussion on the counter-terms, the terms $\sum_i m_i^2$ merely shift the bare mass parameters as

$$-\mu_i^2 \to -\mu_i^2 + \frac{T^2}{24} \left(6\lambda_i + 4\lambda_3 + 2\lambda_4 + \frac{9}{2} g^2 + \frac{3}{2} g'^2 + 6 y_t \, \delta_{i2} \right) \tag{3.12}$$

with $i \in \{1, 2\}$. Thus, at high enough temperatures, thermal corrections will cause these parameters to become positive, and the potential will have a single minimum at the origin: electroweak symmetry is restored.

3.1.1 Daisy resummation

Such a drastic change in the shape of the potential due to radiative corrections may be an indicative of a possible breakdown of the perturbative expansion. Indeed, let λ denote a general expansion parameter, such that the introduction of an extra vertex in a diagram corresponds to the addition of an extra power of this coupling in the perturbative series. Now, an extra loop adds not only an additional vertex but also an extra propagator, and in the thermal case the latter comes with an extra factor of T due to the Matsubara sums in eq. (3.5). Thus each additional loop comes with a factor of λT, so the relevant expansion parameter (apart from numerical factors) is actually $\lambda T / m_{\text{eff}}$, where m_{eff} is some relevant mass scale introduced for dimensional reasons [250, 251]. Clearly, the perturbative approach breaks down at high temperatures.

---

eq. (2.33) as

$$\begin{aligned} V_1 &= \sum_i \frac{n_i}{2} \int \frac{d^3k}{(2\pi)^3} \int \frac{dk^0}{2\pi} \log\left[(k^0)^2 + E_i^2 \right] \\ &= \sum_i \frac{n_i}{2} \int \frac{d^3k}{(2\pi)^3} \int \frac{dk^0}{2\pi} \int dE_i \frac{2E_i}{(k^0)^2 + E_i^2}, \end{aligned} \tag{3.8}$$

ignoring field-independent constants. The integral in k^0 can be performed by closing the contour in the complex plane and using Cauchy's integral theorem, yielding

$$V_1 = \sum_i n_i \int \frac{d^3k}{(2\pi)^3} \int d\left(\frac{E_i}{2} \right), \tag{3.9}$$

which is the first integral in eq. (3.7).

Related to this problem is the existence of an infrared divergence in eq. (3.6) for the $n = 0$ bosonic Matsubara mode. This zeroth mode is responsible for the cubic term in eq. (3.11), as can be seen by direct computation from eq. (3.6),

$$\frac{\partial V_1^{T,\,n=0}}{\partial m_B^2} = \frac{n_B}{2\beta}\int \frac{d^3k_E}{(2\pi)^3}\frac{1}{k_E^2 + m_B^2(\phi_{\rm cl})} = n_B\,T\left[\frac{\Lambda}{4\pi^2} - \frac{m_B}{8\pi} + \mathcal{O}\left(\frac{m_B^2}{\Lambda}\right)\right]. \tag{3.13}$$

Because the purely thermal contribution in eq. (3.7) is UV finite, there can be no temperature dependence in UV divergences. Therefore the Λ-dependent term above should be cancelled by contributions from the $n \neq 0$ modes, and we are left with

$$V_1^{T,\,n=0} = -\sum_B \frac{n_B}{12\pi} T m_B^3 \tag{3.14}$$

as promised. That this non-analytic cubic term is intimately related to infrared divergences is further emphasized by the fact that they do not arise from fermionic contributions, for which the lowest Matsubara mode is non-vanishing and the limit $m_F \to 0$ is therefore always well-defined.

As we go to higher orders in the perturbative expansion, other odd powers of m appear, but it can be shown that they are all related to the $n = 0$ mode of bosonic contributions. For instance, one trivial 2-loop contribution to the effective potential is

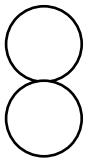

$$\sim \lambda\left(\sum_n T\int\frac{d^3k}{(2\pi)^3}\frac{1}{4\pi^2T^2n^2 + k^2 + m_B^2}\right)^2 = \lambda\left(\frac{1}{m_B}\frac{\partial V_1^T}{\partial m_B}\right)^2$$
$$\overset{T\gg m_B}{\approx} \lambda\left(\frac{T^2}{12} - \frac{Tm_B}{4\pi} + \ldots\right)^2 = \lambda\frac{T^4}{144} - \lambda\frac{T^3 m_B}{24\pi} + \ldots$$

with the same particle running in both loops and λ its quartic self-coupling. We see that the linear term arises from crossing terms with even and odd powers of m_B, i.e. from diagrams where one loop corresponds to a zero mode, the other to a non-zero (heavy) one [252]. Similarly, we can compute the contribution from a 3-loop diagram where one zero mode loop (larger loop in diagram) is surrounded by two loops of heavy modes (smaller loops),

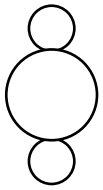

$$\sim \lambda^2\left(\frac{T^2}{12} + \ldots\right)^2\left(T\int\frac{d^3k}{(2\pi)^3}\frac{1}{(k^2 + m_B^2)^2}\right) = \lambda^2\frac{T^4}{144}\frac{T}{8\pi m_B} + \ldots,$$

which diverges as $m_B \to 0$. Note, furthermore, that each order in this expansion gets a contribution $\mathcal{O}(\lambda T^2/m_B^2)$, which becomes large in this IR limit.

We can therefore interpret these IR divergences as a side-effect of the breakdown of this naïve perturbative expansion, as we have already indicated previously. And, indeed, it

turns out that all these terms with odd powers of m_B can be resummed to a closed analytic form in what is called *ring* or *daisy resummation*, in such a way that the improved potential is IR finite. This is equivalent to resumming all diagrams of the form shown in fig. 3.2, with a loop of a zero Matsubara mode "dressed" by loops of heavy modes, resulting in a modified propagator for the former.

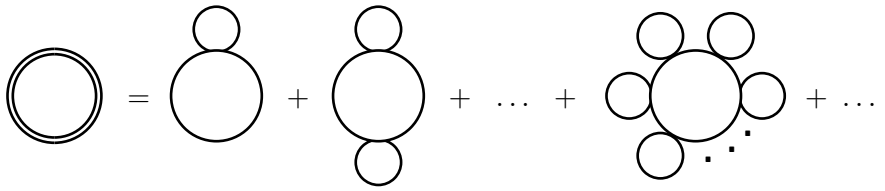

Figure 3.2: Resummation of daisy diagrams.

Note that this resummation is only relevant in the high-temperature (or, equivalently, low-mass) approximation, $m_B/T \ll 1$, since only then can the lightest zeroth mode be of any relevance. In this case the result is a thermal shift in the mass of the bosonic zero modes, effectively obtained by absorbing the leading term of the high-temperature expansion into the quadratic terms of the zero-temperature potential, in analogy to eq. (3.12) [250, 251, 252, 253, 254]. And since only zero modes are affected, the resummed mass should enter only in the cubic term, so that eq. (3.14) becomes

$$V_{1,\,\text{resummed}}^{T,\,n=0} = -\sum_B \frac{n_B}{12\pi} T \left(m_B^2 + \frac{T^2}{24}\mathcal{O}(\lambda) \right)^{3/2}. \tag{3.15}$$

The effect is $\mathcal{O}(\lambda^{3/2})$, which means it is dominant with respect to ordinary 2-loop contributions of $\mathcal{O}(\lambda^2)$ and *must* be taken into account in any perturbative expansion going beyond next-to-leading order.

More than that, these resummations also improve the 1-loop perturbative expansion, as the expansion parameter at high temperatures is now [255]

$$\frac{\lambda T}{\pi m_{\text{eff}}} \sim \frac{\lambda T}{\pi T\sqrt{\lambda}} \sim \frac{\sqrt{\lambda}}{\pi}, \tag{3.16}$$

where we have introduced the numerical factor π^{-1} coming from loop integrations [256, 257, 250]. Thus, as long as the expansion parameter is small, the 1-loop thermal potential is a good effective description of physics at high temperatures. The related problem of IR divergences is also tamed by this procedure, since the limit $m_B \to 0$ can now be taken even for zero modes, thus confirming that this problem was indeed merely a consequence of the breakdown of perturbation theory.

According to the prescription delineated above, resummations modify the 2HDM scalar

mass matrix as [84]

$$(M_T)_{ij} = \frac{\partial^2}{\partial\phi_i^*\partial\phi_j}\left(V_{\rm tree} + \frac{T^2}{24}\sum_B n_B m_B^2 + \frac{T^2}{48}\sum_F |n_F| m_F^2\right). \tag{3.17}$$

We do not consider resummation of the gauge bosons, as their effect is subdominant with respect to the scalar contributions [83]. Moreover, including them would cause the mass of gauge bosons' transverse components to increase with temperature, thus enhancing the non-convex cubic term in the effective potential and, consequently, the phase transition strength. By neglecting this effect the latter is therefore underestimated, so that our analysis is in fact conservative.

The problem of IR divergences will be most relevant for the Goldstone bosons, since they are massless at the minima of the thermal effective potential. But there is also another reason why the Goldstones must be handled with extra care, as in the zero temperature case. Namely, in a large portion of the field space their squared masses are negative, $m_G^2 < 0$, in which case the thermal part of the effective potential, V_T in eq. (3.7), is *not* well defined. First, the result has a non-vanishing imaginary part which is *not* related to instabilities, and in fact cannot have any physical significance since it is gauge-dependent [139, 140]. Moreover, the integrand has poles in the integration interval when $|m_G| > 2\pi T$.

Both these problems can also be solved with daisy resummations, since for high enough temperatures the thermal contributions will make all masses positive. But this requires that thermal masses be implemented directly in the integral for V_T in eq. (3.7), while strictly speaking these corrections affect only the zeroth Matsubara mode and should enter only in the cubic term, as in eq. (3.15). We choose nevertheless the former implementation for definiteness [84], checking that it will result in an overestimation of the phase transition strength by at most 15% as compared to the latter. The small impact of this choice on the final result is expected: resummations are only relevant at high temperatures, and their leading contributions to the phase transition strength comes from the cubic term, since resumming the quadratic term of the high temperature expansion merely shifts the potential by a field-independent quantity.

3.1.2 Nature of the phase transition and validity of 1-loop approximation

In computing the effective action in section 2.3 an important step was to take the Legendre transform of $W[J] \equiv -i\log Z[J]$ in order to exchange the dependence from the current J

to the field configuration $\phi_{\rm cl}$. Since a Legendre transform is a convex function, we would expect that the graph of the effective potential would not have any "bumps" or barriers. However, such barriers do eventually appear in the end result[3], as shown in fig. 3.1, and the effective potential then displays multiple local minima $\phi^i_{\rm cl}$. This can be seen as indicative of a breakdown of the initial hypothesis, stated in eq. (2.32), of homogeneity of the classical configuration. In these cases, the actual configuration of minimum energy would be a spatially-dependent combination of these $\phi^i_{\rm cl}$ which averages to $\phi_{\rm cl}$ [135], i.e. one in which space is filled with bubbles of different vacuum states. Therefore the existence of a barrier in the effective potential points to a first order phase transition proceeding via nucleation of vacuum bubbles at different points in space.

At this stage one could wonder whether the existence of the barrier is not a mere artifact of the 1-loop approximation which disappears upon the inclusion of higher-order terms in the perturbative expansion. This is known to happen in a pure $\lambda\phi^4$ theory, where the phase transition is actually of second order, in contradiction to the 1-loop prediction [251]. However, in non-abelian gauge theories, and especially in models with additional scalars such as the MSSM, both the 2-loop perturbative analysis as well as lattice computations typically yield a phase transition stronger than the 1-loop estimative [74, 251, 258, 259]. This means that our results are actually too conservative, and we could in fact relax the bound on the condition defining a strong phase transition in eq. (1.9). For peace of mind, we checked that our results are essentially unaffected if we use a modified criterion $(v_c/T_c)_{\rm relaxed} \gtrsim 0.7$. However, it should be noted that the computation leading to eq. (1.9) is far from being precise, and other bounds have sometimes been adopted in the literature, depending on the exact determination of the sphaleron rate and how much baryon washout is considered acceptable [260]. With all these uncertainties involved, we stick to $v_c/T_c \gtrsim 1.0$ as a good reference value for defining a strong phase transition for the purpose of the present work.

But there is a yet stronger argument supporting the validity of our results, namely that the thermal evolution of the system is to a large extent determined by the *zero-temperature* potential. More specifically, *the electroweak phase transition tends to be stronger as the zero-temperature vacuum energy* $|\mathcal{F}_0|$ *becomes smaller*. For as $|\mathcal{F}_0|$ decreases, so do the thermal corrections necessary to uplift the electroweak minimum until it becomes degenerate with (and eventually less energetically favoured than) the symmetric one. This means that the critical temperature T_c will tend to decrease with $|\mathcal{F}_0|$, while the critical VEV v_c

[3]For instance, in the high temperature expansion the cubic term is non-convex.

will approach the zero-temperature value $v \approx 246$ GeV, thus increasing the ratio v_c/T_c.

Because our zero-temperature loop expansion is well under control, we expect our results to be trustworthy at least at a qualitative level. For greater quantitative precision a computation of the full 2-loop effective potential would be required, which, although definitely worth pursuing, is beyond the scope of the present work.

We note in passing that, for the purpose of studying the phase transition, it is pointless to compute the effective potential to an accuracy better than three loops. This is because the masses of the gauge bosons vanish at the symmetric minimum, leading to a non-perturbative IR divergence which introduces uncertainties of the same order of magnitude as contributions from four-loop diagrams [251].

3.2 Parameter Scan

In order to understand how the nature of the electroweak phase transition depends on the parameters of the model, we perform a Monte-Carlo scan over an extensive region of the parameter space, imposing the constraints discussed in section 2.4. Vacuum stability is checked by directly searching for secondary minima of the effective potential up to a cutoff $\Lambda = 10$ TeV, rather than by using the RG improved potential, as detailed in section 2.4.1. We explicitly verified that the two methods are equivalent for about 99.4% of the points, our method being more constraining for the remaining 0.6%. We also impose a perturbativity bound on the scalar quartic couplings,

$$g_{ijkl} < 2\pi. \tag{3.18}$$

The constraint is imposed on the self-couplings of the *physical* fields rather than on the quartic couplings λ_{1-5} appearing in the potential, since it is the former that enters in contributions from higher-order diagrams. Note that we require perturbativity and unitarity at tree-level only. A more stringent constraint would be to require these couplings to remain small all the way up to the cutoff scale of the model [100, 105]. A rather thorough treatment of this issue in 2HDMs showed that the bound stated above generally implies perturbativity up to $\Lambda \approx 1.5$ TeV [94].

In our scan, the lightest CP-even Higgs h^0 is assumed to be the particle recently discovered at the LHC, so that $m_{h^0} = 125$ GeV. All other masses are required to lie below 1 TeV, in which case $B^0 - \overline{B^0}$ mixing puts a type-independent lower bound $\tan\beta > 0.8$ (cf. fig. 2.4). Furthermore, the fact that the observed scalar behaves much like the SM Higgs enforces $|\beta - \alpha| \leq \pi/4$, since outside this region it is the heavier H^0 who is more

SM-like. We therefore vary the physical parameters uniformly within the ranges

$$\begin{aligned} 0.8 \leq\ & \tan\beta \leq 10, \\ -\tfrac{\pi}{4} <\ & \beta - \alpha\ \leq \tfrac{\pi}{4}, \\ 0\ \text{GeV} \leq\ & M \leq 1\ \text{TeV}, \\ 100\ \text{GeV} \leq\ & m_{A^0},\ m_{H^\pm} \leq 1\ \text{TeV}, \\ 130\ \text{GeV} \leq\ & m_{H^0} \leq 1\ \text{TeV}. \end{aligned}$$

Eqs. (2.18) and (2.19) are then used to obtain the respective parameters of the potential.

A point passing all the constraints is said to be *physical*, and we proceed to evaluate the phase transition strength. This we do first by increasing the temperature of the plasma by small steps of $T_{\text{step}} = 1$ GeV and computing the free energy $\mathcal{F}_T$ of the broken phase, eq. (3.2), until $\mathcal{F}_T > 0$ or until we hit a maximum temperature $T_{\text{max}} = 300$ GeV beyond which only exotic (e.g. two-stepped) phase transitions could be strongly first order, which are not considered here. In the former case, the critical temperature is known to a precision of T_{step}. For greater accuracy, we then proceed to iterate the following process:

- define the interval $[T_{\text{below}}, T_{\text{above}}] \ni T_c$ and evaluate $\mathcal{F}_{T'}$ for some T' in it;
- if $\mathcal{F}_{T'} > 0$ (resp. $\mathcal{F}_{T'} < 0$), set $T_{\text{above}} = T'$ (resp. $T_{\text{below}} = T'$);
- iterate until T_c is found at which this vacuum energy difference is vanishing.

The strength of the phase transition is then defined as[4]

$$\xi = \frac{\sqrt{\langle \Phi_1^\dagger \Phi_1 + \Phi_2^\dagger \Phi_2 \rangle_c}}{T_c}\ .$$

Following the discussion leading to eq. (1.9), the phase transition is considered to be strong if $\xi > 1$, in order to ensure that the baryon asymmetry generated during the phase transition is not washed out afterwards. A point in the parameter space for which this condition is satisfied will be called a "strong PT point".

Impact of constraints

We have already mentioned in section 2.4.3 that only points with an approximate mass degeneracy between charged and neutral scalars are expected to pass the ρ parameter test,

[4]Note that this evaluation of the phase transition strength, even though widely used in the literature, does not yield a gauge invariant result [138, 260]. This is because the effective potential itself is gauge dependent, and so are the positions of its minima. The critical temperature T_c also inherits a gauge-dependence from the way it is computed, namely by evaluating the potential at the position of its minima calculated in a fixed gauge. An appropriate gauge invariant evaluation of the strength of the electroweak phase transition has been proposed in [260, 261]. However, the quantitative impact of the gauge choice has been shown to be small [262], and this issue can be overlooked without incurring in significant errors in the end result.

so that varying the masses of all scalars independently is bound to be a very inefficient scanning method. In fact, about 87% of points produced this way would be discarded due to electroweak precision constraints alone. A natural criterion to quantitatively estimate the size of the required degeneracy is to compare it to the electroweak scale, in which case we expect that $\Delta\rho \approx 0$ will force $m_{H^\pm}$ to lie in an interval of size $\mathcal{O}(v)$ around the mass of some other scalar. Indeed, among the points that do pass the electroweak precision tests, 92% satisfy this condition[5]. Thus, in an attempt to optimize the yield of physical points without biasing the scan towards a specific spectrum, we adopt the following procedure: if a randomly generated point does not pass the electroweak precision constraints, we pick a *random* neutral scalar s^0 and set the charged mass such that $|m_{H^\pm} - m_{s^0}| < v/2$; if the constraints are still not satisfied, the attempt is repeated for a second neutral scalar, and eventually for the third and last one, until the point is deemed physical or is discarded altogether. This improved method increases the efficiency of our scan by 550%, with approximately 72% of scanned points passing the electroweak precision constraints.

Perturbativity and unitarity bounds are responsible for excluding another 70.6% of the initial sample, which is also due to the random nature of the scan[6]. Indeed, we have already argued that the role of the quartic couplings is to regulate the splittings of the scalars' masses among themselves, as well as their deviation from their base values, given by the two dimensionful parameters v and $M \equiv \mu/\sqrt{\sin(2\beta)}$ — cf. eq. (2.19). Therefore these couplings will be naturally large in a scan where the values of μ, $\tan\beta$ and the masses are all chosen independently. In particular, note that close to alignment eq. (2.19) reads

$$\begin{aligned} \lambda_1 &\gtrsim \tan^2\beta\,\frac{m_{H^0}^2 - M^2}{v^2}, \\ \lambda_2 &\gtrsim \frac{1}{\tan^2\beta}\,\frac{m_{H^0}^2 - M^2}{v^2} \end{aligned} \tag{3.19}$$

so that small couplings requires $\tan\beta \sim 1$ and $m_{H^0} \sim M \sim v$.

The Yukawa couplings to down-type quarks and leptons enter only in flavour and collider constraints. Since flavour constraints cannot differentiate Types I and X (resp. II and Y), and because the collider constraints look similar for Types II, X and Y (cf. fig. 2.7), we will show here the results for Types I and II only, which are the most widely studied cases. In Type I the collider bounds are not very constraining, and we observe

[5] For the remaining 8% the mentioned interval of degeneracy has a size $\sim 2v$.

[6] Recently an alternative scanning method has been proposed to avoid this problem, where the scanned parameters are $m_{h^0}, m_{H^0}, \tan\beta$ and $\beta - \alpha$ together with 3 additional self-couplings [263]. This has been named the "hybrid basis". Having m_{h^0}, $\beta - \alpha$ and $\tan\beta$ as inputs enables us to tune these quantities towards the experimentally allowed regions, whereas using quartic couplings as inputs allows for better control over perturbativity.

Type	Total	EW precision	$\lambda_i < 2\pi$ Unitarity	Flavour Collider bounds	Stability	Strong PT
I	3.00×10^8 (100%)	2.16×10^8 (72.0%)	4.27×10^6 (1.4%)	9.48×10^5 (0.32%)	1.80×10^5 (0.06%)	1.45×10^4 (0.0048%)
II				2.78×10^5 (0.09%)	4.99×10^4 (0.017%)	4.18×10^3 (0.0014%)

Table 3.1: Number of points of the initial sample that survive after each step of tests.

that 22% of points surviving previous constraints pass also the phenomenological bounds. For Type II this rate is a meagre 6.5%, since the bounds are much tighter, as discussed in section 2.4.5.

Among the surviving points, about 21.6% pass the stability test. Hence, for Type I (resp. Type II) only 0.06% (resp. 0.017%) of the initial sample are *physical* points which are tested for phase transition. Nevetheless, because we scan over a total of 3×10^8 points, the number of physical points is still about 1.80×10^5 for Type I (resp. 4.99×10^4 for Type II).

Finally, approximately 8% of these physical points have a strong phase transition, so we end up with 1.45×10^4 points (resp. 4.18×10^3), which is large enough to provide significant statistics concerning the general behaviour of the electroweak phase transition with respect to the input parameters, as will be shown in Section 3.3.

Table 3.1 summarizes the discussion of this section.

3.3 Analysis and Results

The data will be presented as distributions of the number of physical and strong PT points as functions of some given parameters. Since these distributions will of course depend heavily on the priors of the scan, the actual information that interests us is encoded in their ratio,

$$\mathcal{P}_{\xi>1} \equiv \frac{\#\text{ strong PT points}}{\#\text{ physical points}}, \tag{3.20}$$

which indicates the probability of having a strong phase transition as a function of the parameters under consideration. This quantity will be plotted in solid lines. Still, the actual distribution of the counting rates is important, especially because $\mathcal{P}_{\xi>1}$ becomes a less precise indicative of that probability, the smaller the number of physical points in a given range.

We start by proving our previous statement that a small zero-temperature vacuum energy plays a crucial role in leading to a strong phase transition. For convenience, we

normalize the vacuum energy by the SM value at 1-loop, $|\mathcal{F}_0^{\rm SM}| \approx 1.26 \times 10^8$ GeV^4. Fig. 3.3 shows the distribution of physical points and the contours of the probability $\mathcal{P}_{\xi>1}$ as a function of the critical temperature and the vacuum energy. Clearly T_c decreases, and the probability of having a strong phase transition increases, as $|\mathcal{F}_0| \to 0$. Notice, furthermore, that the phase transition is *never* strong for low enough vacuum energies, namely $\mathcal{F}_0 \lesssim -1.081 \times |\mathcal{F}_0^{\rm SM}|$. This can be used as an effective criterion to judge the nature of the phase transition, as it does not require the evalutation of the thermal potential (but it is not used in what follows).

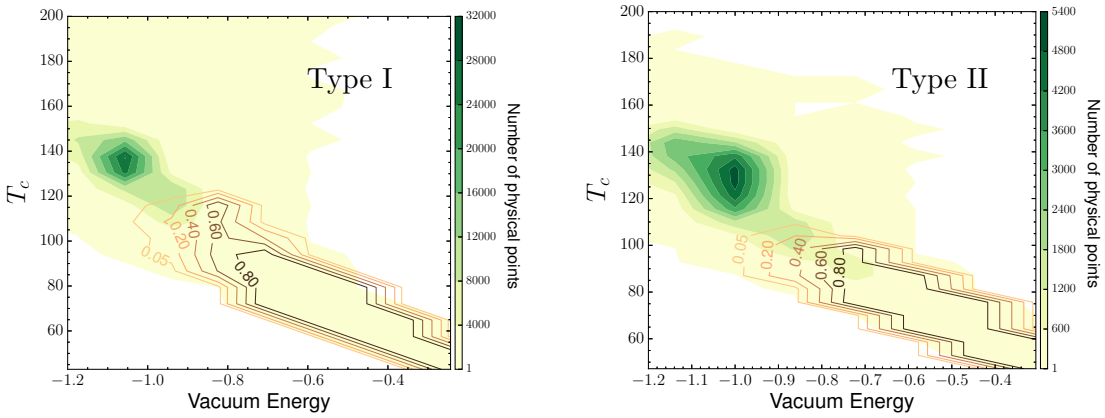

Figure 3.3: Distribution of physical points and $\mathcal{P}_{\xi>1}$ contours in the $(T_c, |\mathcal{F}_0|)$ plane.

At the risk of redundancy, we emphasize that the details of the temperature-dependent part of the effective potential are obviously important for the thermal evolution of the system. In fact, we can see already from fig. 3.3 that a few ($\approx 16.3\%$) points with a moderately uplifted vacuum energy, $\mathcal{F}_0 \gtrsim -0.8 \times |\mathcal{F}_0^{\rm SM}|$, still have a large critical temperature and therefore a weak phase transition. For these points either the masses of the extra scalars are too large, so their effect in the plasma is Boltzmann suppressed and their presence is barely felt unless the temperature is also large, or there is a large mixing between the light h^0 and a rather heavy H^0 which suppresses the phase transition strength, for reasons we will discuss in the following paragraphs. Yet it is certainly true that, the smaller $|\mathcal{F}_0|$ is, the more likely it is for the phase transition to be strong. Our claim is simply that the central features of our results can be understood in light of this general tendency.

The zero-temperature vacuum energy can be written as

$$\begin{aligned}\mathcal{F}_0 =& \mathcal{F}_0^{\rm SM} - \frac{v^2}{8}\sin^2(\beta-\alpha)\,(m_H^2 - m_h^2) \\ &+ \Delta\left[\sum_{s\neq h^0}\frac{m_s^4}{64\pi^2}\left(\log\frac{|m_s^2|}{v^2} - \frac{1}{2}\right)\right] + \text{counter terms},\end{aligned} \tag{3.21}$$

where $\Delta[\ldots]$ is to be understood as the difference of the Coleman-Weinberg terms evaluated at the electroweak minimum and at the origin[7]. The absolute value in the argument of the logarithm ensures we evaluate only the real part of the potential.

Since away from alignment the vacuum energy gets a negative tree-level contribution which increases with m_{H^0}, we expect a strong phase transition to favour the alignment limit, and the more so, the heavier H^0 is. This behaviour can also be explained by appealling to the fact that the phase transition is typically weaker when it is driven by heavier particles [34]. In the general non-aligned case, where both h^0 and H^0 "share" the VEV, the contribution of the lighter h^0 to the phase transition is suppressed by a factor of $\cos(\beta-\alpha)$ whereas that from the heavier H^0 grows with $\sin(\beta-\alpha)$. In contrast, the alignment limit is the optimal case, since it implies that only the light h^0 gets a VEV, thus behaving like the SM Higgs and being the sole driver of the phase transition.

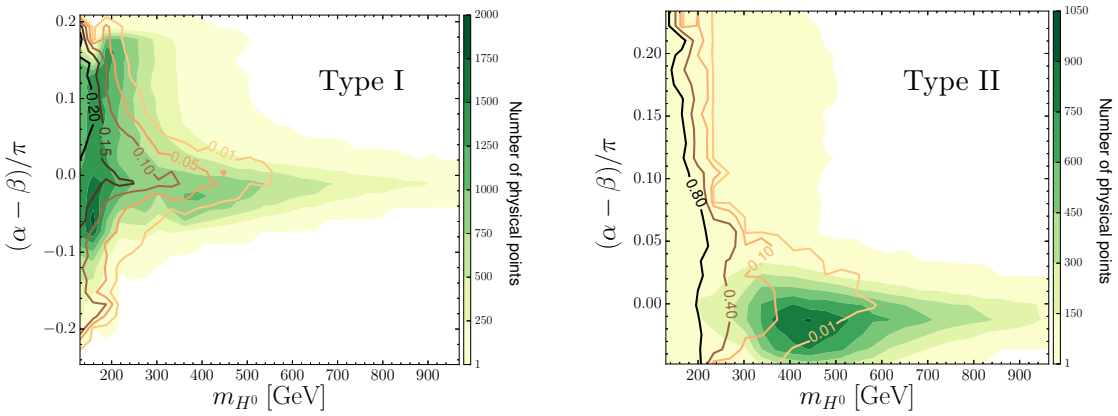

Figure 3.4: Distribution of physical points and $\mathcal{P}_{\xi>1}$ contours in the $(\alpha-\beta, m_{H^0})$ plane.

These expectations are confirmed by the data, as shown in fig. 3.4. In both model types the probability contours show that it becomes more difficult to have a strong phase transition as m_{H^0} grows, with alignment being increasingly more favoured. In fact, *all* points with a strong phase transition satisfy $m_{H^0} \lesssim 650$ GeV. This is not to say that a strong phase transition is excluded for heavier H^0, but that these cases are likely to be very fine tuned, thus escaping our random scan. Note also that the narrowing of the $\mathcal{P}_{\xi>1}$ band around alignment is not due merely to physicality constraints, as there are many points with $\alpha-\beta \gtrsim 0.05\pi$ and $m_{H^0} \gtrsim 300$ GeV which are physical but do not yield a strong phase transition. For Type II the lower bound $m_{H^\pm} > 380$ GeV from flavour constraints tends to shift the masses of the additional scalars towards rather large values,

[7]The masses of the scalars do *not* vanish at the origin in general.

which is why the physical points are mostly concentrated in the region $m_{H^0} \gtrsim 300$ GeV. The region $m_{H^0} \lesssim 200$ GeV is populated by only 2.3% of the total amount of physical points, but they are all favoured by a strong phase transition requirement, thus explaining the large $\mathcal{P}_{\xi>1}$ values there.

The overall scale M affects the vacuum energy via the loop correction term. Indeed, close to alignment the scalar masses in the symmetric phase are $m_s^2(\text{sym}) \approx M^2 - \frac{m_h^2}{2}$. This means that for $M \gg \max(m_{H^0}, m_{A^0}, m_{H^\pm})$ the "Δ-term" in eq. (3.21) is negative and the phase transition strength is suppressed. Moreover, if M *as well as* the masses of all additional scalars are large we approach the decoupling limit, recovering the SM prediction of a cross-over.

The converse of this argument then leads to a strong phase transition being favoured by a moderately light M, with at least some particles heavier than this scale. Alternatively, we could argue that a strong phase transition typically requires some couplings to be large, so that some large mass splittings are expected. But if $M \gg v$, then the large mass splittings will quickly lead to negative couplings and therefore to an unstable potential (in case the masses are smaller than M) or to a rapid blowup of the perturbativity bound.

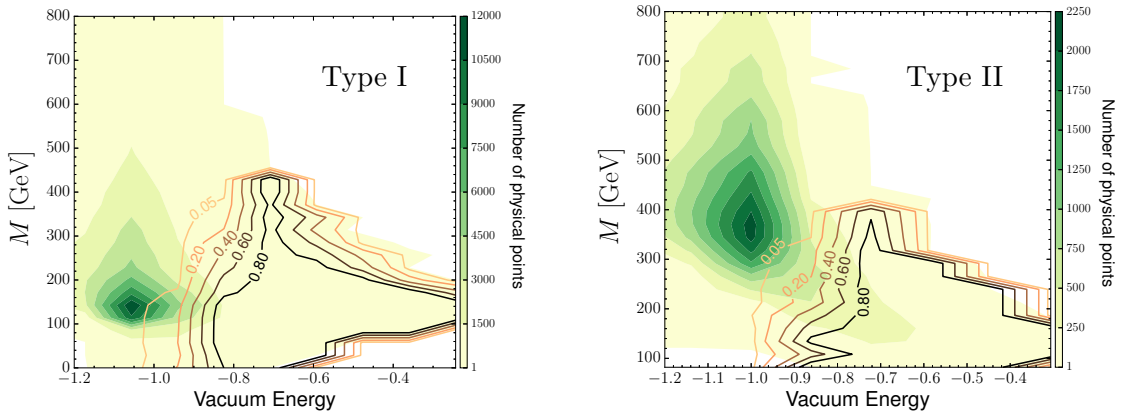

Figure 3.5: Distribution of physical points and $\mathcal{P}_{\xi>1}$ contours in the $(M, |\mathcal{F}_0|)$ plane.

The distribution of physical points and the probability contours are shown in fig. 3.5 varying with M and the vacuum energy. In Type II the physical points are peaked around slightly large mass values (compared to the electroweak scale), due to the lower bound on $m_{H^\pm}$ imposed by $\overline{B} \to X_s\gamma$ constraints. But in both types a moderate uplifting of the vacuum energy is achieved only if $M \lesssim 400$ GeV, with $M \to v$ as $\mathcal{F}_0 \to 0$.

Now, we have already seen in eq. (3.19) that, close to alignment, a large $m_{H^0} - M$ splitting is disfavoured by perturbativity constraints, whereas far from alignment a heavy

m_{H^0} suppresses the phase transition strength by pulling the vacuum energy towards more negative values already at tree-level. As for the charged scalar, electroweak precision observables forces it to pair with one of the neutral ones. This leaves A^0 as the only scalar whose mass is free to be large, and fig. 3.6 (top) confirms this as indeed the most favoured scenario, with virtually all (98%) strong PT points lying above the lower bound $m_{A^0} \gtrsim 300$ GeV. As for $H^\pm$ (fig. 3.6 (bottom)), in Type I we see two spikes corresponding to the cases when the charged scalar aligns with H^0 ($m_{H^\pm} \approx v$) or with the heavier A^0. Clearly the latter is the most favoured scenario for a strong phase transition, since the extra heavy scalar introduces yet another large coupling. Indeed, a rather heavy $m_{H^\pm} \approx m_{A^0} \gtrsim 300$ GeV is the only possibility for a significant vacuum energy uplift, $|\mathcal{F}_0| \lesssim 0.6 \times |\mathcal{F}_0^{\rm SM}|$.

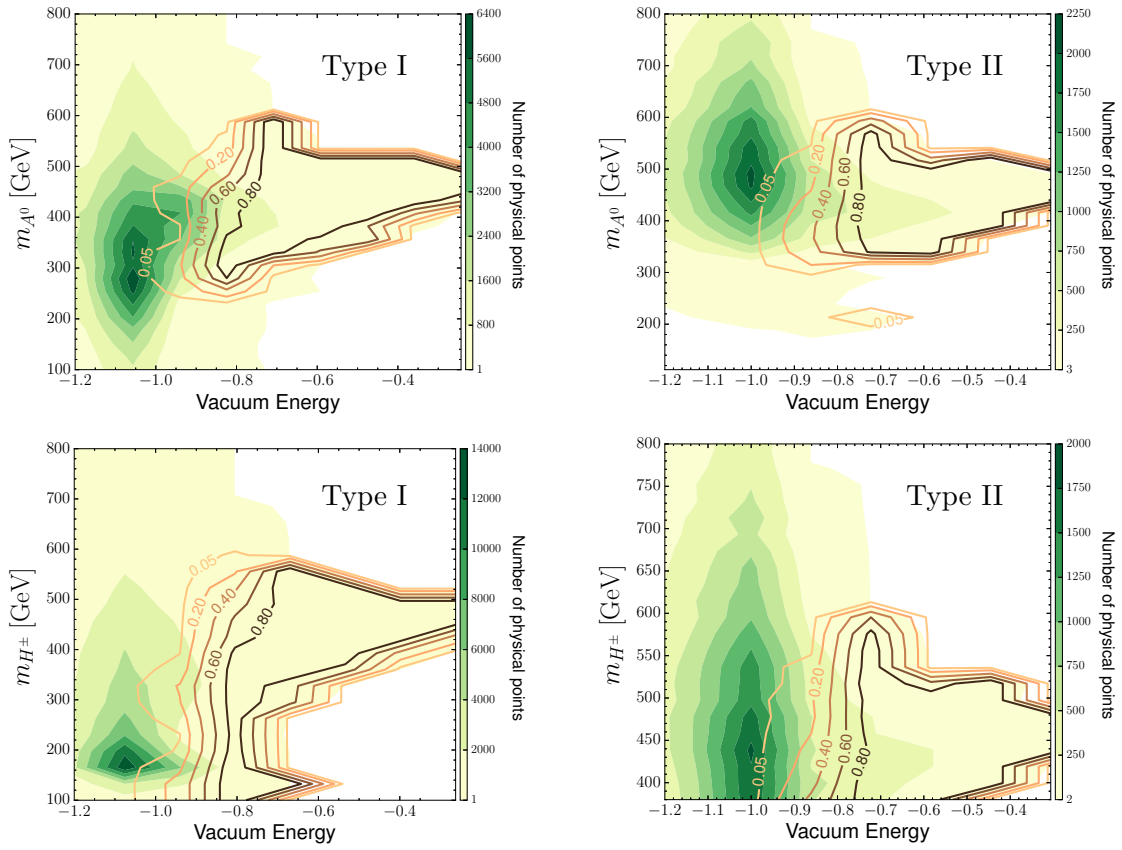

Figure 3.6: (Top) Distribution of physical points and $\mathcal{P}_{\xi>1}$ contours in the $(m_{A^0}, |\mathcal{F}_0|)$ plane. (Bottom) Same as above, now in the $(m_{H^\pm}, |\mathcal{F}_0|)$ plane.

Finally, we show in fig. 3.7 the distribution of physical (green) and strong PT (yellow) points varying with $\tan\beta$, as well as the ratio $\mathcal{P}_{\xi>1}$ in solid black lines. The yellow bars have been rescaled by a factor of 5 for convenience. As shown in eq. (3.19), perturbativity requirements tend to favour $\tan\beta \approx 1$, and more pronouncedly so in Type II due to the

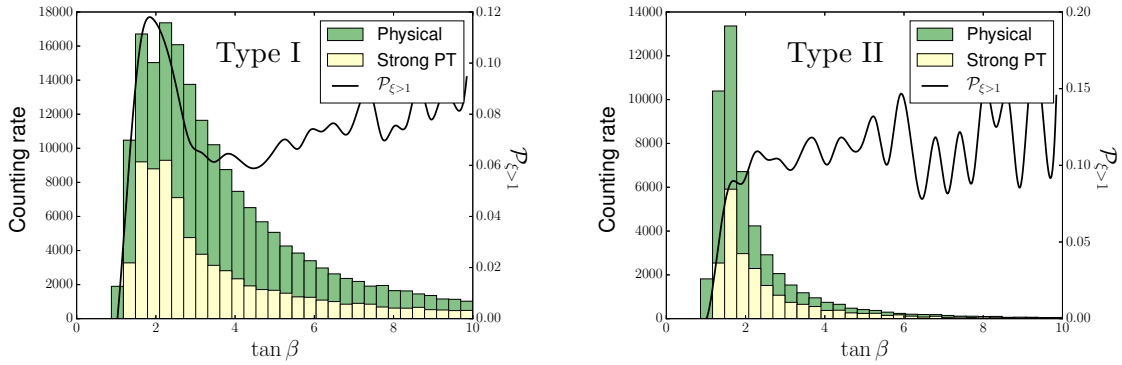

Figure 3.7: Distribution of physical and strong PT points as functions of $\tan\beta$. The yellow bars have been rescaled by a factor of 5 for convenience. The probability $\mathcal{P}_{\xi>1}$ is shown as a black line.

mass scales being typically larger in this case. The highly oscillatory behaviour of $\mathcal{P}_{\xi>1}$ for $\tan\beta \gtrsim 5$, particularly for Type II, is a consequence of the small sample of physical points in this region. But the wiggly data still allows us to conclude that, on average, $\tan\beta$ hardly influences the phase transition, if at all. And, when there is some preference, it is for $\tan\beta \approx 1$.

This is an excellent result from the baryogenesis perspective. For the computation of the baryon asymmetry the important additional source of CP violation comes from the variation of the particle masses along the wall of a vacuum bubble, whose complex parts (emerging from the complex phase in the doublet VEVs) induce an asymmetrical particle-antiparticle flow in and out of the bubble [113]. Due to its large mass, the top quark gives by far the most relevant contribution to this process. However, for $\tan\beta \gg 1$ the top coupling to the scalar sector is suppressed and this effect becomes rapidly negligible. In fact, it can be shown that the net baryon number scales as $n_B \sim (\tan\beta)^{-2}$ [264]. Therefore, the fact that $\tan\beta \sim 1$ is not ruled out from the phase transition perspective shows that there is no tension with the demand for sufficient additional CP violation.

Chapter 4

Collider phenomenology

In the previous chapter we have investigated the regions of the 2HDM parameter space that favour a strong first order phase transition, as required for solving the problem of the matter-antimatter asymmetry of the Universe. With this information at hand, the natural question that follows is: what can we say about the phenomenological predictions of these models in collider experiments? Can a cosmological observable be used to point at effective search strategies for new particles at the LHC? This chapter is devoted to exploring this interface between particle cosmology and collider phenomenology. We will answer these questions, showing that the 2HDM with a strong phase transition has a rather exotic phenomenology which has been little explored in the current searches for heavy scalars at the LHC [86]. For other theoretical works exploring exotic channels without our cosmological motivation we refer the reader to refs. [107, 265].

4.1 Motivating a search via $A^0 \to ZH^0$

We have seen in section 2.4.5 that searches for heavy scalars have focused mainly on the diboson, diphoton and $\tau^+\tau^-$ channels, not the least because these are the most relevant modes to look for the SM Higgs at hadron colliders. For decays specific to the 2HDM, searches have focused on $H^0 \to h^0 h^0$ and $A^0 \to Zh^0$ [207], mainly motivated by the supersymmetric case, where the additional scalars can be rather heavy but are nearly degenerate among themselves. In particular, note that

$$\begin{aligned} m^2_{h^0} + m^2_{H^0} - m^2_{A^0} &= \left(\lambda_1 \cos^2\beta + \lambda_2 \sin^2\beta + \lambda_5\right) v^2, \\ m^2_{h^0} + m^2_{H^0} - m^2_{H^\pm} &= \left(\lambda_1 \cos^2\beta + \lambda_2 \sin^2\beta + \frac{\lambda_4+\lambda_5}{2}\right) v^2, \\ m^2_{A^0} - m^2_{H^\pm} &= \frac{\lambda_4-\lambda_5}{2}\, v^2, \end{aligned} \tag{4.1}$$

and since SUSY requires that the quartic couplings be given by the gauge couplings according to

$$\begin{aligned} \lambda_1 &= \lambda_2 = \frac{g^2 + g'^2}{4}, \\ \lambda_4 &= \frac{g^2}{2}, \qquad\qquad \lambda_5 = 0, \end{aligned} \tag{4.2}$$

it follows that

$$\begin{aligned} |m^2_{H^0} - m^2_{A^0}| &= |m^2_Z - m^2_{h^0}| \approx (85.5 \text{ GeV})^2 < m^2_Z, \\ |m^2_{H^0} - m^2_{H^\pm}| &= |m^2_Z + m^2_W - m^2_{h^0}| \approx (29.1 \text{ GeV})^2 < m^2_W, \\ |m^2_{A^0} - m^2_{H^0}| &= m^2_W. \end{aligned} \tag{4.3}$$

This means that in supersymmetric scenarios a decay $S_i \to S_j V$ (with $S = H^0, A^0, H^\pm$ and $V = W, Z$) is kinematically forbidden, and have for this reason been little explored experimentally.

But we have seen in the previous chapter that a strong phase transition in 2HDMs typically requires a large $m_{A^0} - M$ splitting in order to induce large couplings in the scalar sector. On the other hand, because H^0 in general shares the electroweak VEV with the lightest h^0, its being heavy is largely disfavoured except in very special circumstances, e.g. very close to alignment and for $\tan\beta \approx 1$ to avoid non-perturbative couplings.

These results are put together in fig. 4.1, showing how the likelihood of a strong phase transition varies with m_{H^0} and m_{A^0}. In both types it is clear that the favoured scenario has a large splitting $m_{A^0} > m_{H^0} + m_Z$, pointing to the $A^0 \to ZH^0$ decay as a *smoking gun signature* of a 2HDM with a strong phase transition.

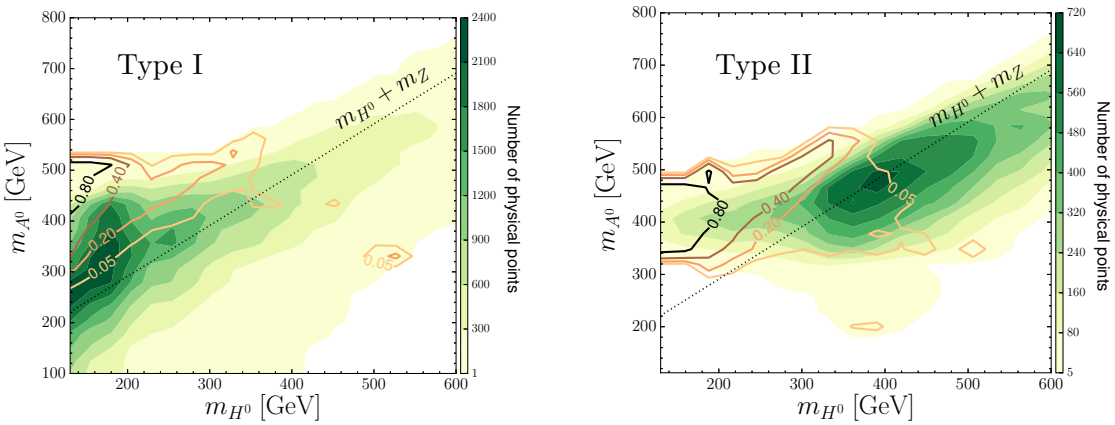

Figure 4.1: Distribution of physical points and $\mathcal{P}_{\xi>1}$ contours in the $m_{H^0} \times m_{A^0}$ plane.

This is further reinforced by the fact that a strong PT also favours the alignment limit, in which case the decays usually searched for are strongly disfavoured (including the

important diboson channel) because $g_{HVV} \sim g_{Hhh} \sim g_{hAZ} \sim \sin(\beta-\alpha)$[1]. On the other hand, $g_{HAZ} \sim \cos(\beta-\alpha)$ is unsuppressed.

Now, is it viable to study this decay at the LHC? To start answering this question note first that, for a heavy pseudoscalar, the main competing channels are $A^0 \to t\bar{t}$, which is suppressed as $(\tan\beta)^{-2}$, together with $A^0 \to Zh^0$ and $A^0 \to W^\pm H^\mp$ when available. The former is subdominant close to alignment, as just discussed. As for the latter, recall that $H^\pm$ has to be nearly degenerate with a neutral scalar to satisfy $\Delta\rho \approx 1$, so this decay will be forbidden when $m_{H^0} \approx m_{A^0}$. This is typically the case in Type II, as can be seen from fig. 3.6, whereas in Type I a pairing with CP-even states is still possible and the decay of the pseudoscalar into a charged Higgs is still open, thus reducing $\mathrm{BR}(A^0 \to ZH^0)$ by $\sim 50\%$.

For a more detailed investigation of the detection prospects we will henceforth focus on two benchmark points, representatives of the favoured scenarios discussed in chapter 3. Based on fig. 3.6 we pick $m_{A^0} = 400$ GeV and will consider $m_{H^\pm} = m_{A^0}$ for simplicity, thus closing the competing decay into charged scalars. Since H^0 has to be relatively light we choose $m_{H^0} = 180$ GeV, as well as $\mu = 100$ GeV and a moderate $\tan\beta = 2$ (so that $M \approx 111.8$ GeV). Finally, the two benchmarks differ among themselves in that one (called Benchmark A) is close to alignment, with $\alpha - \beta = 0.001\pi$, whereas the other (Benchmark B) has $\alpha - \beta = 0.1\pi$ (cf. fig 3.4). We will also assume Type I fermionic couplings, since the other types are a lot more constrained to be close alignment (see fig. 2.7). These values are summarized in Table 4.1. We checked that these points pass all the constraints discussed in section 2.4 and that they both yield a strong phase transition.

Benchmark	M	$\tan\beta$	m_{H^0}	m_{A^0}	$m_{H^\pm}$	$\alpha-\beta$	T_c	v_c/T_c
A	111.8	2	400	400	180	0.001π	85.712	2.268
B	111.8	2	400	400	180	0.1π	86.748	2.201

Table 4.1: The two benchmark scenarios considered in our collider analysis. Mass parameters and critical temperature are given in GeV.

The branching ratios of the pseudoscalar varying with m_{H^0} are shown in fig. 4.2 (left) for benchmarks A (solid lines) and B (dotted lines). In both cases $A^0 \to ZH^0$ largely dominates when $m_{H^0} \lesssim 200$ GeV. As for the subsequent decays of H^0, its branching ratios are depicted in fig. 4.2 (right). Close to alignment the couplings of H^0 to gauge bosons are nearly vanishing, leaving $b\bar{b}$ as the main decay mode. But the diboson channel

[1] In fact $g_{Hhh} = \frac{\sin(\beta-\alpha)}{v^2\sin(2\beta)}\left\{\sin(2\alpha)\left(2m_{h^0}^2 + m_{H^0}^2\right) - 2M^2\left[\sin(\beta+\alpha)\cos(\beta-\alpha) + \sin(2\alpha)\right]\right\}$.

quickly dominates as the coupling grows, and we see that, for benchmark B, the heavy CP-even scalar decays almost exclusively into W^+W^-.

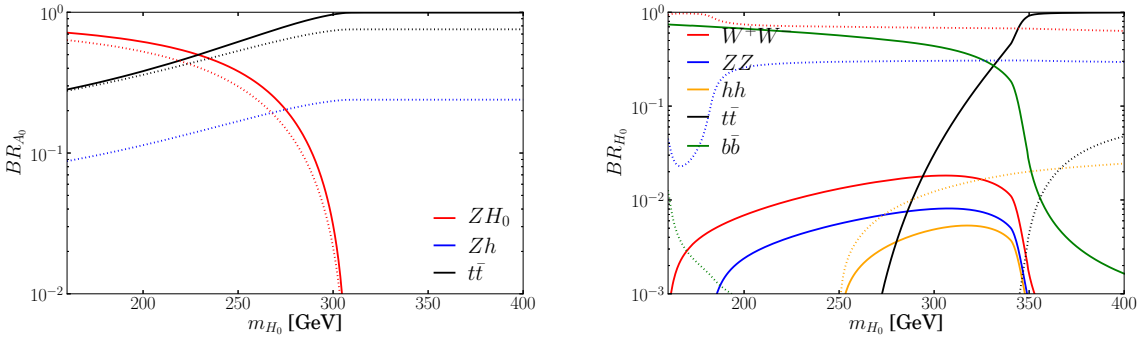

Figure 4.2: Branching ratios of A^0 (left) and H^0 (right) varying with m_{H^0}. Solid and dotted lines correspond to benchmarks A and B, respectively.

Focusing on the leptonic decays of gauge bosons, which are the cleanest and easiest to detect, it follows that a 2HDM with a strong phase transition should leave its imprint at the LHC in $pp \to A^0 \to ZH^0 \to \ell\ell b\bar{b}$ or $4\ell + \not{E}_T$ (where $\not{E}_T$ is the missing transverse energy corresponding to the neutrinos from the leptonic W decay).

4.2 Search for A^0 in $\ell\ell b\bar{b}$ and $4\ell + \not{E}_T$

We turn now to a more detailed analysis of the prospects for these searches in the next LHC run at 13 TeV. For this purpose we implement the Type I 2HDM in FeynRules 1.6 [266] with a 5D effective operator [267, 228]

$$\mathcal{L}_{ggA} \equiv \frac{\alpha_S}{8\pi v} \frac{\mathcal{F}_{ggA}}{\tan\beta} \left(G^a_{\mu\nu} \widetilde{G}^{a\,\mu\nu} A^0 \right) \tag{4.4}$$

to reproduce the $gg \to A^0$ production cross section at leading order. Here

$$\widetilde{G}^{a\,\mu\nu} \equiv \frac{1}{2} \epsilon^{\mu\nu\rho\sigma} G^a_{\rho\sigma} \tag{4.5}$$

is the dual of the gluon field strength tensor and

$$\mathcal{F}_{ggA} \equiv \frac{f(\tau)}{\tau}, \qquad f(\tau) \equiv \begin{cases} \arcsin^2(\sqrt{\tau}), & \tau \leq 1 \\ -\frac{1}{4}\left[\log\frac{\tau+\sqrt{\tau-1}}{\tau+\sqrt{\tau+1}} - i\pi\right], & \tau > 1 \end{cases} \tag{4.6}$$

(with $\tau \equiv m^2_{A^0}/4m^2_t$) is the form factor for the top quark loop.

Events are then generated with MadGraph5_aMC@NLO [268, 269], a program designed for performing Monte-Carlo simulations at parton level. This means that its output final states still involve isolated quarks. Due to confinement, long before they can reach

the detector these quarks emit a myriad of gluons, which can also emit other gluons before all of them ultimately give rise to quark-antiquark pairs. This process is called *parton showering*. Finally, the multitude of quarks and gluons thus generated eventually hadronize into colorless objects (mesons and baryons), so that the detector signature of a single quark in the event final state is actually a *jet* of multiple hadrons. These showering and hadronization processes are taken into account using PYTHIA [270], a code especially designed for this task. Lastly, the events are passed to DELPHES [271] for simulation of detector effects such as b-tagging efficiency, i.e. the efficiency of the detector in recognizing that a certain jet originated from a b quark.

Close to the alignment limit the dominant final state is $\ell\ell b\bar{b}$, for which the main SM backgrounds are (in order of relevance) (i) $t\bar{t}$ production (with subsequent $t \to W^+ b \to \ell\nu_\ell b$ and the conjugate process for $\bar{t}$); (ii) $Zb\bar{b}$ production; (iii) ZZ production and (iv) associated production of a SM-like Higgs with a Z boson. We take NLO effects into account by rescaling the signal and the two dominant backgrounds by K-factors. For the signal, $K_{\text{signal}} \simeq 1.6$ (computed with SUSHI), whereas $K_{t\bar{t}} \simeq 1.5$ [272] and $K_{Zb\bar{b}} \simeq 1.4$ [273].

	Signal	$t\bar{t}$	$Z\,b\bar{b}$	ZZ	$Z\,h$
Event selection	14.6	1578	424	7.3	2.7
$80 < m_{\ell\ell} < 100$ GeV	13.1	240	388	6.6	2.5
$H_T^{b\bar{b}} > 150\,\text{GeV}$ $H_T^{\ell\ell b\bar{b}} > 280\,\text{GeV}$	8.2	57	83	0.8	0.74
$\Delta R_{b\bar{b}} < 2.5$, $\Delta R_{\ell\ell} < 1.6$	5.3	5.4	28.3	0.75	0.68
$m_{b\bar{b}}$, $m_{\ell\ell b\bar{b}}$ signal region	3.2	1.37	3.2	< 0.01	< 0.02

Table 4.2: Cut-flow chart for $\ell\ell b\bar{b}$ final state considering event selection and background reduction. The NLO cross section (in fb) is shown after successive cuts for the signal $A_0 \to ZH_0 \to \ell\ell b\bar{b}$ and the dominant backgrounds $t\bar{t}$ and $Zb\bar{b}$, while ZZ and Zh are shown at LO.

We use standard event selection criteria, requiring the presence of two isolated same flavour leptons and two b-tagged jets [274] in the final state, with minimum transverse momenta $p_T^{\ell_1,b_1} > 40$ GeV, $p_T^{\ell_2,b_2} > 20$ GeV, and maximum pseudorapidities $|\eta_b| < 2.5$ and $|\eta_\ell| < 2.5$ (2.7) for electrons (muons). Demanding the two leptons to reconstruct the Z mass eliminates most of the $t\bar{t}$ background, whereas further cuts in $H_T \equiv \sum p_T$ and on the angular separation ΔR between the two jets or the two leptons help increasing the signal to background ratio. Finally, the signal is defined by requiring the two b-jets to reconstruct the H^0 mass and $\ell\ell b\bar{b}$ to reconstruct A^0 (taking into account eventual losses

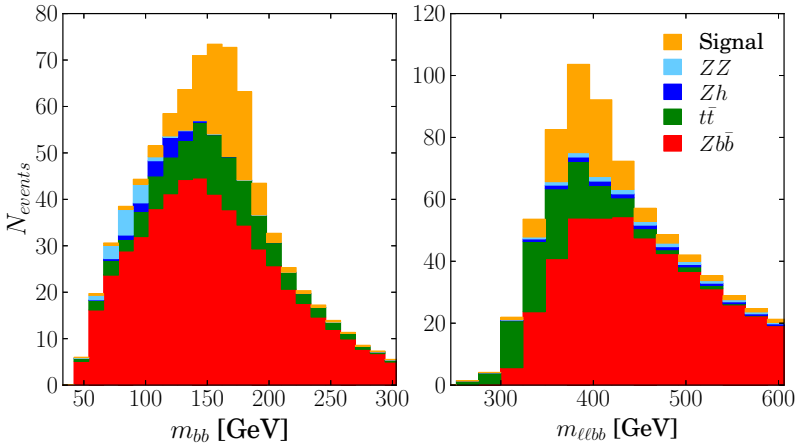

Figure 4.3: Stacked distributions of $m_{b\bar{b}}$ (left) and $m_{\ell\ell b\bar{b}}$ (right) for signal and backgrounds for $\mathcal{L} = 20$ fb^{-1} after applying all cuts.

due to hadronization effects),

$$\begin{aligned} m_{b\bar{b}} &= (m_{H^0} - 20) \pm 30 \text{ GeV}, \\ m_{\ell\ell b\bar{b}} &= (m_{A^0} - 20) \pm 40 \text{ GeV}. \end{aligned} \tag{4.7}$$

Table 4.2 shows the cross sections (in fb) of signal and backgrounds after the successive cuts. The number of signal (S) and background (B) events are obtained by multiplying the respective cross sections by the total luminosity $\mathcal{L}$, from which we conclude that a 5σ statistical-only significance, $S/\sqrt{S+B} = 5$, is reached for $\mathcal{L} \sim 20$ fb^{-1}. Systematic errors can be estimated by marginalizing over a (conservative) 10% uncertainty in the background prediction, yielding $\mathcal{L} \sim 40$ fb^{-1}.

The invariant mass distributions for the final decay products are shown in fig. 4.3 for a luminosity $\mathcal{L} = 20$ fb^{-1} after all the cuts have been applied, from which a clear excess can be seen in the signal region.

Away from alignment the $\ell\ell b\bar{b}$ final state comes mostly from $A^0 \to Zh^0$, since BR$(H^0 \to b\bar{b}) \ll 1$ (fig. 4.2 (right)). But for $m_{H_0} \lesssim 250$ GeV the pseudoscalar decay into the light h^0 is suppressed (see fig. 4.2 (left)), which renders the search in the $\ell\ell b\bar{b}$ final state challenging. As we have already argued, in this regime the characteristic signature is $pp \to A^0 \to ZH^0 \to \ell\ell W^+W^- \to 4\ell + \not{E}_T$.

The main irreducible SM backgrounds in this case is diboson (ZZ) production with $ZZ \to \ell\ell\ell\ell$. Other backgrounds, such as $Zt\bar{t}$, ZWW and Zh yield a combined cross section which is $< \sigma_{\text{signal}}/4$ after event selection. We follow the same selection and analysis procedure as before, except for requiring the presence of *four* isolated leptons (in two same flavour pairs) in the final state with $p_T^{\ell_1} > 40$ GeV, $p_T^{\ell_{2,3,4}} > 20$ GeV. Again, we require at least one of the same flavour lepton pairs to reconstruct m_Z within ~ 20 GeV, and rescale

the signal and dominant background by their respective K factors, $K_{ZZ} \simeq 1.2$ [275] and $K_{Zt\bar{t}} \simeq 1.35$ [276].

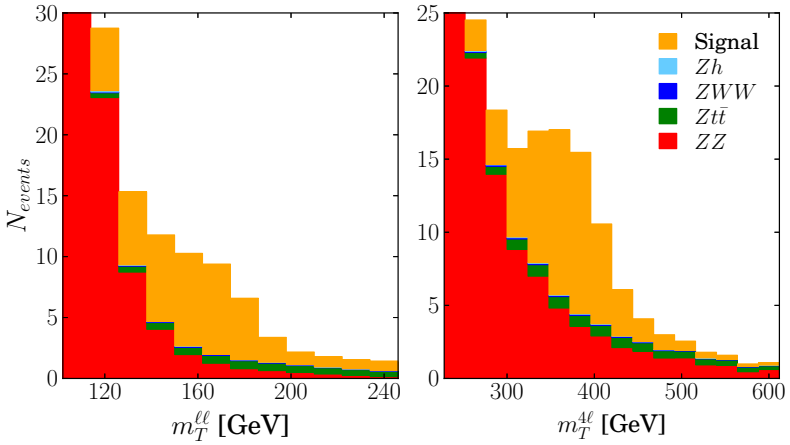

Figure 4.4: Stacked distributions of the defined invariant masses, $m_T^{\ell\ell}$ (left) and $m_T^{4\ell}$ (right) after event selection for an integrated luminosity of $\mathcal{L} = 40$ fb^{-1}.

In order to take into account the missing energy in the reconstruction of the decaying particle's mass, we define the following transverse mass variables

$$\begin{aligned} \left(m_T^{\ell\ell}\right)^2 &= \left(\sqrt{p_{T,\ell\ell}^2 + m_{\ell\ell}^2} + \not{p}_T\right)^2 - \left(\vec{p}_{T,\ell\ell} + \vec{\not{p}}_T\right)^2, \\ m_T^{4\ell} &= \sqrt{p_{T,\ell'\ell'}^2 + m_{\ell'\ell'}^2} + \sqrt{p_{T,\ell\ell}^2 + \left(m_T^{\ell\ell}\right)^2}, \end{aligned} \tag{4.8}$$

($\ell'\ell'$ are the two same flavour leptons most closely reconstructing m_Z). The distribution of the data in these mass variables is shown in fig. 4.4, from which we see that the region of $m_T^{4\ell} > 260$ GeV allows for extraction of a clean signal.

The NLO cross sections after event selection and this background selection is shown in Table 4.3. A final signal cross section of 0.88 fb compared to a background of 1.39 fb yields a 5σ significance with $\mathcal{L} \sim 70$ fb^{-1}, which increases to $\mathcal{L} \simeq 200$ fb^{-1} assuming a 10% systematic uncertainty on the background prediction.

	Signal	ZZ	Rare
Event selection $80 < m_{\ell\ell} < 100$ GeV	1.49	6.72	0.34
$m_T^{4\ell} > 260$ GeV	0.88	1.18	0.21

Table 4.3: Cut-flow chart for $\ell\ell\ell\ell$ final state considering event selection and the background reduction, showing the NLO cross sections (in fb) after successive cuts.

These are all very promising prospects, considering that the next LHC run at 13 TeV is designed to reach up to 300 fb^{-1}, in which case even our less favourable scenario could

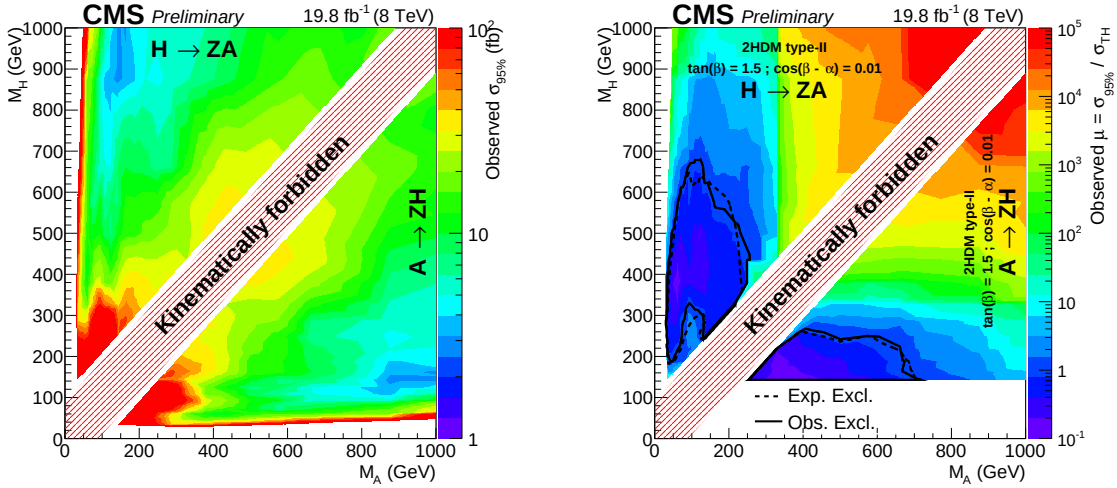

Figure 4.5: (Left) Observed 95% C.L. upper limits on $H^0/A^0 \to A^0/H^0 + Z \to \ell\ell b\bar{b}$ cross section. (Right) Signal strength limits for a theoretical value calculated with $\tan\beta = 1.5$ in a Type II 2HDM. Figures taken from ref. [277].

yield a 5σ discovery. Indeed, the results even suggest that the current $7-8$ TeV data set can already be sensitive to these final states. Motivated by this, the CMS collaboration has recently performed a search in $H^0/A^0 \to A^0/H^0 + Z \to \ell\ell b\bar{b}$ and $\ell\ell\tau\tau$, imposing limits on the corresponding cross sections and signal strengths [277]. The results are shown in figs. 4.5 and 4.6. For the signal strength modifiers, the theoretical value has been computed considering a Type II 2HDM with $\tan\beta = 1.5$ and near alignment[2], but extending for other parameter choices is a straightforward exercise.

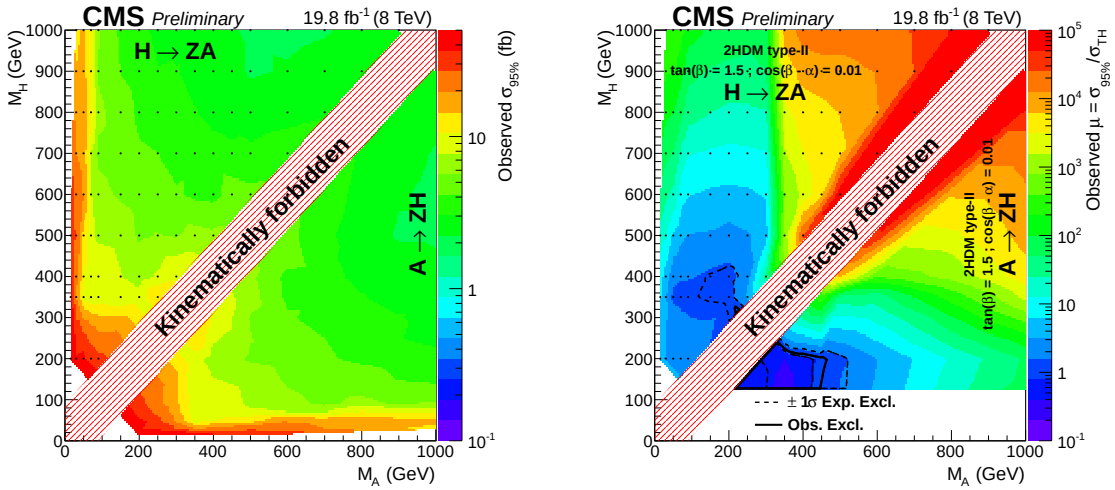

Figure 4.6: (Left) Observed 95% C.L. upper limits on $H^0/A^0 \to A^0/H^0 + Z \to \ell\ell\tau\tau$ cross section. (Right) Signal strength limits for a theoretical value calculated with $\tan\beta = 1.5$ in a Type II 2HDM. Figures taken from ref. [277].

[2]Note that their convention for $\beta - \alpha$ differs from ours by an additive factor of $\pi/2$.

Chapter 5

Conclusions

The origin of the matter-antimatter asymmetry of the Universe figures among the few experimental observations that the Standard Model of Particle Physics (SM) cannot explain. The reason is that the SM lacks enough CP violation as well as a strong source of displacement from thermodynamical equilibrium occurring during the history of the Universe. In this work we take a step further towards a broad study of the viability of two-Higgs-doublet models (2HDM) as minimal alternatives for explaining baryogenesis. Focusing on the CP conserving case for simplicity, we evaluate the strength of the electroweak phase transition in an extended region of the model's parameter space, showing that the most likely scenario for successful baryogenesis has:

- a SM-like light Higgs (alignment limit);
- a rather heavy pseudoscalar, $m_{A^0} \gtrsim 300$ GeV;
- a large mass splitting between the pseudoscalar and the CP-even states, $m_{A^0} - m_{H^0} \gtrsim v$.

Altogether, the findings point to an exotic phenomenology which has been little explored in collider searches for heavy Higgs bosons so far. In particular, not only is the decay $A^0 \to ZH^0$ open, in contrast to supersymmetric scenarios, it is also among the most favourable search channels, since decays of H^0 into gauge bosons and of the pseudoscalar into a light SM-like Higgs are suppressed near alignment. We have performed a detailed analysis of the detection prospects of this proposed channel in the $\ell\ell b\bar{b}$ and $4\ell + \not{E}_T$ final states, showing that a 5σ discovery could be achieved at the 13 TeV LHC run with a luminosity of $\mathcal{L} \sim 20 - 200$ fb^{-1}, and with some sensitivity even with the current $7 - 8$ TeV data, as proven by recent searches performed by the CMS collaboration.

It is worth emphasizing that a search in the $A^0 \to ZH^0$ channel, as proposed in this work, has the potential to unveil valuable information about physics beyond the SM. If a resonance is found in this channel, we would not only know that the symmetry-breaking sector is non-SM like, but also that the UV complete theory is likely to be strongly coupled at relatively low energies, $\Lambda \sim 10$ TeV. In particular, supersymmetric scenarios would be very much disfavoured, while Composite Higgs theories would be put in the spotlight as promising candidates.

Of course, the most natural completion of this work would be to compute the actual baryon asymmetry generated during the phase transition. The first step in this direction is to reintroduce the additional source of CP violation in the scalar sector, which have been neglected in this first analysis. In the 2HDM this has the side effect of generating contributions to electron and neutron electric dipole moments already at 2-loop level[1] [110, 278, 279], while in the SM they first appear at 4-loop and are therefore highly suppressed. Experimental searches for these effects have consistently returned negative results [280, 281, 282], thus putting tight bounds on the 2HDM CP violating phase [111, 112]. Preliminary studies indicate that the allowed values could be just enough to obtain the observed baryon asymmetry, but a more detailed analysis taking into account the non-equilibrium hydrodynamical properties of the phase transition, such as the bubble profile, the particle transport along its wall [113, 283, 284] as well as its expansion velocity [285, 286], is still largely missing.

On the more field-theoretic side, it would be interesting to compute the 2-loop contributions to the effective potential and investigate their impact on our results for the phase transition strength. This becomes even more important as we advance into an era of precision measurements of Higgs properties, with a consequent increasing relevance in knowing more accurately the dependence of phenomenological observables on parameters of the Higgs sector. The functions appearing in the computation of the relevant diagrams (without assuming a high-temperature expansion, which is not always a valid approximation in our case) have been worked out in ref. [287], making the full 2-loop computation in the 2HDM a bookkeeping exercise, albeit a time-consuming one.

From a more collider-oriented perspective, we plan to extend our previous analysis to include more benchmark points and cover cases that we have not considered in this first approach. In particular, we aim at exploring the rich phenomenology of the CP violating 2HDM. In this case the pseudoscalar A^0 can also decay into gauge boson and scalar pairs,

[1] See Appendix C for the expressions of the electron, neutron and mercury EDMs in 2HDMs.

possibly altering its branching fractions significantly, even for small CP violating phases. For other studies in this direction see refs. [112, 288, 289].

An extended analysis of the recent CMS data on $A^0 \to H^0 Z$, showing the exclusion regions for various $\tan\beta$ values, is already in preparation.

Appendix A

Mass matrix of scalars

For the evaluation of the effective potential it is necessary to compute the masses of the scalars at an arbitrary point in field space. Recall that, in a charge conserving case, a gauge rotation can be performed to write the doublets in the form

$$\Phi_1 = \frac{1}{\sqrt{2}} \begin{pmatrix} 0 \\ h_1 \end{pmatrix}, \qquad \Phi_2 = \frac{1}{\sqrt{2}} \begin{pmatrix} 0 \\ h_2 + i\,\eta_2 \end{pmatrix}. \tag{A.1}$$

The squared mass matrix is given by the second derivative of the tree-level potential with respect to the fields $\phi_i = \big(\mathrm{Re}(\varphi_1^+), \mathrm{Re}(\varphi_2^+), \mathrm{Im}(\varphi_1^+), \mathrm{Im}(\varphi_2^+), h_1, h_2, \eta_1, \eta_2\big)$,

$$M_{ij} = \frac{\partial^2 V_{\mathrm{tree}}}{\partial\phi_i^* \partial\phi_j}, \tag{A.2}$$

whose eigenvalues are the scalars' squared masses. The field array ϕ_i is organized in such a way that M_{ij} is block diagonal, each block a 4×4 symmetric matrix. For the charged scalars the matrix elements are

$$2M_{11}^{\pm} = -2\mu_1^2 + \lambda_1 h_1^2 + \lambda_3\,(h_2^2 + \eta_2^2), \tag{A.3}$$

$$2M_{22}^{\pm} = -2\mu_2^2 + \lambda_3 h_1^2 + \lambda_2\,(h_2^2 + \eta_2^2), \tag{A.4}$$

$$2M_{12}^{\pm} = -\mathrm{Re}(\mu^2 e^{i\xi}) + \Big[\lambda_4 + \mathrm{Re}(\lambda_5 e^{2i\xi})\Big]\, h_1 h_2 - \mathrm{Im}(\lambda_5 e^{2i\xi})\, h_1 \eta_2, \tag{A.5}$$

$$2M_{13}^{\pm} = 0, \tag{A.6}$$

$$-2M_{23}^{\pm} = 2M_{14}^{\pm} = \mathrm{Im}(\lambda_5 e^{2i\xi})\,\big(v^2 \sin\beta\cos\beta - h_1 h_2\big) + \Big[\lambda_4 - \mathrm{Re}(\lambda_5 e^{2i\xi})\Big]\, h_1 \eta_2. \tag{A.7}$$

For the neutral scalars,

$$2M_{11}^{0} = -2\mu_1^2 + 3\lambda_1 h_1^2 + \lambda_{345}^{+}\, h_2^2 + \lambda_{345}^{-}\, \eta_2^2 - 2\,\mathrm{Im}(\lambda_5 e^{2i\xi})\, h_2\, \eta_2, \tag{A.8}$$

$$2M_{22}^{0} = -2\mu_2^2 + \lambda_{345}^{+}\, h_1^2 + \lambda_2\,(3h_2^2 + \eta_2^2), \tag{A.9}$$

$$2M_{33}^{0} = -2\mu_1^2 + \lambda_1 h_1^2 + \lambda_{345}^{-}\, h_2^2 + \lambda_{345}^{+}\, \eta_2^2 + 2\,\mathrm{Im}(\lambda_5 e^{2i\xi})\, h_2\, \eta_2, \tag{A.10}$$

$$2M_{44}^{0} = -2\mu_2^2 + \lambda_{345}^{-}\, h_1^2 + \lambda_2\,(h_2^2 + 3\eta_2^2), \tag{A.11}$$

and the off-diagonal elements,

$$2M^0_{12} = -\mathrm{Re}(\mu^2 e^{i\xi}) + 2\lambda^+_{345}\, h_1\, h_2 - 2\,\mathrm{Im}(\lambda_5 e^{2i\xi})\, h_1\, \eta_2, \tag{A.12}$$

$$2M^0_{13} = 2\,\mathrm{Re}(\lambda_5 e^{2i\xi})\, h_2\, \eta_2 + \mathrm{Im}(\lambda_5 e^{2i\xi})\, (h_2^2 - \eta_2^2), \tag{A.13}$$

$$2M^0_{14} = \mathrm{Im}(\lambda_5 e^{2i\xi}) \left(v^2 \sin\beta\cos\beta - 2h_1 h_2\right) + 2\lambda^-_{345}\, h_1\, \eta_2, \tag{A.14}$$

$$2M^0_{23} = 2\,\mathrm{Re}(\lambda_5 e^{2i\xi})\, h_1\, \eta_2 - \mathrm{Im}(\lambda_5 e^{2i\xi})\, (v^2 \sin\beta\cos\beta - 2h_1\, h_2), \tag{A.15}$$

$$2M^0_{24} = 2\lambda_2\, h_2\, \eta_2 - \mathrm{Im}(\lambda_5 e^{2i\xi})\, h_1^2, \tag{A.16}$$

$$2M^0_{34} = -\mathrm{Re}(\mu^2 e^{i\xi}) + 2\,\mathrm{Re}(\lambda_5 e^{2i\xi})\, h_1\, h_2 - 2\,\mathrm{Im}(\lambda_5 e^{2i\xi})\, h_1\, \eta_2, \tag{A.17}$$

where

$$\lambda^\pm_{345} \equiv \lambda_3 + \lambda_4 \pm \mathrm{Re}(\lambda_5 e^{2i\xi}) \tag{A.18}$$

and $\mu_{1,2}$ are given by eq. (2.18) with $\lambda_{345} \to \lambda^+_{345}$.

In the CP conserving case, $\eta_2 = 0 = \mathrm{Im}(\lambda_5 e^{2i\xi})$ and these matrices are themselves block diagonal, each block a 2×2 matrix corresponding to the CP-even and CP-odd sectors.

Appendix B

Decay widths

We list here the expressions we use for calculating the scalar decay widths, as discussed in section 2.4.5.

$H_i \to f\bar{f}$

The decay width of neutral scalars into a pair of fermions is given by [221]

$$\Gamma(H_i \to f\bar{f}) = N_c\, m_{H_i} m_f^2\, \frac{\sqrt{2}G_f}{8\pi}\left[\beta_f^3\,|y_{f,i}|^2\,(1+\Delta_H) + \beta_f\,|\widetilde{y}_{f,i}|^2\,(1+\Delta_A)\right] \tag{B.1}$$

with $\beta_f \equiv \sqrt{1-\frac{4m_f^2}{m_{H_i}^2}}$ the phase space factor, m_f the mass of the fermion and N_c the color factor (3 for quarks, 1 for leptons). For quarks, most QCD corrections are taken into account if we use the running quark mass $m_q(m_{H_i})$ in the computation of the width, rather than the pole or the $\overline{\text{MS}}$ mass $m_q(m_q)$. We therefore compute the running of α_s [225] and of quark masses [225, 226] (including matching conditions) to NNNLO[1]. The remaining QCD corrections are given by the $\Delta_{H,A}$ factors.

For light quarks these corrections read [221]

$$\begin{aligned}\Delta_H^{\text{light } f} &= \Delta_{qq} + \left(\frac{\alpha_s}{\pi}\right)^2\left(1.57 - \frac{4}{3}\log\frac{m_H}{m_t} + \frac{4}{9}\log^2\frac{m_f}{m_H}\right),\\ \Delta_A^{\text{light } f} &= \Delta_{qq} + \left(\frac{\alpha_s}{\pi}\right)^2\left(\frac{23}{6} - 2\log\frac{m_A}{m_t} + \frac{2}{3}\log^2\frac{m_f}{m_A}\right),\end{aligned} \tag{B.2}$$

with $\alpha_s \equiv \alpha_s(m_{H_i})$ and the common term for both scalar and pseudoscalar [290, 220],

$$\begin{aligned}\Delta_{qq} =& \frac{17}{3}\frac{\alpha_s}{\pi} + \left[\overbrace{\frac{10801}{144} - \frac{19}{2}\zeta(2) - \frac{39}{2}\zeta(3)}^{\approx 35.9399612} - n_f\overbrace{\left(\frac{65}{24} - \frac{1}{3}\zeta(2) - \frac{2}{3}\zeta(3)\right)}^{\approx 1.35865070}\right]\left(\frac{\alpha_s}{\pi}\right)^2\\ &+ \left(164.14 - 25.77\,n_f + 0.26\,n_f^2\right)\left(\frac{\alpha_s}{\pi}\right)^3.\end{aligned} \tag{B.3}$$

[1] That is, we consider the 4-loop RGE and 3-loop matching conditions.

On the other hand, for decays into top quarks the QCD corrections are [221]

$$\begin{aligned}\Delta_H^{\text{top}} &= \frac{4}{3}\frac{\alpha_s}{\pi}\left[\frac{A(\beta_f)}{\beta_f} + \frac{1}{16\beta_f^3}(3+34\beta_f^2-13\beta_f^4)\log\frac{1+\beta_f}{1-\beta_f} + \frac{3}{8\beta_f^2}(7\beta_f^2-1)\right],\\ \Delta_A^{\text{top}} &= \frac{4}{3}\frac{\alpha_s}{\pi}\left[\frac{A(\beta_f)}{\beta_f} + \frac{1}{16\beta_f}(19+2\beta_f^2+3\beta_f^4)\log\frac{1+\beta_f}{1-\beta_f} + \frac{3}{8}(7-\beta_f^2)\right],\end{aligned} \tag{B.4}$$

with

$$A(\beta_f) = (1+\beta_f^2)\left[4\text{Li}_2(x_\beta) + 2\text{Li}_2(-x_\beta) + \log x_\beta \log\frac{8\beta_f^2}{(1+\beta_f)^3}\right] - 3\beta_f \log\frac{4\beta_f^{4/3}}{1-\beta_f^2}, \tag{B.5}$$

where $x_\beta \equiv (1-\beta_f)/(1+\beta_f)$.

$H^+ \to f\bar{f}'$

The decay width of a charged Higgs boson into a pair of quarks can be written as [221]

$$\begin{aligned}\Gamma(H^+ \to u\bar{d}) = N_c\, m_{H^\pm}\frac{\sqrt{2}G_f}{8\pi}|V_{ud}|^2\sqrt{\lambda(x_u,x_d)}\,(1+\Delta_{qq})\,\times\\ \left[(1-x_u-x_d)\left(|y_{d,H^+}|^2 m_d^2 + |y_{u,H^+}|^2 m_u^2\right) + 4\sqrt{x_u x_d}\, m_u m_d\, y_{u,H^+} y_{d,H^+}\right],\end{aligned} \tag{B.6}$$

where $x_f \equiv m_f^2/m_{H^\pm}^2$, V_{ud} is the corresponding CKM matrix element, and the kinematic factor

$$\begin{aligned}\lambda(x,y) &\equiv (1-x-y)^2 - 4xy\\ &= 1 + x^2 + y^2 - 2x - 2y - 2xy.\end{aligned} \tag{B.7}$$

For the $H^+ \to t\bar{b}$ the off-shell contribution $H^+ \to t^*\bar{b} \to W^+ b\bar{b}$ is also relevant and has width [224]

$$\begin{aligned}\Gamma(H^+ \to t^*\bar{b} \to W^+ b\bar{b}) = N_c\, m_{H^\pm}\frac{(\sqrt{2}G_f)^2}{64\pi^3}|V_{ud}|^2 m_W^2\,\times\\ \times\int_0^{1-x_W} dx_1 \int_{1-x_w-x_1}^{1-\frac{x_W}{1-x_1}} dx_2 \frac{F(x_1,x_2)}{(1-x_2-x_t+x_b)^2 + x_t w_t},\end{aligned} \tag{B.8}$$

with $w_t \equiv (\Gamma_t^{\text{tot}}/m_{H^\pm})^2$ and

$$\begin{aligned}F(x_1,x_2) \equiv |y_{u,H^+}|^2 m_u^2\; x_t\left(\frac{(1-x_1)(1-x_2)}{x_W} + 2x_1 + 2x_2 + 2x_W - 2x_b - 3\right) +\\ + |y_{d,H^+}|^2 m_d^2\left[\frac{x_2^3 + x_1 x_2^2 - 3x_2^2 - 2x_1x_2 + 3x_2 + x_1 - 1}{x_W}\right.\\ + x_2^2 + 2x_1x_2 - 4x_2 - 2x_1 - 2x_W + 3\\ \left. + x_b\left(2x_W - 2x_b - 2x_1 + 3 + \frac{5x_2 + x_1 - 2x_2^2 - x_1x_2 - 3}{x_W}\right)\right]\\ - 2\sqrt{x_b x_t}\, m_u m_d\, y_{u,H^+} y_{d,H^+}\left(\frac{(x_2-1)^2}{x_W} - x_2 - 2x_W + 2x_b + 1\right).\end{aligned} \tag{B.9}$$

The decay of a charged Higgs into a lepton pair is given by eq. (B.6) with the appropriate adjustments, such that

$$\Gamma(H^+ \to \ell^+ \nu_\ell) = m_{H^\pm} \frac{\sqrt{2} G_f}{8\pi} |y_{\ell,H^+}|^2 m_\ell^2 \left(1 - \frac{m_\ell^2}{m_{H^\pm}^2}\right)^2 . \tag{B.10}$$

$H_i \to W^+W^-, ZZ$

The decay $H_i \to V^*V^*$ into two offshell gauge bosons ($V = Z, W$) which later decay into into pairs of fermions is implemented as [227]

$$\begin{aligned}\Gamma(H_i \to VV) = \delta_V \frac{\sqrt{2} G_f m_{H_i}^3}{32\pi} |g_{H_i VV}|^2 \times \\ \int_0^{m_{H_i}^2} dp_1^2 \frac{1}{\pi} \frac{\Gamma_V m_V}{(p_1^2 - m_V^2)^2 + \Gamma_V^2 m_V^2} \int_0^{\left(m_{H_i} - p_1\right)^2} dp_2^2 \frac{1}{\pi} \frac{\Gamma_V m_V}{(p_2^2 - m_V^2)^2 + \Gamma_V^2 m_V^2} \times \\ \times \sqrt{\lambda\left(\frac{p_1^2}{m_{H_i}^2}, \frac{p_2^2}{m_{H_i}^2}\right)} \left[\lambda\left(\frac{p_1^2}{m_{H_i}^2}, \frac{p_2^2}{m_{H_i}^2}\right) + 12 \frac{p_1^2 p_2^2}{m_{H_i}^4}\right],\end{aligned} \tag{B.11}$$

where m_V is the mass of the gauge boson V, Γ_V its total fermionic decay width and $\delta_V = 2(1)$ for $V = W(Z)$.

The on-shell decay width is obtained by taking the limit $\Gamma_V m_V \to 0$ and recalling that in this case

$$\frac{1}{\pi} \frac{\Gamma_V m_V}{(p_i^2 - m_V^2)^2 + \Gamma_V^2 m_V^2} \to \delta(p_i^2 - m_V^2), \tag{B.12}$$

yielding

$$\Gamma(H_i \to VV) = \delta_V \frac{\sqrt{2} G_f m_{H_i}^3}{32\pi} |g_{H_i VV}|^2 \sqrt{1 - 4\frac{m_V^2}{m_{H_i}^2}} \left(1 - 4\frac{m_V^2}{m_{H_i}^2} + 12\frac{m_V^4}{m_{H_i}^4}\right) \tag{B.13}$$

for $m_{H_i} \geq 2m_V$.

$H_i \to \gamma\gamma$

The decay of a neutral Higgs to two photons is a loop mediated process with fermions, W bosons and charged scalars $H^\pm$ as mediators. Denoting the corresponding amplitudes by A_f, A_W and $A_{H^\pm}$, the decay width reads [228]

$$\Gamma(H_i \to \gamma\gamma) = \frac{\sqrt{2} G_f \alpha_{EW}^2 m_{H_i}^3}{256\pi^3} \left(|S_i^{\gamma\gamma}|^2 + |P_i^{\gamma\gamma}|^2\right), \tag{B.14}$$

with

$$\begin{aligned} S_i^{\gamma\gamma} &= \sum_f 2N_c Q_f^2 y_{f,i} A_{f(s)}(\tau_f) + g_{H_i WW} A_W(\tau_W) - g_{H_i H^+ H^-} \frac{v^2}{m_{H^\pm}^2} A_{H^\pm}(\tau_{H^\pm}), \\ P_i^{\gamma\gamma} &= \sum_f N_c Q_f^2 \widetilde{y}_{f,i} A_{f(p)}(\tau_f) \end{aligned} \tag{B.15}$$

the amplitudes for the decay of the scalar and pseudo-scalar components of H_i, respectively. Here $\tau_k \equiv m_{H_i}^2/(4m_k^2)$ and the 1-loop form factors are

$$\begin{aligned} A_W &= \left[-2\tau^2+3\tau+3(2\tau-1)f(\tau)\right]/\tau^2, \\ A_{H^\pm} &= -\left[\tau-f(\tau)\right]/\tau^2, \\ A_{f(s)} &= \left[\tau+(\tau-1)f(\tau)\right]/\tau^2, \\ A_{f(p)} &= f(\tau)/\tau, \end{aligned} \tag{B.16}$$

with $f(\tau)$ given in eq. (4.6).

$H_i \to Z\gamma$

Similarly to the digamma decay channel, the decay into $Z\gamma$ is given by [221] (see also [229])

$$\Gamma(H_i \to Z\gamma) = \frac{G_f^2\,\alpha_{EW}\,m_W^2 m_{H_i}^3}{64\pi^4}\left(1-\frac{m_Z^2}{m_{H_i}^2}\right)^3\left(\left|S_i^{Z\gamma}\right|^2+\left|P_i^{Z\gamma}\right|^2\right), \tag{B.17}$$

with

$$\begin{aligned} S_i^{Z\gamma} &= \sum_f 2N_c Q_f \frac{I_3^f-2Q_f s_W^2}{c_W}\,y_{f,i}\,A_{f(s)}^{Z\gamma}(\tau_f,\lambda_f) \\ &\quad + g_{H_iWW}\,A_W^{Z\gamma}(\tau_W,\lambda_W) - (2c_W^2-1)\,g_{H_iH^+H^-}\frac{v^2}{m_{H^\pm}^2}A_{H^\pm}^{Z\gamma}(\tau_{H^\pm},\lambda_{H^\pm}), \\ P_i^{\gamma\gamma} &= \sum_f 2N_c Q_f \frac{I_3^f-2Q_f s_W^2}{c_W}\,\widetilde{y}_{f,i}\,A_{f(p)}^{Z\gamma}(\tau_f,\lambda_f), \end{aligned} \tag{B.18}$$

for $\tau_i \equiv 4m_i^2/m_{H_i}^2$ and $\lambda_i \equiv 4m_i^2/m_Z^2$. The 1-loop form factors in this case read

$$\begin{aligned} A_{f(s)}^{Z\gamma}(\tau,\lambda) &= I_1(\tau,\lambda)-I_2(\tau,\lambda), \\ A_{f(p)}^{Z\gamma}(\tau,\lambda) &= I_2(\tau,\lambda), \\ A_W^{Z\gamma}(\tau,\lambda) &= c_W\left\{4\left(3-\frac{s_W^2}{c_W^2}\right)I_2(\tau,\lambda)+\left[\left(1+\frac{2}{\tau}\right)\frac{s_W^2}{c_W^2}-\left(5+\frac{2}{\tau}\right)\right]I_1(\tau,\lambda)\right\}, \\ A_{H^\pm}^{Z\gamma}(\tau,\lambda) &= I_1(\tau,\lambda), \end{aligned} \tag{B.19}$$

with the functions

$$\begin{aligned} g(\tau) &= (1-\tau)f'(\tau), \\ I_1(\tau,\lambda) &= \frac{\tau\lambda}{2(\tau-\lambda)}+\frac{\tau^2\lambda}{2(\tau-\lambda)^2}\left\{\tau\left[f(\tau^{-1})-f(\lambda^{-1})\right]+2\left[g(\tau^{-1})-g(\lambda^{-1})\right]\right\}, \\ I_2(\tau,\lambda) &= -\frac{\tau\lambda}{2(\tau-\lambda)}\left[f(\tau^{-1})-f(\lambda^{-1})\right]. \end{aligned} \tag{B.20}$$

$H_i \to gg$

Decays of a neutral scalar into pairs of gluons are mediated by quark loops, with a width [228, 221]

$$\Gamma(H_i \to gg) = \frac{\sqrt{2} G_f \alpha_s(\mu)^2 m_{H_i}^3}{128\pi^3} \left(\left| \sum_f y_{f,i} A_{f(s)}(\tau_f) \right|^2 K_s^{gg} + \left| \sum_f \widetilde{y}_{f,i} A_{f(p)}(\tau_f) \right|^2 K_p^{gg} \right), \quad \text{(B.21)}$$

where the renormalization scale is $\mu = m_{H_i}$ and K^{gg} are the relevant K-factors to account for higher order corrections, which must be taken into account since they can alter the result by up to 70%.

Expressions for the full NLO QCD corrections can be found in refs. [228, 221], but the various integrals involved are computationally expensive to calculate. We adopt here the alternative of implementing the K-factors obtained from an effective theory approach with the top-quark taken to be heavy (more precisely, $m_{H_i} \ll 2m_t$). In this approach we can obtain the K-factors at NNLO [231, 232],

$$\begin{aligned} K_s^{gg} = 1 + \frac{a_s(\mu)}{\pi}\left(\frac{95}{4} - \frac{7}{6}n_f\right) + \left(\frac{a_s(\mu)}{\pi}\right)^2 \Bigg[& \frac{149533}{288} - \frac{121}{16}\pi^2 - \frac{495}{8}\zeta_3 - \frac{19}{4}\log\left(\frac{m_t(\mu)}{m_{H_i}}\right) \\ & + n_l\left[-\frac{4157}{72} + \frac{11}{12}\pi^2 + \frac{5}{4}\zeta_3 - \frac{4}{3}\log\left(\frac{m_t(\mu)}{m_{H_i}}\right)\right] \\ & + n_l^2\left(\frac{127}{108} - \frac{\pi^2}{36}\right)\Bigg], \end{aligned}$$

$$\begin{aligned} K_p^{gg} = 1 + \frac{a_s(\mu)}{\pi}\left(\frac{97}{4} - \frac{7}{6}n_f\right) + \left(\frac{a_s(\mu)}{\pi}\right)^2 \Bigg[& \frac{51959}{96} - \frac{121}{16}\pi^2 - \frac{495}{8}\zeta_3 - \frac{19}{4}\log\left(\frac{m_t}{m_{H_i}}\right) \\ & + n_l\left[-\frac{473}{8} + \frac{11}{12}\pi^2 + \frac{5}{4}\zeta_3 - 2\log\left(\frac{m_t}{m_{H_i}}\right)\right] \\ & + n_l^2\left(\frac{251}{216} - \frac{\pi^2}{36}\right)\Bigg], \end{aligned}$$

where $m_t(\mu)$ is the running top mass at $\mu = m_{H_i}$ and $n_l = 5$ (since we are considering a theory with 5 effective flavours, the top-quark being integrated out). In principle one must be careful to use these expressions only in their region of validity, for Higgs masses well below the top-quark threshold. But it turns out that this is a good approximation for the full result for heavy scalars as well, with a mere 6% deviation when $m_{H_i} = 1$ TeV.

Decays into other scalars

The width for the decay of a scalar into another plus an off-shell gauge boson V is [233]

$$\Gamma(S_i \to S_j V) = \frac{m_i^3 |g_{S_i S_j V}|^2}{16\pi m_V^2} \int_0^{(1-\sqrt{k_H})^2} dx \frac{1}{\pi} \frac{\sqrt{w_V k_V}}{(x-k_V)^2 + w_V k_V} \lambda^{3/2}(k_H, x), \quad \text{(B.22)}$$

with $w_V = \Gamma_V^2/m_{S_i}^2$, $k_V = m_V^2/m_{S_i}^2$ and $k_H = m_{S_j}^2/m_{S_i}^2$. For the decay $S_i \to H^\pm W^\mp$ the above result must be multiplied by 2 to include the two possible final states (H^+W^- and H^-W^+).

As for the decay into two scalars, $H_i \to H_j H_k$, we consider only the on-shell width [227, 221]

$$\Gamma(H_i \to H_j H_k) = \frac{g_{H_i H_j H_k}}{32\pi\, m_{H_i}} \sqrt{\lambda(x_j, x_k)}, \tag{B.23}$$

with $x_{j,k} \equiv m_{H_{j,k}}/m_{H_i}$, neglecting cascade decays.

Appendix C

Electric dipole moments

In the case of a CP violating scalar sector one must also ensure that the resulting EDMs of particles, nucleons, atoms and molecules are still below the experimental bounds. In the 2HDM only six-dimensional effective operators can contribute to these effects, namely the EDM and cEDM operators [278, 279] as well as the Weinberg three-gluon operator [112],

$$\mathcal{L} \supset -i\sum_f \frac{d_f}{2}\bar{f}\sigma_{\mu\nu}\gamma_5 f F^{\mu\nu} - i\sum_f \frac{\widetilde{d}_f}{2} g_s \bar{f}\sigma_{\mu\nu}\gamma_5 f T^a G_a^{\mu\nu} + \frac{d_W}{6} f_{abc}\epsilon^{\mu\nu\rho\sigma} G^a_{\mu\lambda} G^{b\ \lambda}_{\nu} G^c_{\rho\sigma}. \quad \text{(C.1)}$$

It will be convenient to work with the dimensionless quantities

$$\delta_f \equiv \frac{d_f}{e}\frac{v^2}{m_f}, \qquad \widetilde{\delta}_f \equiv \widetilde{d}_f \frac{v^2}{m_f}, \qquad \delta_W \equiv d_W \frac{v^2}{g_s}. \quad \text{(C.2)}$$

The Weinberg operator originates from the diagram in fig. C.1 (right), the dominant contribution coming from a top running in the central loop, and its coefficient reads [112]

$$\delta_W = -\frac{g_s^2}{256\pi^4}\sum_{i=1,2,3} y_{u,i}\,\widetilde{y}_{u,i}\,h\left(\frac{m_i^2}{m_t^2}\right). \quad \text{(C.3)}$$

The coefficients $d_f, \widetilde{d}_f$ come from two-loop Barr-Zee diagrams shown in fig. C.1 (left and centre, respectively). In the cEDM case there are only contributions from quarks running in the loop and one has [278]

$$\widetilde{\delta}_f = -\frac{g_s^2}{128\pi^4}\sum_{\substack{q=t,b\\ i=1,2,3}} y_{q,i}\,\widetilde{y}_{f,i}\,f\left(\frac{m_q^2}{m_i^2}\right) + \widetilde{y}_{q,i}\,y_{f,i}\,g\left(\frac{m_q^2}{m_i^2}\right). \quad \text{(C.4)}$$

As for the effective EDM operator, the shaded blob in fig C.1 (left) represents effective vertices $h\gamma\gamma$ and $hZ\gamma$ with contributions from quarks, $W^\pm$ or $H^\pm$ running in the loop, as well as an effective vertex $H^\mp W^\pm\gamma$. These vertices and their contributions to the EDM

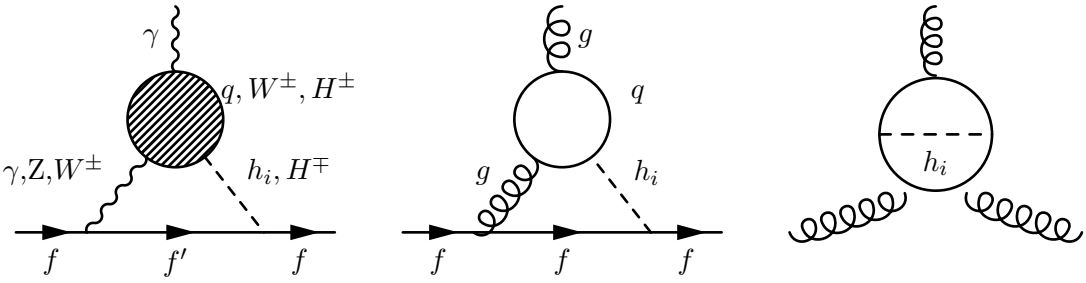

Figure C.1: Diagrams contributing to the fermionic EDM (left), cEDM (centre) and the Weinberg operator (right) in the 2HDM.

coefficient d_f have been computed in [278], yielding

$$(\delta_f)^q_{hV\gamma} = -\frac{g_{Vff}}{64\pi^4}\sum_{\substack{q=t,b\\ i=1,2,3}} N_c Q_q\, g_{Vqq}\left[y_{q,i}\,\widetilde{y}_{f,i}\hat{f}\left(\frac{m_q^2}{m_i^2},\frac{m_q^2}{m_V^2}\right)+\widetilde{y}_{q,i}\,y_{f,i}\,\hat{g}\left(\frac{m_q^2}{m_i^2},\frac{m_q^2}{m_V^2}\right)\right],$$

$$(\delta_f)^W_{hV\gamma} = \frac{g_{Vff}\,g_{VWW}}{256\pi^4}\sum_{i=1,2,3}\widetilde{y}_{f,i}\,g_{H_iWW}\left\{\left[6-\frac{m_V^2}{m_W^2}+\left(1-\frac{m_V^2}{2m_W^2}\right)\frac{m_i^2}{m_W^2}\right]\hat{f}\left(\frac{m_W^2}{m_i^2},\frac{m_W^2}{m_V^2}\right)\right.$$
$$\left.+\left[10-\frac{3m_V^2}{m_W^2}-\left(1-\frac{m_V^2}{2m_W^2}\right)\frac{m_i^2}{m_W^2}\right]\hat{g}\left(\frac{m_W^2}{m_i^2},\frac{m_W^2}{m_V^2}\right)\right\},$$

$$(\delta_f)^{H^\pm}_{hV\gamma} = -\frac{g_{Vff}\,g_{VH^+H^-}}{128\pi^4}\sum_{i=1,2,3}\widetilde{y}_{f,i}\left(\frac{g_{H_iH^+H^-}}{\sqrt{2}v}\right)\frac{v^2}{m_{H^\pm}^2}\left[\hat{f}\left(\frac{m_{H^\pm}^2}{m_i^2},\frac{m_{H^\pm}^2}{m_V^2}\right)\right.$$
$$\left.-\hat{g}\left(\frac{m_{H^\pm}^2}{m_i^2},\frac{m_{H^\pm}^2}{m_V^2}\right)\right],$$

$$(\delta_f)_{hH^\mp W^\pm} = -\frac{s_f}{512\pi^4}\sum_{i=1,2,3}\widetilde{y}_{f,i}\left[g_{H_iWW}\frac{g^2}{2}\mathcal{I}_4(m_i^2,m_{H^\pm}^2)+\frac{g_{H_iH^+H^-}}{\sqrt{2}v}\mathcal{I}_5(m_i^2,m_{H^\pm}^2)\right],$$

with all the functions involved defined in eqs. (C.12) and (C.13) below and with the couplings

$$\begin{aligned}
&g_{\gamma ff} = eQ_f, && g_{Zff} = \frac{g\,(T_{3,f}-2Q_f\sin^2\theta_W)}{2\cos\theta_W},\\
&g_{\gamma WW} = e, && g_{ZWW} = g\cos\theta_W,\\
&g_{\gamma H^+H^-} = e, && g_{ZH^+H^-} = g\,\frac{2\cos^2\theta_W-1}{2\cos\theta_W},\\
&s_f = \begin{cases} -1, & f = u,c,t\\ 1, & \text{otherwise}\end{cases}.
\end{aligned} \tag{C.5}$$

To obtain the coefficient of the EDM operator one must then sum all these contributions,

$$\delta_f = (\delta_f)_{hH^\mp W^\pm} + \sum_{V=\gamma,Z}\left[(\delta_f)^q_{hV\gamma}+(\delta_f)^W_{hV\gamma}+(\delta_f)^{H^\pm}_{hV\gamma}\right]. \tag{C.6}$$

To compute the neutron and atomic EDMs the coefficients in eqs. (C.4) and (C.6) must be runned from the electroweak scale $\Lambda_{\rm EW}\approx v$ down to the nuclear scale $\Lambda_n\simeq 1$ GeV.

Following [291] the RGEs read

$$\frac{d}{d\log\mu}\begin{pmatrix}\delta_f/Q_f\\ \widetilde{\delta}_f\\ \delta_W\end{pmatrix}=\frac{\alpha_s}{4\pi}\begin{pmatrix}32/3 & -32/3 & 0\\ 0 & 28/3 & 6\\ 0 & 0 & 14+4n_f(\mu)/3\end{pmatrix}\begin{pmatrix}\delta_f/Q_f\\ \widetilde{\delta}_f\\ \delta_W\end{pmatrix}. \tag{C.7}$$

At $\mu = m_b$, we impose the matching conditions [112]

$$\begin{aligned}
\widetilde{\delta}_b(m_b) &= \widetilde{\delta}_b - \frac{1}{8\pi^2}\log\frac{\Lambda_{\rm EW}}{m_b}\sum_{i=1,2,3}\frac{m_b^2(\Lambda_{\rm EW})}{m_i^2}\,y_{d,i}\,\widetilde{y}_{d,i},\\
\widetilde{\delta}_q(m_b) &= \widetilde{\delta}_q - \frac{g_s^2}{64\pi^4}\frac{m_b}{m_q}\left(\log\frac{\Lambda_{\rm EW}}{m_b}\right)^2\sum_{i=1,2,3}\frac{m_b(\Lambda_{\rm EW})\,m_q(\Lambda_{\rm EW})}{m_i^2}\left(y_{d,i}\,\widetilde{y}_{q,i}+\widetilde{y}_{d,i}\,y_{b,i}\right),\\
\delta_W(m_b) &= \delta_W - \frac{\alpha_s(m_b)}{8\pi}\widetilde{\delta}_b(m_b),
\end{aligned} \tag{C.8}$$

where the $\widetilde{\delta}_b(m_b)$ entering in the last equation is the shifted value obtained from the first one. These coefficients are then runned further from $\mu = m_b$ down to $\mu = \Lambda_n$.

Finally, the EDM of the neutron and mercury (Hg) can be written as [279, 112]

$$\begin{aligned}
\frac{d_n}{e} &= -(\zeta_n^u\,\delta_u+\zeta_n^d\,\delta_d)-(\widetilde{\zeta}_n^u\,\widetilde{\delta}_u+\widetilde{\zeta}_n^d\,\widetilde{\delta}_d)+\frac{2}{3}\frac{\beta_n^W}{e}\,\delta_W,\\
\frac{d_{\rm Hg}}{e} &= \kappa_S\frac{2\,m_n\,g_A}{F_\pi}\left\{\left(\frac{a_0}{e}\right)\left[-\widetilde{\eta}_0\left(\widetilde{\delta}_u+\widetilde{\delta}_d\right)+\frac{2\gamma_0}{3}\,\delta_W\right]\right.\\
&\qquad\left.+\left(\frac{a_1}{e}\right)\left[-\widetilde{\eta}_1\left(\widetilde{\delta}_u-\widetilde{\delta}_d\right)+\frac{2\gamma_1}{3}\,\delta_W\right]\right\},
\end{aligned} \tag{C.9}$$

with [279]

$$\begin{aligned}
\zeta_n^u &= 0.82\times10^{-21}\,\text{cm}, & \zeta_n^d &= -3.3\times10^{-21}\,\text{cm},\\
\widetilde{\zeta}_n^u &= 0.82\times10^{-21}\,\text{cm}, & \widetilde{\zeta}_n^d &= 1.63\times10^{-21}\,\text{cm},\\
\beta_n^W &= 2.0\times10^{-20}\,e\cdot\text{cm}, & g_A &= 1.26,\\
\kappa_S\cdot a_0 &= -2.8\times10^{-19}\,e\cdot\text{cm}, & \kappa_S\cdot a_1 &= \mp5.6\times10^{-19}\,e\cdot\text{cm},\\
m_n &= 939.565379\,\text{MeV}, & F_\pi &= 186\,\text{MeV},\\
\widetilde{\eta}_1 &= 2\widetilde{\eta}_0 = -4\times10^{-7}, & \gamma_0 &= \gamma_1 = 2\times10^{-6}.
\end{aligned} \tag{C.10}$$

The results should be compared to the experimental bounds for the EDMs of the electron, neutron and Hg atom [280, 281, 282],

$$\begin{aligned}
|d_e| &< 8.7\times10^{-29}\ e\cdot\text{cm},\\
|d_n| &< 2.9\times10^{-26}\ e\cdot\text{cm},\\
|d_{\rm Hg}| &< 3.1\times10^{-29}\ e\cdot\text{cm}.
\end{aligned} \tag{C.11}$$

The functions involved in the computations above are

$$h(z) = \frac{z^4}{2}\int_0^1 dx \int_0^1 dy\, \frac{x^3y^3(1-x)}{\left[z^2x(1-xy)+(1-x)(1-y)\right]^2},$$

$$f(z) \equiv \frac{z}{2}\int_0^1 dx\, \frac{1-2x(1-x)}{x(1-x)-z}\log\left(\frac{x(1-x)}{z}\right),$$

$$g(z) \equiv \frac{z}{2}\int_0^1 dz\, \frac{1}{x(1-x)-z}\log\left(\frac{x(1-x)}{z}\right), \tag{C.12}$$

$$I_4(m^2_{H^\pm}, m_1^2, m_h^2) \equiv \int_0^1 dx\,(1-x)^2\left(x-4+\frac{m^2_{H^\pm}-m_h^2}{m_W^2}x\right) \times \frac{m_1^2}{m_W^2(1-x)+m_h^2x-m_1^2x(1-x)}\log\left(\frac{m_W^2(1-x)+m_h^2x}{m_1^2x(1-x)}\right),$$

$$I_5(m^2_{H^\pm}, m_1^2, m_h^2) \equiv 2\int_0^1 dx\, \frac{m_1^2x(1-x)^2}{m^2_{H^\pm}(1-x)+m_h^2x-m_1^2x(1-x)}\log\left(\frac{m^2_{H^\pm}(1-x)+m_h^2x}{m_1^2x(1-x)}\right),$$

and

$$\hat{f}(x,y) \equiv \frac{x\,f(y)-y\,f(x)}{x-y},$$

$$\hat{g}(x,y) \equiv \frac{x\,g(y)-y\,g(x)}{x-y}, \tag{C.13}$$

$$\mathcal{I}_{4(5)}(m_h^2, m^2_{H^\pm}) \equiv \frac{m_W^2}{m^2_{H^\pm}-m_W^2}\left[I_{4(5)}(m^2_{H^\pm}, m_W^2, m_h^2) - I_{4(5)}(m^2_{H^\pm}, m^2_{H^\pm}, m_h^2)\right].$$

Notice that

$$\lim_{z\to\infty} f'(z) = 0, \tag{C.14}$$

so that

$$\lim_{y\to\infty} \hat{f}(x,y) = f(x). \tag{C.15}$$

Bibliography

[1] C. D. Anderson, "*The Positive Electron* ", *Phys. Rev.* **43** (1933) 491–494.

[2] G. Steigman, "*Observational tests of antimatter cosmologies* ", *Ann.Rev.Astron.Astrophys.* **14** (1976) 339–372.

[3] **AMS** , J. Alcaraz et al., "*Search for anti-helium in cosmic rays* ", *Phys.Lett.* **B461** (1999) 387–396, [hep-ex/0002048].

[4] K. Abe, H. Fuke, S. Haino, T. Hams, M. Hasegawa, et al., "*Search for Antihelium with the BESS-Polar Spectrometer* ", *Phys.Rev.Lett.* **108** (2012) 131301, [arXiv:1201.2967].

[5] A. G. Cohen, A. De Rujula, and S. Glashow, "*A matter - antimatter universe?* ", *Astrophys.J.* **495** (1998) 539–549, [astro-ph/9707087].

[6] **WMAP9** , G. Hinshaw et al., "*Nine-year Wilkinson Microwave Anisotropy Probe (WMAP) Observations: Cosmological Parameter Results* ", *The Astrophysical Journal Supplement Series* **208** (Oct., 2013) 19, [arXiv:1212.5226].

[7] **Planck** , P. Ade et al., "*Planck 2013 results. XVI. Cosmological parameters* ", *Astron.Astrophys.* **571** (2014) A16, [arXiv:1303.5076].

[8] L. Canetti, M. Drewes, and M. Shaposhnikov, "*Matter and antimatter in the Universe* ", *New J.Phys.* **14** (2012) 095012, [arXiv:1204.4186].

[9] A. Sakharov, "*Violation of CP invariance, C asymmetry, and baryon asymmetry of the Universe* ", *Pisma Zh.Eksp.Teor.Fiz.* **5** (1967) 32–35.

[10] N. Cabibbo, "*Unitary symmetry and leptonic decays* ", *Phys.Rev.Lett.* **10** (1963) 531–533.

[11] M. Kobayashi and T. Maskawa, "*CP violation in the renormalizable theory of weak interaction* ", *Prog.Theor.Phys.* **49** (1973) 652–657.

[12] A. Rasin, "*Diagonalization of quark mass matrices and the Cabibbo-Kobayashi-Maskawa matrix* ", hep-ph/9708216.

[13] J. Christenson, J. Cronin, V. Fitch, and R. Turlay, "*Evidence for the* 2π *Decay of the* K_2^0 *Meson* ", *Phys.Rev.Lett.* **13** (1964) 138–140.

[14] G. D'Ambrosio and G. Isidori, "*CP violation in kaon decays* ", *Int.J.Mod.Phys.* **A13** (1998) 1–94, [hep-ph/9611284].

[15] A. Liddle, "*An introduction to modern cosmology", 2nd ed.* Wiley, Chichester, 2003.

[16] M. Gockeler, R. Horsley, A. Irving, D. Pleiter, P. Rakow, et al., "*A Determination of the Lambda parameter from full lattice QCD* ", *Phys.Rev.* **D73** (2006) 014513, [hep-ph/0502212].

[17] G. W. Anderson and L. J. Hall, "*The electroweak phase transition and baryogenesis* ", *Phys.Rev.* **D45** (1992) 2685–2698.

[18] D. Kirzhnits and A. D. Linde, "*Macroscopic Consequences of the Weinberg Model* ", *Phys.Lett.* **B42** (1972) 471–474.

[19] D. Kirzhnits and A. D. Linde, "*Symmetry behavior in gauge theories* ", *Annals Phys.* **101** (1976) 195–238.

[20] J. Bell and R. Jackiw, "*A PCAC puzzle:* $\pi^0 \to \gamma\gamma$ *in the sigma model* ", *Nuovo Cim.* **A60** (1969) 47–61.

[21] S. L. Adler, "*Axial vector vertex in spinor electrodynamics* ", *Phys.Rev.* **177** (1969) 2426–2438.

[22] R. Jackiw and C. Rebbi, "*Vacuum periodicity in a Yang-Mills quantum theory* ", *Phys.Rev.Lett.* **37** (1976) 172–175.

[23] J. Callan, Curtis G., R. Dashen, and D. J. Gross, "*The Structure of the Gauge Theory Vacuum* ", *Phys. Lett.* **B63** (1976) 334–340.

[24] A. G. Cohen, D. B. Kaplan and A. E. Nelson, "*Progress in electroweak baryogenesis* ", *Ann. Rev. Nucl. Part. Sci.* **43** (1993) 27 [hep-ph/9302210].

[25] S. R. Coleman, "*The fate of the false vacuum. 1. Semiclassical theory* ", *Phys.Rev.* **D15** (1977) 2929–2936.

[26] G. 't Hooft, "*Symmetry breaking through Bell-Jackiw anomalies* ", *Phys.Rev.Lett.* **37** (1976) 8–11.

[27] V. Kuzmin, V. Rubakov, and M. Shaposhnikov, "*On the Anomalous Electroweak Baryon Number Nonconservation in the Early Universe* ", *Phys. Lett.* **B155** (1985) 36.

[28] P. B. Arnold and L. D. McLerran, "*Sphalerons, Small Fluctuations and Baryon Number Violation in Electroweak Theory* ", *Phys.Rev.* **D36** (1987) 581.

[29] A. D. Linde, "*Fate of the false vacuum at finite temperature: theory and applications* ", *Phys. Lett.* **B100** (1981) 37.

[30] F. R. Klinkhamer and N. Manton, "*A Saddle Point Solution in the Weinberg-Salam Theory* ", *Phys.Rev.* **D30** (1984) 2212.

[31] S. Y. Khlebnikov and M. Shaposhnikov, "*The Statistical Theory of Anomalous Fermion Number Nonconservation* ", *Nucl.Phys.* **B308** (1988) 885–912.

[32] J. Ambjorn, T. Askgaard, H. Porter, and M. Shaposhnikov, "*Sphaleron transitions and baryon asymmetry: A Numerical real time analysis*", *Nucl.Phys.* **B353** (1991) 346–378.

[33] M. D'Onofrio, K. Rummukainen, and A. Tranberg, "*The Sphaleron Rate in the Minimal Standard Model*", *Phys.Rev.Lett.* **113** (2014) 141602, [arXiv:1404.3565].

[34] M. Quiros, "*Field theory at finite temperature and phase transitions*", *Helv.Phys.Acta* **67** (1994) 451–583.

[35] G. D. Moore, "*Measuring the broken phase sphaleron rate nonperturbatively*", *Phys.Rev.* **D59** (1999) 014503, [hep-ph/9805264].

[36] K. Kajantie, M. Laine, K. Rummukainen, and M. E. Shaposhnikov, "*Is there a hot electroweak phase transition at m(H) larger or equal to m(W)?*", *Phys.Rev.Lett.* **77** (1996) 2887–2890, [hep-ph/9605288].

[37] F. Karsch, T. Neuhaus, A. Patkos, and J. Rank, "*Critical Higgs mass and temperature dependence of gauge boson masses in the SU(2) gauge Higgs model*", *Nucl.Phys.Proc.Suppl.* **53** (1997) 623–625, [hep-lat/9608087].

[38] F. Csikor, Z. Fodor, and J. Heitger, "*Endpoint of the hot electroweak phase transition*", *Phys.Rev.Lett.* **82** (1999) 21–24, [hep-ph/9809291].

[39] Y. Aoki, F. Csikor, Z. Fodor, and A. Ukawa, "*The endpoint of the first order phase transition of the SU(2) gauge Higgs model on a four-dimensional isotropic lattice*", *Phys.Rev.* **D60** (1999) 013001, [hep-lat/9901021].

[40] **ATLAS Collaboration** , G. Aad et al., "*Observation of a new particle in the search for the Standard Model Higgs boson with the ATLAS detector at the LHC*", *Phys. Lett.* **B716** (2012) 1–29, [arXiv:1207.7214].

[41] **CMS Collaboration** , S. Chatrchyan et al., "*Observation of a new boson at a mass of 125 GeV with the CMS experiment at the LHC*", *Phys. Lett.* **B716** (2012) 30–61, [arXiv:1207.7235].

[42] M. Gavela, P. Hernandez, J. Orloff, and O. Pene, "*Standard model CP violation and baryon asymmetry*", *Mod.Phys.Lett.* **A9** (1994) 795–810, [hep-ph/9312215].

[43] C. Jarlskog, "*Commutator of the Quark Mass Matrices in the Standard Electroweak Model and a Measure of Maximal CP Violation*", *Phys.Rev.Lett.* **55** (1985) 1039.

[44] **Particle Data Group** , K. Olive et al., "*Review of Particle Physics*", *Chin.Phys.* **C38** (2014) 090001.

[45] C. Jarlskog and R. Stora, "*Unitarity Polygons and CP Violation Areas and Phases in the Standard Electroweak Model*", *Phys.Lett.* **B208** (1988) 268.

[46] G. R. Farrar and M. Shaposhnikov, "*Baryon asymmetry of the universe in the standard electroweak theory*", *Phys.Rev.* **D50** (1994) 774, [hep-ph/9305275].

[47] M. Gavela, P. Hernandez, J. Orloff, O. Pene, and C. Quimbay, "*Standard model CP violation and baryon asymmetry. Part 2: Finite temperature*", *Nucl.Phys.* **B430** (1994) 382–426, [hep-ph/9406289].

[48] P. Huet and E. Sather, "*Electroweak baryogenesis and standard model CP violation*", *Phys.Rev.* **D51** (1995) 379–394, [hep-ph/9404302].

[49] A. Tranberg, A. Hernandez, T. Konstandin, and M. G. Schmidt, "*Cold electroweak baryogenesis with Standard Model CP violation*", *Phys.Lett.* **B690** (2010) 207–212, [arXiv:0909.4199].

[50] A. Hernandez, T. Konstandin, and M. G. Schmidt, "*Sizable CP Violation in the Bosonized Standard Model*", *Nucl.Phys.* **B812** (2009) 290–300, [arXiv:0810.4092].

[51] G. Jungman, M. Kamionkowski, and K. Griest, "*Supersymmetric dark matter*", *Phys. Rept.* **267** (1996) 195–373, [hep-ph/9506380].

[52] N. Arkani-Hamed, S. Dimopoulos, and G. R. Dvali, "*The Hierarchy problem and new dimensions at a millimeter*", *Phys. Lett.* **B429** (1998) 263–272, [hep-ph/9803315].

[53] L. Randall and R. Sundrum, "*A Large mass hierarchy from a small extra dimension*", *Phys. Rev. Lett.* **83** (1999) 3370–3373, [hep-ph/9905221].

[54] A. Pilaftsis, "*CP violation and baryogenesis due to heavy Majorana neutrinos*", *Phys.Rev.* **D56** (1997) 5431–5451, [hep-ph/9707235].

[55] W. Buchmuller, R. Peccei, and T. Yanagida, "*Leptogenesis as the origin of matter*", *Ann.Rev.Nucl.Part.Sci.* **55** (2005) 311–355, [hep-ph/0502169].

[56] G. 't Hooft, "*Naturalness, chiral symmetry, and spontaneous chiral symmetry breaking*", *NATO Sci. Ser. B* **59** (1980) 135.

[57] K. S. Babu, "*TASI Lectures on Flavor Physics*", in *Proceedings of Theoretical Advanced Study Institute in Elementary Particle Physics on The dawn of the LHC era (TASI 2008)*, pp. 49–123, 2010. arXiv:0910.2948.

[58] R. N. Mohapatra and G. Senjanovic, "*Neutrino Mass and Spontaneous Parity Violation*", *Phys. Rev. Lett.* **44** (1980) 912.

[59] J. Schechter and J. W. F. Valle, "*Neutrino Masses in $SU(2) \times U(1)$ Theories*", *Phys. Rev.* **D22** (1980) 2227.

[60] W. Rodejohann, "*Neutrino-less Double Beta Decay and Particle Physics*", *Int. J. Mod. Phys.* **E20** (2011) 1833–1930, [arXiv:1106.1334].

[61] M. Fukugita and T. Yanagida, "*Baryogenesis Without Grand Unification*", *Phys. Lett.* **B174** (1986) 45.

[62] G. R. Farrar and M. Shaposhnikov, "*Baryon asymmetry of the universe in the minimal Standard Model*", *Phys.Rev.Lett.* **70** (1993) 2833–2836, [hep-ph/9305274].

[63] A. G. Cohen, D. Kaplan, and A. Nelson, "*Spontaneous baryogenesis at the weak phase transition* ", *Phys. Lett.* **B263** (1991) 86–92.

[64] A. G. Cohen, D. B. Kaplan, and A. E. Nelson, "*Weak scale baryogenesis* ", *Phys. Lett.* **B245** (1990) 561–564.

[65] M. Joyce, T. Prokopec, and N. Turok, "*Electroweak baryogenesis from a classical force* ", *Phys.Rev.Lett.* **75** (1995) 1695–1698, [hep-ph/9408339].

[66] M. Joyce, T. Prokopec, and N. Turok, "*Nonlocal electroweak baryogenesis. Part 1: Thin wall regime* ", *Phys.Rev.* **D53** (1996) 2930–2957, [hep-ph/9410281].

[67] M. Joyce, T. Prokopec, and N. Turok, "*Nonlocal electroweak baryogenesis. Part 2: The Classical regime* ", *Phys.Rev.* **D53** (1996) 2958–2980, [hep-ph/9410282].

[68] D. E. Morrissey and M. J. Ramsey-Musolf, "*Electroweak baryogenesis* ", *New J.Phys.* **14** (2012) 125003, [arXiv:1206.2942].

[69] J. Espinosa, M. Quiros, and F. Zwirner, "*On the electroweak phase transition in the minimal supersymmetric Standard Model* ", *Phys. Lett.* **B307** (1993) 106–115, [hep-ph/9303317].

[70] M. S. Carena, M. Quiros, and C. Wagner, "*Opening the window for electroweak baryogenesis* ", *Phys. Lett.* **B380** (1996) 81–91, [hep-ph/9603420].

[71] A. Davies, C. Froggatt, and R. Moorhouse, "*Electroweak baryogenesis in the next-to-minimal supersymmetric model* ", *Phys. Lett.* **B372** (1996) 88–94, [hep-ph/9603388].

[72] J. M. Cline and G. D. Moore, "*Supersymmetric electroweak phase transition: Baryogenesis versus experimental constraints* ", *Phys.Rev.Lett.* **81** (1998) 3315–3318, [hep-ph/9806354].

[73] K. Funakubo, S. Otsuki, and F. Toyoda, "*Transitional CP violation in the MSSM and electroweak baryogenesis* ", *Prog.Theor.Phys.* **102** (1999) 389–406, [hep-ph/9903276].

[74] F. Csikor, Z. Fodor, P. Hegedus, A. Jakovac, S. Katz, et al., "*Electroweak phase transition in the MSSM: 4-Dimensional lattice simulations* ", *Phys.Rev.Lett.* **85** (2000) 932–935, [hep-ph/0001087].

[75] M. Carena, G. Nardini, M. Quiros, and C. E. Wagner, "*MSSM Electroweak Baryogenesis and LHC Data* ", *JHEP* **1302** (2013) 001, [arXiv:1207.6330].

[76] D. Curtin, P. Jaiswal, and P. Meade, "*Excluding Electroweak Baryogenesis in the MSSM* ", *JHEP* **1208** (2012) 005, [arXiv:1203.2932].

[77] J. Kozaczuk, "*Bubble Expansion and the Viability of Singlet-Driven Electroweak Baryogenesis* ", arXiv:1506.0474.

[78] S. Profumo, M. J. Ramsey-Musolf, and G. Shaughnessy, "*Singlet Higgs phenomenology and the electroweak phase transition* ", *JHEP* **0708** (2007) 010, [arXiv:0705.2425].

[79] S. Profumo, M. J. Ramsey-Musolf, C. L. Wainwright, and P. Winslow, "*Singlet-Catalyzed Electroweak Phase Transitions and Precision Higgs Studies* ", arXiv:1407.5342.

[80] L. D. McLerran, M. E. Shaposhnikov, N. Turok, and M. B. Voloshin, "*Why the baryon asymmetry of the universe is approximately* 10^{-10} ", *Phys. Lett.* **B256** (1991) 451–456.

[81] N. Turok and J. Zadrozny, "*Electroweak baryogenesis in the two doublet model* ", *Nucl.Phys.* **B358** (1991) 471–493.

[82] J. M. Cline and P.-A. Lemieux, "*Electroweak phase transition in two Higgs doublet models* ", *Phys.Rev.* **D55** (1997) 3873–3881, [hep-ph/9609240].

[83] L. Fromme, S. J. Huber, and M. Seniuch, "*Baryogenesis in the two-Higgs doublet model* ", *JHEP* **0611** (2006) 038, [hep-ph/0605242].

[84] J. M. Cline, K. Kainulainen, and M. Trott, "*Electroweak baryogenesis in two Higgs doublet models and B meson anomalies* ", *JHEP* **1111** (2011) 089, [arXiv:1107.3559].

[85] G. C. Dorsch, S. J. Huber, and J. M. No, "*A strong electroweak phase transition in the 2HDM after LHC8* ", *JHEP* **1310** (2013) 029, [arXiv:1305.6610].

[86] G. Dorsch, S. Huber, K. Mimasu, and J. No, "*Echoes of the Electroweak Phase Transition: Discovering a second Higgs doublet through* $A_0 \to ZH_0$ ", *Phys.Rev.Lett.* **113** (2014), no. 21 211802, [arXiv:1405.5537].

[87] R. D. Peccei, "*The Strong CP problem and axions* ", *Lect. Notes Phys.* **741** (2008) 3–17, [hep-ph/0607268].

[88] C. D. Froggatt and H. B. Nielsen, "*Hierarchy of Quark Masses, Cabibbo Angles and CP Violation* ", *Nucl. Phys.* **B147** (1979) 277.

[89] H. P. Nilles, "*Supersymmetry, Supergravity and Particle Physics* ", *Phys.Rept.* **110** (1984) 1–162.

[90] S. P. Martin, "*A Supersymmetry primer* ", hep-ph/9709356, [Adv. Ser. Direct. High Energy Phys.18, 1 (1998)].

[91] R. Contino, "*The Higgs as a Composite Nambu-Goldstone Boson* ", in *Physics of the large and the small, TASI 09, proceedings of the Theoretical Advanced Study Institute in Elementary Particle Physics, Boulder, Colorado, USA, 1-26 June 2009*, pp. 235–306, 2011. arXiv:1005.4269.

[92] B. Bellazzini, C. Cski, and J. Serra, "*Composite Higgses* ", *Eur. Phys. J.* **C74** (2014), no. 5 2766, [arXiv:1401.2457].

[93] J. E. Kim, "*Light Pseudoscalars, Particle Physics and Cosmology* ", *Phys. Rept.* **150** (1987) 1–177.

[94] R. Barbieri, L. J. Hall, and V. S. Rychkov, "*Improved naturalness with a heavy Higgs: An Alternative road to LHC physics* ", *Phys. Rev.* **D74** (2006) 015007, [hep-ph/0603188].

[95] N. Blinov, S. Profumo, and T. Stefaniak, "*The Electroweak Phase Transition in the Inert Doublet Model*", arXiv:1504.0594.

[96] E. Ma, "*Verifiable radiative seesaw mechanism of neutrino mass and dark matter*", *Phys. Rev.* **D73** (2006) 077301, [hep-ph/0601225].

[97] G. Branco, P. Ferreira, L. Lavoura, M. Rebelo, M. Sher, et al., "*Theory and phenomenology of two-Higgs-doublet models*", *Phys.Rept.* **516** (Dec., 2012) 1–102, [arXiv:1106.0034].

[98] M. Aoki, S. Kanemura, K. Tsumura, and K. Yagyu, "*Models of Yukawa interaction in the two Higgs doublet model, and their collider phenomenology*", *Phys.Rev.* **D80** (2009) 015017, [arXiv:0902.4665].

[99] O. Deschamps, S. Descotes-Genon, S. Monteil, V. Niess, S. T'Jampens, et al., "*The two Higgs doublet of Type II facing flavour physics data*", *Phys.Rev.* **D82** (2010) 073012, [arXiv:0907.5135].

[100] P. Ferreira and D. Jones, "*Bounds on scalar masses in two Higgs doublet models*", *JHEP* **0908** (2009) 069, [arXiv:0903.2856].

[101] M. Jung, A. Pich, and P. Tuzon, "*Charged-Higgs phenomenology in the Aligned two-Higgs-doublet model*", *JHEP* **1011** (2010) 003, [arXiv:1006.0470].

[102] A. Arhrib, P. Ferreira, and R. Santos, "*Are There Hidden Scalars in LHC Higgs Results?*", arXiv:1311.1520.

[103] C.-Y. Chen, S. Dawson, and M. Sher, "*Heavy Higgs Searches and Constraints on Two Higgs Doublet Models*", *Phys.Rev.* **D88** (2013) 015018, [arXiv:1305.1624].

[104] N. Craig, J. Galloway, and S. Thomas, "*Searching for Signs of the Second Higgs Doublet*", arXiv:1305.2424.

[105] B. Grinstein and P. Uttayarat, "*Carving Out Parameter Space in Type-II Two Higgs Doublets Model*", *JHEP* **1306** (2013) 094, [arXiv:1304.0028].

[106] N. Craig, F. D'Eramo, P. Draper, S. Thomas, and H. Zhang, "*The Hunt for the Rest of the Higgs Bosons*", arXiv:1504.0463.

[107] B. Coleppa, F. Kling, and S. Su, "*Exotic decays of a heavy neutral Higgs through HZ/AZ channel*", arXiv:1404.1922.

[108] V. Barger, L. L. Everett, C. B. Jackson, A. D. Peterson, and G. Shaughnessy, "*Measuring the 2HDM Scalar Potential at LHC14*", *Phys.Rev.* **D90** (2014) 095006, [arXiv:1408.2525].

[109] P. B. Dev and A. Pilaftsis, "*Maximally Symmetric Two Higgs Doublet Model with Natural Standard Model Alignment*", *JHEP* **1412** (2014) 024, [arXiv:1408.3405].

[110] M. Jung and A. Pich, "*Electric Dipole Moments in Two-Higgs-Doublet Models*", *JHEP* **1404** (2014) 076, [arXiv:1308.6283].

[111] S. Ipek, "*A Perturbative Analysis of Electron EDM and CP Violation in Two Higgs Doublet Models* ", arXiv:1310.6790.

[112] S. Inoue, M. J. Ramsey-Musolf, and Y. Zhang, "*CPV Phenomenology of Flavor Conserving Two Higgs Doublet Models* ", arXiv:1403.4257.

[113] L. Fromme and S. J. Huber, "*Top transport in electroweak baryogenesis* ", *JHEP* **0703** (2007) 049, [hep-ph/0604159].

[114] I. F. Ginzburg and M. Krawczyk, "*Symmetries of two Higgs doublet model and CP violation* ", *Phys.Rev.* **D72** (2005) 115013, [hep-ph/0408011].

[115] S. Davidson and H. E. Haber, "*Basis-independent methods for the two-Higgs-doublet model* ", *Phys.Rev.* **D72** (2005) 035004; Erratum–ibid. D72 (2005) 099902, [hep-ph/0504050].

[116] H. E. Haber and D. O'Neil, "*Basis-independent methods for the two-Higgs-doublet model. II. The Significance of tan beta* ", *Phys.Rev.* **D74** (2006) 015018, [hep-ph/0602242].

[117] G. C. Branco, M. Rebelo, and J. Silva-Marcos, "*CP-odd invariants in models with several Higgs doublets* ", *Phys. Lett.* **B614** (2005) 187–194, [hep-ph/0502118].

[118] J. F. Gunion and H. E. Haber, "*Conditions for CP-violation in the general two-Higgs-doublet model* ", *Phys.Rev.* **D72** (2005) 095002, [hep-ph/0506227].

[119] G. Branco, W. Grimus, and L. Lavoura, "*Relating the scalar flavor changing neutral couplings to the CKM matrix* ", *Phys. Lett.* **B380** (1996) 119–126, [hep-ph/9601383].

[120] G. D'Ambrosio, G. Giudice, G. Isidori, and A. Strumia, "*Minimal flavor violation: an effective field theory approach* ", *Nucl.Phys.* **B645** (2002) 155–187, [hep-ph/0207036].

[121] F. Botella, G. Branco, and M. Rebelo, "*Minimal flavour violation and multi-Higgs models* ", *Phys. Lett.* **B687** (2010) 194–200, [arXiv:0911.1753].

[122] A. J. Buras, M. V. Carlucci, S. Gori, and G. Isidori, "*Higgs-mediated FCNCs: Natural Flavour Conservation vs. Minimal Flavour Violation* ", *JHEP* **1010** (2010) 009, [arXiv:1005.5310].

[123] A. Pich and P. Tuzon, "*Yukawa alignment in the two-Higgs-doublet model* ", *Phys.Rev.* **D80** (2009) 091702, [arXiv:0908.1554].

[124] T. Cheng and M. Sher, "*Mass Matrix Ansatz and Flavor Nonconservation in Models with Multiple Higgs Doublets* ", *Phys.Rev.* **D35** (1987) 3484.

[125] P. Ferreira, L. Lavoura, and J. P. Silva, "*Renormalization-group constraints on Yukawa alignment in multi-Higgs-doublet models* ", *Phys.Lett.* **B688** (2010) 341–344, [arXiv:1001.2561].

[126] S. L. Glashow and S. Weinberg, "*Natural conservation laws for neutral currents* ", *Phys.Rev.* **D15** (1977) 1958.

[127] J. Diaz-Cruz and A. Mendez, "*Vacuum alignment in multiscalar models*", *Nucl.Phys.* **B380** (1992) 39–50.

[128] G. Branco and M. Rebelo, "*The Higgs mass in a model with two scalar doublets and spontaneous CP violation*", *Phys. Lett.* **B160** (1985) 117.

[129] Y. B. Zeldovich, I. Yu. Kobzarev, and L. B. Okun, "*Cosmological Consequences of the Spontaneous Breakdown of Discrete Symmetry*", *Zh. Eksp. Teor. Fiz.* **67** (1974) 3–11. [Sov. Phys. JETP40,1(1974)].

[130] J. Preskill, S. P. Trivedi, F. Wilczek, and M. B. Wise, "*Cosmology and broken discrete symmetry*", *Nucl. Phys.* **B363** (1991) 207–220.

[131] G. Jona-Lasinio, "*Relativistic field theories with symmetry breaking solutions*", *Nuovo Cim.* **34** (1964) 1790–1795.

[132] S. R. Coleman and E. J. Weinberg, "*Radiative Corrections as the Origin of Spontaneous Symmetry Breaking*", *Phys.Rev.* **D7** (1973) 1888–1910.

[133] P. A. M. Dirac, "*The Lagrangian in quantum mechanics*", *Phys.Z.Sowjetunion* **3** (1933) 64–72.

[134] P. A. M. Dirac, "*The Principles of Quantum Mechanics*". International Series of Monographs on Physics. Oxford University Press, fourth ed., 1958.

[135] M. E. Peskin and D. V. Schroeder, "*An Introduction to Quantum Field Theory*". Westview Press, first ed., 1995.

[136] R. Jackiw, "*Functional evaluation of the effective potential*", *Phys.Rev.* **D9** (1974) 1686.

[137] K. Wilson and J. B. Kogut, "*The Renormalization group and the epsilon expansion*", *Phys.Rept.* **12** (1974) 75–200.

[138] L. Dolan and R. Jackiw, "*Symmetry behavior at finite temperature*", *Phys.Rev.* **D9** (1974) 3320–3341.

[139] J. Elias-Miro, J. R. Espinosa, and T. Konstandin, "*Taming Infrared Divergences in the Effective Potential*", *JHEP* **08** (2014) 034, [arXiv:1406.2652].

[140] S. P. Martin, "*Taming the Goldstone contributions to the effective potential*", *Phys.Rev.* **D90** (2014), no. 1 016013, [arXiv:1406.2355].

[141] I. Krive and A. D. Linde, "*On the Vacuum Stability Problem in Gauge Theories*", *Nucl.Phys.* **B117** (1976) 265.

[142] H. D. Politzer and S. Wolfram, "*Bounds on Particle Masses in the Weinberg-Salam Model*", *Phys.Lett.* **B82** (1979) 242–246.

[143] M. Sher, "*Electroweak Higgs Potentials and Vacuum Stability*", *Phys.Rept.* **179** (1989) 273–418.

[144] M. Lindner, M. Sher, and H. W. Zaglauer, "*Probing Vacuum Stability Bounds at the Fermilab Collider* ", *Phys.Lett.* **B228** (1989) 139.

[145] M. Sher, "*Precise vacuum stability bound in the standard model* ", *Phys.Lett.* **B317** (1993) 159–163, [hep-ph/9307342].

[146] J. Espinosa and M. Quiros, "*Improved metastability bounds on the standard model Higgs mass* ", *Phys.Lett.* **B353** (1995) 257–266, [hep-ph/9504241].

[147] G. Degrassi, S. Di Vita, J. Elias-Miro, J. R. Espinosa, G. F. Giudice, et al., "*Higgs mass and vacuum stability in the Standard Model at NNLO* ", *JHEP* **1208** (2012) 098, [arXiv:1205.6497].

[148] K. Klimenko, "*On Necessary and Sufficient Conditions for Some Higgs Potentials to Be Bounded From Below* ", *Theor.Math.Phys.* **62** (1985) 58–65.

[149] M. Maniatis, A. von Manteuffel, O. Nachtmann, and F. Nagel, "*Stability and symmetry breaking in the general two-Higgs-doublet model* ", *Eur.Phys.J.* **C48** (2006) 805–823, [hep-ph/0605184].

[150] J. Velhinho, R. Santos, and A. Barroso, "*Tree level vacuum stability in two Higgs doublet models* ", *Phys. Lett.* **B322** (1994) 213–218.

[151] A. Barroso, P. Ferreira, and R. Santos, "*Neutral minima in two-Higgs doublet models* ", *Phys. Lett.* **B652** (2007) 181–193, [hep-ph/0702098].

[152] I. Ginzburg and K. Kanishev, "*Different vacua in 2HDM* ", *Phys.Rev.* **D76** (2007) 095013, [arXiv:0704.3664].

[153] I. P. Ivanov, "*Minkowski space structure of the Higgs potential in 2HDM. II. Minima, symmetries, and topology* ", *Phys.Rev.* **D77** (2008) 015017, [arXiv:0710.3490].

[154] P. M. Ferreira, R. Santos, and A. Barroso, "*Stability of the tree-level vacuum in two Higgs doublet models against charge or CP spontaneous violation* ", *Phys. Lett. B* **603** (2004), no. 3-4 219–229; Erratum–ibid.B629(2005)114, [hep-ph/0406231].

[155] A. Barroso, P. Ferreira, and R. Santos, "*Charge and CP symmetry breaking in two Higgs doublet models* ", *Phys. Lett. B* **632** (2006), no. 56 684 – 687.

[156] A. Barroso, P. Ferreira, I. Ivanov, and R. Santos, "*Metastability bounds on the two Higgs doublet model* ", *JHEP* **1306** (2013) 045, [arXiv:1303.5098].

[157] I. P. Ivanov and J. P. Silva, "*Tree-level metastability bounds for the most general two Higgs doublet model* ", arXiv:1507.0510.

[158] W. J. Marciano, G. Valencia, and S. Willenbrock, "*Renormalization Group Improved Unitarity Bounds on the Higgs Boson and Top Quark Masses* ", *Phys.Rev.* **D40** (1989) 1725.

[159] A. Arhrib, "*Unitarity constraints on scalar parameters of the standard and two Higgs doublets model* ", hep-ph/0012353.

[160] B. W. Lee, C. Quigg, and H. Thacker, "*Weak Interactions at Very High-Energies: The Role of the Higgs Boson Mass* ", *Phys.Rev.* **D16** (1977) 1519.

[161] M. S. Chanowitz and M. K. Gaillard, "*The TeV Physics of Strongly Interacting W's and Z's* ", *Nucl.Phys.* **B261** (1985) 379.

[162] H. G. Veltman, "*The Equivalence Theorem* ", *Phys.Rev.* **D41** (1990) 2294.

[163] I. Ginzburg and I. Ivanov, "*Tree level unitarity constraints in the 2HDM with CP violation* ", hep-ph/0312374.

[164] I. Ginzburg and I. Ivanov, "*Tree-level unitarity constraints in the most general 2HDM* ", *Phys.Rev.* **D72** (2005) 115010, [hep-ph/0508020].

[165] **Particle Data Group** , J. Beringer et al., "*Review of Particle Physics (RPP)* ", *Phys.Rev.* **D86** (2012) 010001.

[166] W. Grimus, L. Lavoura, O. Ogreid, and P. Osland, "*A Precision constraint on multi-Higgs-doublet models* ", *J.Phys.* **G35** (2008) 075001, [arXiv:0711.4022].

[167] W. Grimus, L. Lavoura, O. Ogreid, and P. Osland, "*The Oblique parameters in multi-Higgs-doublet models* ", *Nucl.Phys.* **B801** (2008) 81–96, [arXiv:0802.4353].

[168] H. E. Haber and D. O'Neil, "*Basis-independent methods for the two-Higgs-doublet model III: The CP-conserving limit, custodial symmetry, and the oblique parameters S, T, U* ", *Phys.Rev.* **D83** (2011) 055017, [arXiv:1011.6188].

[169] M. E. Peskin and T. Takeuchi, "*Estimation of oblique electroweak corrections* ", *Phys.Rev.* **D46** (1992) 381–409.

[170] I. Maksymyk, C. Burgess, and D. London, "*Beyond S, T and U* ", *Phys.Rev.* **D50** (1994) 529–535, [hep-ph/9306267].

[171] R. Barbieri, A. Pomarol, R. Rattazzi, and A. Strumia, "*Electroweak symmetry breaking after LEP-1 and LEP-2* ", *Nucl. Phys.* **B703** (2004) 127–146, [hep-ph/0405040].

[172] G. Funk, D. O'Neil, and R. M. Winters, "*What the oblique parameters S, T, and U and their extensions reveal about the 2HDM: A numerical analysis* ", *Int.J.Mod.Phys.* **A27** (2012) 1250021, [arXiv:1110.3812].

[173] H. E. Haber and H. E. Logan, "*Radiative corrections to the $Zb\bar{b}$ vertex and constraints on extended Higgs sectors* ", *Phys.Rev.* **D62** (2000) 015011, [hep-ph/9909335].

[174] F. Mahmoudi and O. Stal, "*Flavor constraints on the two-Higgs-doublet model with general Yukawa couplings* ", *Phys.Rev.* **D81** (2010) 035016, [arXiv:0907.1791].

[175] M. Misiak and M. Steinhauser, "*NNLO QCD corrections to the $\overline{B} \to X_s\gamma$ matrix elements using interpolation in m(c)* ", *Nucl.Phys.* **B764** (2007) 62–82, [hep-ph/0609241].

[176] M. Ciuchini, G. Degrassi, P. Gambino, and G. Giudice, "*Next-to-leading QCD corrections to $\overline{B} \to X_s\gamma$: Standard model and two Higgs doublet model* ", *Nucl.Phys.* **B527** (1998) 21–43, [hep-ph/9710335].

[177] F. Borzumati and C. Greub, "*2HDMs predictions for $\overline{B} \to X_s\gamma$ in NLO QCD* ", *Phys.Rev.* **D58** (1998) 074004, [hep-ph/9802391].

[178] P. Ciafaloni, A. Romanino, and A. Strumia, "*Two loop QCD corrections to charged Higgs mediated $b \to s\gamma$ decay* ", *Nucl.Phys.* **B524** (1998) 361–376, [hep-ph/9710312].

[179] T. Hermann, M. Misiak, and M. Steinhauser, "*$\overline{B} \to X_s\gamma$ in the Two Higgs Doublet Model up to Next-to-Next-to-Leading Order in QCD* ", *JHEP* **1211** (2012) 036, [arXiv:1208.2788].

[180] C. Geng and J. N. Ng, "*Charged Higgs effect in $B^0_d - \bar{B}^0_d$ mixing, $K \to \pi\nu\bar{\nu}$ decay, and rare decays of B Mesons* ", *Phys.Rev.* **D38** (1988) 2857.

[181] **DELPHI, OPAL, ALEPH, LEP Working Group for Higgs Boson Searches, L3** , S. Schael et al., "*Search for neutral MSSM Higgs bosons at LEP* ", *Eur. Phys. J.* **C47** (2006) 547–587, [hep-ex/0602042].

[182] **CDF** , T. Aaltonen et al., "*Inclusive Search for Standard Model Higgs Boson Production in the WW Decay Channel using the CDF II Detector* ", *Phys. Rev. Lett.* **104** (2010) 061803, [arXiv:1001.4468].

[183] **ATLAS** , G. Aad et al., "*Combined search for the Standard Model Higgs boson using up to 4.9 fb^{-1} of pp collision data at $\sqrt{s} = 7$ TeV with the ATLAS detector at the LHC* ", *Phys. Lett.* **B710** (2012) 49–66, [arXiv:1202.1408].

[184] **CMS** , S. Chatrchyan et al., "*Combined results of searches for the standard model Higgs boson in pp collisions at $\sqrt{s} = 7$ TeV* ", *Phys. Lett.* **B710** (2012) 26–48, [arXiv:1202.1488].

[185] **ATLAS** , G. Aad et al., "*Search for Scalar Diphoton Resonances in the Mass Range $65 - 600$ GeV with the ATLAS Detector in pp Collision Data at $\sqrt{s} = 8$ TeV* ", *Phys. Rev. Lett.* **113** (2014), no. 17 171801, [arXiv:1407.6583].

[186] **CMS** , S. Chatrchyan et al., "*Search for a standard-model-like Higgs boson with a mass in the range 145 to 1000 GeV at the LHC* ", *Eur.Phys.J.* **C73** (2013) 2469, [arXiv:1304.0213].

[187] **CMS** , V. Khachatryan et al., "*Search for a Higgs boson in the mass range from 145 to 1000 GeV decaying to a pair of W or Z bosons* ", arXiv:1504.0093.

[188] **CMS** , V. Khachatryan et al., "*Search for diphoton resonances in the mass range from 150 to 850 GeV in pp collisions at $\sqrt{s} = 8$ TeV* ", arXiv:1506.0230.

[189] **CMS** , S. Chatrchyan et al., "*Search for a Higgs boson decaying into a Z and a photon in pp collisions at $\sqrt{s} = 7$ and 8 TeV* ", *Phys.Lett.* **B726** (2013) 587–609, [arXiv:1307.5515].

[190] **ATLAS** , G. Aad et al., "*Search for Higgs boson decays to a photon and a Z boson in pp collisions at $\sqrt{s} = 7$ and 8 TeV with the ATLAS detector* ", *Phys. Lett.* **B732** (2014) 8–27, [arXiv:1402.3051].

[191] **CDF** , T. Aaltonen et al., "*Search for Higgs bosons predicted in two-Higgs-doublet models via decays to tau lepton pairs in 1.96-TeV $p\bar{p}$ collisions* ", *Phys. Rev. Lett.* **103** (2009) 201801, [arXiv:0906.1014].

[192] **D0** , V. M. Abazov et al., "*Search for Higgs bosons decaying to $\tau\tau$ pairs in $p\bar{p}$ collisions at $\sqrt{s} = 1.96$ TeV* ", *Phys. Lett.* **B707** (2012) 323–329, [arXiv:1106.4555].

[193] **ATLAS** , G. Aad et al., "*Search for neutral MSSM Higgs bosons decaying to $\tau^+\tau^-$ pairs in proton-proton collisions at $\sqrt{s} = 7$ TeV with the ATLAS detector* ", *Phys. Lett.* **B705** (2011) 174–192, [arXiv:1107.5003].

[194] **CMS** , S. Chatrchyan et al., "*Search for neutral Higgs bosons decaying to τ pairs in pp collisions at $\sqrt{s} = 7$ TeV* ", *Phys. Lett.* **B713** (2012) 68–90, [arXiv:1202.4083].

[195] **ATLAS** , G. Aad et al., "*Search for neutral Higgs bosons of the minimal supersymmetric standard model in pp collisions at $\sqrt{s} = 8$ TeV with the ATLAS detector* ", *JHEP* **11** (2014) 056, [arXiv:1409.6064].

[196] **ATLAS** , G. Aad et al., "*Measurement of the Higgs boson mass from the $H \to \gamma\gamma$ and $H \to ZZ^* \to 4\ell$ channels with the ATLAS detector using 25 fb^{-1} of pp collision data* ", *Phys. Rev.* **D90** (2014), no. 5 052004, [arXiv:1406.3827].

[197] **ATLAS** , G. Aad et al., "*Measurement of Higgs boson production in the diphoton decay channel in pp collisions at center-of-mass energies of 7 and 8 TeV with the ATLAS detector* ", *Phys. Rev.* **D90** (2014), no. 11 112015, [arXiv:1408.7084].

[198] **CMS** , V. Khachatryan et al., "*Observation of the diphoton decay of the Higgs boson and measurement of its properties* ", *Eur. Phys. J.* **C74** (2014), no. 10 3076, [arXiv:1407.0558].

[199] **CDF, D0** , T. Aaltonen et al., "*Evidence for a particle produced in association with weak bosons and decaying to a bottom-antibottom quark pair in Higgs boson searches at the Tevatron* ", *Phys. Rev. Lett.* **109** (2012) 071804, [arXiv:1207.6436].

[200] **CMS** , S. Chatrchyan et al., "*Search for the standard model Higgs boson produced in association with a W or a Z boson and decaying to bottom quarks* ", *Phys. Rev.* **D89** (2014), no. 1 012003, [arXiv:1310.3687].

[201] **ATLAS** , G. Aad et al., "*Search for the $b\bar{b}$ decay of the Standard Model Higgs boson in associated $(W/Z)H$ production with the ATLAS detector* ", *JHEP* **01** (2015) 069, [arXiv:1409.6212].

[202] **CMS** , V. Khachatryan et al., "*Search for the standard model Higgs boson produced through vector boson fusion and decaying to* $\mathrm{b\bar{b}}$ ", arXiv:1506.0101.

[203] **ATLAS** , G. Aad et al., "*Search for invisible decays of the Higgs boson produced in association with a hadronically decaying vector boson in pp collisions at $\sqrt{s} = 8$ TeV with the ATLAS detector* ", arXiv:1504.0432.

[204] **ATLAS** , G. Aad et al., "*Search for Invisible Decays of a Higgs Boson Produced in Association with a Z Boson in ATLAS* ", *Phys. Rev. Lett.* **112** (2014) 201802, [arXiv:1402.3244].

[205] **CMS** , S. Chatrchyan et al., "*Search for invisible decays of Higgs bosons in the vector boson fusion and associated ZH production modes* ", *Eur. Phys. J.* **C74** (2014) 2980, [arXiv:1404.1344].

[206] **CMS** , V. Khachatryan et al., "*Search for exotic decays of a Higgs boson into undetectable particles and photons* ", arXiv:1507.0035.

[207] **CMS** , V. Khachatryan et al., "*Searches for heavy Higgs bosons in two-Higgs-doublet models and for tch decay using multilepton and diphoton final states in pp collisions at 8 TeV* ", *Phys. Rev.* **D90** (2014) 112013, [arXiv:1410.2751].

[208] **ATLAS** , G. Aad et al., "*Search for a CP-odd Higgs boson decaying to Zh in pp collisions at $\sqrt{s} = 8$ TeV with the ATLAS detector* ", *Phys. Lett.* **B744** (2015) 163–183, [arXiv:1502.0447].

[209] **CMS** , V. Khachatryan et al., "*Search for a pseudoscalar boson decaying into a Z boson and the 125 GeV Higgs boson in llbb final states* ", arXiv:1504.0471.

[210] **ALEPH** , A. Heister et al., "*Search for charged Higgs bosons in e^+e^- collisions at energies up to $\sqrt{s}$ = 209-GeV* ", *Phys.Lett.* **B543** (2002) 1–13, [hep-ex/0207054].

[211] **DELPHI** , J. Abdallah et al., "*Search for charged Higgs bosons in e^+e^- collisions at $\sqrt{s}$=189-GeV - 202-GeV* ", *Phys.Lett.* **B525** (2002) 17–28, [hep-ex/0201023].

[212] **L3** , P. Achard et al., "*Search for charged Higgs bosons at LEP* ", *Phys.Lett.* **B575** (2003) 208–220, [hep-ex/0309056].

[213] **ALEPH, DELPHI, L3, OPAL, LEP** , G. Abbiendi et al., "*Search for Charged Higgs bosons: Combined Results Using LEP Data* ", *Eur.Phys.J.* **C73** (2013) 2463, [arXiv:1301.6065].

[214] **D0** , V. Abazov et al., "*Search for charged Higgs bosons in top quark decays* ", *Phys.Lett.* **B682** (2009) 278–286, [arXiv:0908.1811].

[215] **CDF** , T. Aaltonen et al., "*Search for charged Higgs bosons in decays of top quarks in $p\bar{p}$ collisions at $\sqrt{s} = 1.96$ TeV* ", *Phys.Rev.Lett.* **103** (2009) 101803, [arXiv:0907.1269].

[216] **ATLAS** , G. Aad et al., "*Search for charged Higgs bosons decaying via $H^+ \to \tau\nu$ in top quark pair events using pp collision data at $\sqrt{s} = 7$ TeV with the ATLAS detector* ", *JHEP* **1206** (2012) 039, [arXiv:1204.2760].

[217] **ATLAS** , G. Aad et al., "*Search for a light charged Higgs boson in the decay channel $H^+ \to c\bar{s}$ in $t\bar{t}$ events using pp collisions at $\sqrt{s} = 7$ TeV with the ATLAS detector* ", *Eur.Phys.J.* **C73** (2013), no. 6 2465, [arXiv:1302.3694].

[218] **D0** , V. Abazov et al., "*Search for charged Higgs bosons decaying to top and bottom quarks in $p\bar{p}$ collisions* ", *Phys.Rev.Lett.* **102** (2009) 191802, [arXiv:0807.0859].

[219] **ATLAS** , G. Aad et al., "*Search for charged Higgs bosons decaying via $H^\pm \to \tau^\pm\nu$ in fully hadronic final states using pp collision data at $\sqrt{s} = 8$ TeV with the ATLAS detector* ", *JHEP* **1503** (2015) 088, [arXiv:1412.6663].

[220] A. Djouadi, "*The anatomy of electro-weak symmetry breaking. I: The Higgs boson in the standard model* ", *Phys.Rept.* **457** (2008) 1–216, [hep-ph/0503172].

[221] A. Djouadi, "*The anatomy of electro-weak symmetry breaking. II. The Higgs bosons in the minimal supersymmetric model* ", *Phys.Rept.* **459** (2008) 1–241, [hep-ph/0503173].

[222] T. Plehn, "*Lectures on LHC Physics* ", *Lect. Notes Phys.* **844** (2012) 1–193, [arXiv:0910.4182].

[223] R. V. Harlander, S. Liebler, and H. Mantler, "*SusHi: A program for the calculation of Higgs production in gluon fusion and bottom-quark annihilation in the Standard Model and the MSSM* ", *Comput.Phys.Commun.* **184** (2013) 1605–1617, [arXiv:1212.3249].

[224] J. Lee, M. Carena, J. Ellis, A. Pilaftsis, and C. Wagner, "*CPsuperH2.0: an Improved Computational Tool for Higgs Phenomenology in the MSSM with Explicit CP Violation* ", *Comput.Phys.Commun.* **180** (2009) 312–331, [arXiv:0712.2360].

[225] K. Chetyrkin, B. A. Kniehl, and M. Steinhauser, "*Decoupling relations to $\mathcal{O}(\alpha_s^3)$ and their connection to low-energy theorems* ", *Nucl.Phys.* **B510** (1998) 61–87, [hep-ph/9708255].

[226] Z.-z. Xing, H. Zhang, and S. Zhou, "*Updated Values of Running Quark and Lepton Masses* ", *Phys.Rev.* **D77** (2008) 113016, [arXiv:0712.1419].

[227] A. Djouadi, J. Kalinowski, and P. Zerwas, "*Two and three-body decay modes of SUSY Higgs particles* ", *Z.Phys.* **C70** (1996) 435–448, [hep-ph/9511342].

[228] M. Spira, A. Djouadi, D. Graudenz, and P. Zerwas, "*Higgs boson production at the LHC* ", *Nucl.Phys.* **B453** (1995) 17–82, [hep-ph/9504378].

[229] J. Lee, M. Carena, J. Ellis, A. Pilaftsis, and C. Wagner, "*CPsuperH2.3: an Updated Tool for Phenomenology in the MSSM with Explicit CP Violation*", *Comput.Phys.Commun.* **184** (2013) 1220–1233, [arXiv:1208.2212].

[230] **LHC Higgs Cross Section Working Group** , S. Heinemeyer et al., "*Handbook of LHC Higgs Cross Sections: 3. Higgs Properties*", arXiv:1307.1347.

[231] K. Chetyrkin, B. A. Kniehl, and M. Steinhauser, "*Hadronic Higgs decay to order α_s^4*", *Phys.Rev.Lett.* **79** (1997) 353–356, [hep-ph/9705240].

[232] K. Chetyrkin, B. A. Kniehl, M. Steinhauser, and W. A. Bardeen, "*Effective QCD interactions of CP odd Higgs bosons at three loops*", *Nucl.Phys.* **B535** (1998) 3–18, [hep-ph/9807241].

[233] S. Choi, K. Hagiwara, and J. S. Lee, "*Higgs boson decays in the minimal supersymmetric standard model with radiative Higgs sector CP violation*", *Phys.Rev.* **D64** (2001) 032004, [hep-ph/0103294].

[234] A. Djouadi, J. Kalinowski, and M. Spira, "*HDECAY: A Program for Higgs boson decays in the standard model and its supersymmetric extension*", *Comput.Phys.Commun.* **108** (1998) 56–74, [hep-ph/9704448].

[235] D. Eriksson, J. Rathsman, and O. Stal, "*2HDMC: Two-Higgs-Doublet Model Calculator Physics and Manual*", *Comput. Phys. Commun.* **181** (2010) 189–205, [arXiv:0902.0851].

[236] I. I. Y. Bigi, Y. L. Dokshitzer, V. A. Khoze, J. H. Kuhn, and P. M. Zerwas, "*Production and Decay Properties of Ultraheavy Quarks*", *Phys. Lett.* **B181** (1986) 157.

[237] P. Bechtle, O. Brein, S. Heinemeyer, G. Weiglein, and K. E. Williams, "*HiggsBounds: Confronting Arbitrary Higgs Sectors with Exclusion Bounds from LEP and the Tevatron*", *Comput.Phys.Commun.* **181** (2010) 138–167, [arXiv:0811.4169].

[238] P. Bechtle, O. Brein, S. Heinemeyer, O. Stl, T. Stefaniak, et al., "*HiggsBounds-4: Improved Tests of Extended Higgs Sectors against Exclusion Bounds from LEP, the Tevatron and the LHC*", *Eur.Phys.J.* **C74** (2014) 2693, [arXiv:1311.0055].

[239] **ATLAS** , G. Aad et al., "*Evidence for the spin-0 nature of the Higgs boson using ATLAS data*", *Phys.Lett.* **B726** (2013) 120–144, [arXiv:1307.1432].

[240] **CMS** , V. Khachatryan et al., "*Constraints on the spin-parity and anomalous HVV couplings of the Higgs boson in proton collisions at 7 and 8 TeV*", arXiv:1411.3441.

[241] **ATLAS, CMS** , G. Aad et al., "*Combined Measurement of the Higgs Boson Mass in pp Collisions at $\sqrt{s} = 7$ and 8 TeV with the ATLAS and CMS Experiments*", *Phys. Rev. Lett.* **114** (2015) 191803, [arXiv:1503.0758].

[242] **ATLAS** , G. Aad et al., "*Measurements of Higgs boson production and couplings in diboson final states with the ATLAS detector at the LHC*", *Phys.Lett.* **B726** (2013) 88–119, [arXiv:1307.1427].

[243] **CMS** , V. Khachatryan et al., "*Precise determination of the mass of the Higgs boson and tests of compatibility of its couplings with the standard model predictions using proton collisions at 7 and 8 TeV* ", *Eur. Phys. J.* **C75** (2015), no. 5 212, [arXiv:1412.8662].

[244] **ATLAS** , G. Aad et al., "*Measurements of the Higgs boson production and decay rates and coupling strengths using pp collision data at $\sqrt{s} = 7$ and 8 TeV in the ATLAS experiment* ", arXiv:1507.0454.

[245] M. Gorbahn, J. M. No, and V. Sanz, "*Benchmarks for Higgs Effective Theory: Extended Higgs Sectors* ", arXiv:1502.0735.

[246] P. M. Ferreira, R. Guedes, M. O. P. Sampaio, and R. Santos, "*Wrong sign and symmetric limits and non-decoupling in 2HDMs* ", *JHEP* **12** (2014) 067, [arXiv:1409.6723].

[247] P. M. Ferreira, J. F. Gunion, H. E. Haber, and R. Santos, "*Probing wrong-sign Yukawa couplings at the LHC and a future linear collider* ", *Phys. Rev.* **D89** (2014), no. 11 115003, [arXiv:1403.4736].

[248] P. Bechtle, S. Heinemeyer, O. Stl, T. Stefaniak, and G. Weiglein, "*HiggsSignals: Confronting arbitrary Higgs sectors with measurements at the Tevatron and the LHC* ", *Eur.Phys.J.* **C74** (2014), no. 2 2711, [arXiv:1305.1933].

[249] A. D. Linde, "*Decay of the false vacuum at finite temperature* ", *Nucl.Phys.* **B216** (1983) 421.

[250] M. Laine, "*Basics of thermal field theory*", http://www.laine.itp.unibe.ch/basics.pdf.

[251] P. B. Arnold and O. Espinosa, "*The Effective potential and first order phase transitions: Beyond leading-order* ", *Phys.Rev.* **D47** (1993) 3546, [hep-ph/9212235].

[252] M. Carrington, "*The Effective potential at finite temperature in the Standard Model* ", *Phys.Rev.* **D45** (1992) 2933–2944.

[253] P. Fendley, "*The Effective Potential and the Coupling Constant at High Temperature* ", *Phys.Lett.* **B196** (1987) 175.

[254] C. Delaunay, C. Grojean, and J. D. Wells, "*Dynamics of Non-renormalizable Electroweak Symmetry Breaking* ", *JHEP* **0804** (2008) 029, [arXiv:0711.2511].

[255] P. B. Arnold, "*Quark-Gluon Plasmas and Thermalization* ", *Int.J.Mod.Phys.* **E16** (2007) 2555–2594, [arXiv:0708.0812].

[256] K. Farakos, K. Kajantie, K. Rummukainen, and M. E. Shaposhnikov, "*3-D physics and the electroweak phase transition: Perturbation theory* ", *Nucl.Phys.* **B425** (1994) 67–109, [hep-ph/9404201].

[257] K. Kajantie, M. Laine, K. Rummukainen, and M. E. Shaposhnikov, "*The Electroweak phase transition: A Nonperturbative analysis* ", *Nucl.Phys.* **B466** (1996) 189–258, [hep-lat/9510020].

[258] Z. Fodor and A. Hebecker, "*Finite temperature effective potential to order g^4, λ^2 and the electroweak phase transition* ", *Nucl.Phys.* **B432** (1994) 127–146, [hep-ph/9403219].

[259] M. Laine and K. Rummukainen, "*Two Higgs doublet dynamics at the electroweak phase transition: A nonperturbative study* ", *Nucl.Phys.* **B597** (2001) 23–69, [hep-lat/0009025].

[260] H. H. Patel and M. J. Ramsey-Musolf, "*Baryon Washout, Electroweak Phase Transition, and Perturbation Theory* ", *JHEP* **1107** (2011) 029, [arXiv:1101.4665].

[261] C. Wainwright, S. Profumo, and M. J. Ramsey-Musolf, "*Gravity Waves from a Cosmological Phase Transition: Gauge Artifacts and Daisy Resummations* ", *Phys.Rev.* **D84** (2011) 023521, [arXiv:1104.5487].

[262] M. Garny and T. Konstandin, "*On the gauge dependence of vacuum transitions at finite temperature* ", *JHEP* **1207** (2012) 189, [arXiv:1205.3392].

[263] H. E. Haber and O. Stal, "*New LHC Benchmarks for the CP-conserving Two-Higgs-Doublet Model* ", arXiv:1507.0428.

[264] S. Huber and M. Schmidt, "*Electroweak baryogenesis: Concrete in a SUSY model with a gauge singlet* ", *Nucl.Phys.* **B606** (2001) 183–230, [hep-ph/0003122].

[265] S. Kanemura, S. Moretti, Y. Mukai, R. Santos, and K. Yagyu, "*Distinctive Higgs Signals of a Type II 2HDM at the LHC* ", *Phys.Rev.* **D79** (2009) 055017, [arXiv:0901.0204].

[266] N. D. Christensen and C. Duhr, "*FeynRules - Feynman rules made easy* ", *Comput. Phys. Commun.* **180** (2009) 1614–1641, [arXiv:0806.4194].

[267] R. P. Kauffman and W. Schaffer, "*QCD corrections to production of Higgs pseudoscalars* ", *Phys. Rev.* **D49** (1994) 551–554, [hep-ph/9305279].

[268] J. Alwall, M. Herquet, F. Maltoni, O. Mattelaer, and T. Stelzer, "*MadGraph 5 : Going Beyond* ", *JHEP* **1106** (2011) 128, [arXiv:1106.0522].

[269] J. Alwall, R. Frederix, S. Frixione, V. Hirschi, F. Maltoni, O. Mattelaer, H. S. Shao, T. Stelzer, P. Torrielli, and M. Zaro, "*The automated computation of tree-level and next-to-leading order differential cross sections, and their matching to parton shower simulations* ", *JHEP* **07** (2014) 079, [arXiv:1405.0301].

[270] T. Sjostrand, S. Mrenna, and P. Z. Skands, "*A Brief Introduction to PYTHIA 8.1* ", *Comput. Phys. Commun.* **178** (2008) 852–867, [arXiv:0710.3820].

[271] **DELPHES 3** , J. de Favereau et al., "*DELPHES 3, A modular framework for fast simulation of a generic collider experiment* ", *JHEP* **1402** (2014) 057, [arXiv:1307.6346].

[272] G. Bevilacqua, M. Czakon, A. van Hameren, C. G. Papadopoulos, and M. Worek, "*Complete off-shell effects in top quark pair hadroproduction with leptonic decay at next-to-leading order* ", *JHEP* **02** (2011) 083, [arXiv:1012.4230].

[273] J. M. Campbell, R. K. Ellis, F. Maltoni, and S. Willenbrock, "*Production of a Z boson and two jets with one heavy-quark tag* ", *Phys. Rev.* **D73** (2006) 054007, [hep-ph/0510362]. [Erratum: Phys. Rev.D77,019903(2008)].

[274] **CMS**, "*Performance of b tagging at* $\sqrt{s} = 8$ *TeV in multijet, ttbar and boosted topology events* ", CMS-PAS-BTV-13-001.

[275] J. Ohnemus, "*Hadronic ZZ,* W^-W^+*, and* $W^\pm Z$ *production with QCD corrections and leptonic decays* ", *Phys. Rev.* **D50** (1994) 1931–1945, [hep-ph/9403331].

[276] A. Lazopoulos, T. McElmurry, K. Melnikov, and F. Petriello, "*Next-to-leading order QCD corrections to* $t\bar{t}Z$ *production at the LHC* ", *Phys. Lett.* **B666** (2008) 62–65, [arXiv:0804.2220].

[277] **CMS** , "*Search for H/A decaying into Z+A/H, with Z to ll and A/H to fermion pair* ", CMS-PAS-HIG-15-001.

[278] T. Abe, J. Hisano, T. Kitahara, and K. Tobioka, "*Gauge invariant Barr-Zee type contributions to fermionic EDMs in the two-Higgs doublet models* ", arXiv:1311.4704.

[279] J. Engel, M. J. Ramsey-Musolf, and U. van Kolck, "*Electric Dipole Moments of Nucleons, Nuclei, and Atoms: The Standard Model and Beyond* ", *Prog.Part.Nucl.Phys.* **71** (2013) 21–74, [arXiv:1303.2371].

[280] **ACME** , J. Baron et al., "*Order of Magnitude Smaller Limit on the Electric Dipole Moment of the Electron* ", *Science* **343** (2014) 269–272, [arXiv:1310.7534].

[281] C. Baker, D. Doyle, P. Geltenbort, K. Green, M. van der Grinten, et al., "*An Improved experimental limit on the electric dipole moment of the neutron* ", *Phys.Rev.Lett.* **97** (2006) 131801, [hep-ex/0602020].

[282] W. C. Griffith, M. D. Swallows, T. H. Loftus, M. V. Romalis, B. R. Heckel, and E. N. Fortson, "*Improved Limit on the Permanent Electric Dipole Moment of Hg-199* ", *Phys. Rev. Lett.* **102** (2009) 101601.

[283] T. Konstandin, "*Quantum Transport and Electroweak Baryogenesis* ", arXiv:1302.6713.

[284] T. Konstandin, G. Nardini, and I. Rues, "*From Boltzmann equations to steady wall velocities* ", *JCAP* **1409** (2014), no. 09 028, [arXiv:1407.3132].

[285] D. Bodeker and G. D. Moore, "*Can electroweak bubble walls run away?* ", *JCAP* **0905** (2009) 009, [arXiv:0903.4099].

[286] S. J. Huber and M. Sopena, "*An efficient approach to electroweak bubble velocities* ", arXiv:1302.1044.

[287] M. Laine and M. Losada, "*Two loop dimensional reduction and effective potential without temperature expansions* ", *Nucl.Phys.* **B582** (2000) 277–295, [hep-ph/0003111].

[288] J. Shu and Y. Zhang, "*Impact of a CP Violating Higgs: from LHC to Baryogenesis* ", arXiv:1304.0773.

[289] C.-Y. Chen, S. Dawson, and Y. Zhang, "*Complementarity of LHC and EDMs for Exploring Higgs CP Violation* ", arXiv:1503.0111.

[290] L. R. Surguladze, "*Quark mass effects in fermionic decays of the Higgs boson in $\mathcal{O}(\alpha_s^2)$ perturbative QCD* ", *Phys.Lett.* **B341** (1994) 60–72, [hep-ph/9405325].

[291] W. Dekens and J. de Vries, "*Renormalization Group Running of Dimension-Six Sources of Parity and Time-Reversal Violation* ", *JHEP* **1305** (2013) 149, [arXiv:1303.3156].